Institute of Pharmacology and Toxicology

Head: Prof. Dr. Holger Barth

Bacillus anthracis´ protective antigen as molecular transporter for the pharmacologically relevant biomolecule His-NDPK-A

Dissertation

Submitted in partial fulfillment of the requirements for the degree of

“Doctor rerum naturalium” (Dr. rer. nat.)

of the International Graduate School of Molecular Medicine Ulm

Submitted by

Ina Felix

Born in Überlingen, Germany

Ulm 2021

Current Dean of the Medical Faculty:	Prof. Dr. rer. nat. Thomas Wirth
Current Chairman of the Graduate School:	Prof. Dr. Bernd Knöll

Thesis Advisory Committee

First Supervisor:	Prof. Dr. Holger Barth
Second Supervisor:	Prof. Dr. Manfred Frick
Third Supervisor:	Prof. Dr. Thomas Wieland
External Reviewer:	Prof. Dr. Gudula Schmidt
Day of Doctorate Awarded:	01.03.2022

Results gained in my thesis have previously been published in the following publication:

Felix I, Lomada SK, Barth H, Wieland T. Bacillus anthracis' PA63 Delivers the Tumor Metastasis Suppressor Protein NDPK-A/NME1 into Breast Cancer Cells. Int J Mol Sci. 2020 May 6;21(9):3295. doi: 10.3390/ijms21093295

"CC BY 4.0, https://creativecommons.org/licenses/by/4.0"

Table of Content

Table of Content I
List of Figures I
List of Abbreviations I
1. Introduction 1
1.1. Bacterial Exotoxins 1
1.1.1. Structure, Cellular Uptake and Mode of Action of Bacterial Exotoxins 2
1.2. Bacterial Toxins as Molecular Tools and Therapeutics – From Basic Research to Scientific and Medical Applications 5
1.2.1. Anthrax Toxin 9
1.2.2. PA_{63} as a Molecular Transporter 13
1.2.3. NDPK-A as Model Cargo for PA-mediated Transport into the Cytosol of Cancer Cells 15
1.3. Aim of the Thesis 18
2. Materials and Methods 19
2.1. Materials 19
2.1.1. Chemicals 19
2.1.2. Ready-to-use Solutions, Enzymes and Kits 22
2.1.3. Consumables 23
2.1.4. Devices 24
2.1.5. Buffers and Solutions 26
2.1.6. Antibodies and Binding Proteins 31
2.1.7. Mammalian Cell Lines 32
2.1.8. *Escherichia coli* Strains 33
2.1.9. Toxins and Plasmids 33
2.1.10. Software 34
2.2. Methods 35
2.2.1. Culture of Mammalian Cell Lines 35
2.2.2. Preparation of MDA-MB-231 Cell Lysate 37
2.2.3. Bradford Assay 38
2.2.4. Expression and Purification of Proteins 38
2.2.5. Protein analysis 43
2.2.6. His-NDPK-A Kinase Assays 45
2.2.7. Overview of the Performed Assays 48
2.2.8. Cell Binding Assay 49

2.2.9. Uptake Assays 50
2.2.10. Migration Assay 53
2.2.11. Reproducibility and Statistics 54
3. Results 55
3.1. Purification and Characterization of Recombinantly Expressed Proteins 55
3.1.1. Purification and Characterization of His-NDPK-A 55
3.1.2. Purification and Characterization of PA_{63} 57
3.2. Susceptibility of Human cells to PA_{63}-mediated Delivery of His-tagged DTA 59
3.2.1. MDA-MB-231 cells are Susceptible to His-DTA Delivery via PA_{63} 59
3.2.2. HeLa cells are Susceptible to His-DTA Delivery via PA_{63} 61
3.3. PA_{63} mediates Delivery of His-DTA into Human cells 62
3.3.1. PA_{63} mediates Delivery of His-DTA into MDA-MB-231 cells 62
3.3.2. PA_{63} mediates Delivery of His-DTA into HeLa cells 64
3.4. PA_{63} mediates the Binding of His-NDPK-A to MDA-MB-231 and HeLa cells 67
3.5. PA_{63} Mediates Delivery of His-NDPK-A into the Cytosol of MDA-MB-231 and HeLa cells 68
3.5.1. PA_{63} Mediates Delivery of His-NDPK-A into MDA-MB-231 cells..... 68
3.5.2. PA_{63} Mediates Delivery of His-NDPK-A into HeLa cells..... 70
3.6. Treatment of MDA-MB-231 cells with His-NDPK-A plus PA_{63} Decreased Migration 72
4. Discussion 76
4.1. The Human Breast Cancer Cell line MDA-MB-231 is Susceptible to the Delivery of His-tagged Cargo Proteins via PA_{63} 78
4.2. Delivery of His-NDPK-A into the Cytosol of MDA-MB-231 cells via PA_{63} Decreases Cellular Migration 79
4.3. Conclusions 80
4.4. Perspective and Outlook 81
Optimization of the PA_{63}-mediated Delivery of Recombinant Tumor Metastasis Suppressor Protein NDPK-A into the Cytosol of Certain Cancer Cells 81
5. Summary 84
List of References 86
6. List of Publications 104
7. Curriculum Vitae 105
8. Acknowledgements 106
9. Statutory Declaration 107

List of Figures

Figure 1:Scheme of the cellular uptake and intracellular trafficking of AB-type protein toxins. 3
Figure 2: Structural model of PA. 10
Figure 3: Scheme representing the cytosolic delivery of LF/EF via the central transport protein PA..... 11
Figure 4: NDPK-A and its multiple functions during endocytosis. 16
Figure 5: Exemplary nucleoside diphosphate activity of NDPK-A in vitro. 45
Figure 6: Migration assay set-up using the Ibidi® culture-insert 2 well. 53
Figure 7: Characterization of the cargo protein His-NDPK-A. 56
Figure 8: Characterization of the transporter protein PA_{63}: 58
Figure 9: PA_{63} mediates delivery of His-DTA into MDA-MB-231 cells. 60
Figure 10: PA_{63} mediates delivery of His-DTA into HeLa cells. 61
Figure 11: His-DTA is delivered via PA_{63} into MDA-MB-231 breast cancer cells.. 64
Figure 12: His-DTA delivered via PA_{63} reaches the cytosol HeLa cells as enzymatically active protein. 66
Figure 13: PA_{63} mediates the binding of His-NDPK-A to HeLa and MDA-MB-231 cells. 67
Figure 14: PA_{63} delivers His-NDPK-A into MDA-MB-231 cells. 70
Figure 15: PA_{63} delivers His-NDPK-A into HeLa cells. 72
Figure 16: His-NDPK-A delivered by PA_{63} reduces cell-migration of MDA-MB-231 cells in vitro. 74
Figure 18: Schematic proposed route of uptake of His-NDPK-A via PA_{63}. 80

List of Abbreviations

Abbreviation	Description
°C	degree celsius
µL	microliter(s)
µM	micromolar
6-Biotin-17-NAD^+	biotinylated NAD^+
A-component	enzymatically active component of the AB-type toxins
ADP	adenosine triphosphate
α-MSH	α-melanocyte stimulating hormone
AP	Autophosphorylation Assay
APB	Autophosphorylation Assay buffer
APS	ammonium persulfate
ARB	Sequential ADP-ribosylation buffer
Arg	arginine
ATP	adenosine triphosphate
BafA1	bafilomycinA1
B. anthracis	*Bacillus anthracis*
B. pertussis	*Bordatella pertussis*
B-component	binding and translocation domain of AB-type toxins
BoNT	botulinum neurotoxin of *C. botulinum*
BoNT/A	botulinum neurotoxin of *C. botulinum* serotype A
BSA	bovine serum albumin
cAMP	cyclic adenosine monophosphate
C. botulinum	*Clostridium botulinum*
C. difficile	*Clostridium difficile*
C. diphtheriae	*Corynebacterium diphtheriae*
CHO	Chinese hamster ovary cells
C. perfringens	*Clostridium perfringens*
CMG2 (ANTXR2)	capillary morphogenesis gene 2
C2	binary AB-type toxin of *C. botulinum*
C2I	catalytic component of the C2 toxin

C2IIa	activated binding and translocation component of the C2 toxin
C2IN	N-terminal domain of the C2I
C2IN-C3	fusion toxin of N-terminal domain of C2I of *C. botulinum* and the catalytic domain of C3 *C. limosum*
C3	Rho-ADP-ribosylating toxin of *C. limosum/C. botulinum*
cAMP	cyclic adenosine monophosphate
CHO-K1	chines hamster ovary cells
Cyp	cyclophilin
Cys	cysteine
DMEM	Dulbecco´s modified eagles medium
DMSO	dimethyl sulfoxide
DT	AB-type toxin of *C. diphtheriae*
DTT	dithiothreitol
E. coli	*Escherichia coli*
ECL	enhanced chemiluminescence
EDTA	ethyleneediaminetetraacetic acid
EE	early endosome
EF	edema factor of the anthrax toxin of *B. anthracis*
EF-2	eucaryotic elongation factor 2
EGA	(4-bromobenzaldehyde N-(2,6-dimethylphenyl) semicarbazone)
EGFR	epidermal growth factor
ER	endoplasmic reticulum
ET	edema toxin of *B. anthracis*
ETEC	enterotoxigenic *E. coli* (ETEC)
f-actin	filamentous actin
FCS	fetal calf serum
FGFR	fibroblast growth factor
FKBP	FK506 binding protein
g	gram(s)
GDP	guanosine diphosphate
GTP	guanosine triphosphate

h	hour(s)
H_2O	water
H_2O_2	hydrogen peroxide
HCl	hydrogen chloride
HRP	horseradish peroxidase
Hsp90	heat shock protein 90
IF	Immunofluorescence microscopy
IL-2	interleukin-2
IMAC	Immobilized Metal Affinity Chromatography
IPTG	isopropyl β-D-1-thiogalactopyranoside
KA	Kinase assay
KCl	potassium chloride
KH_2PO_4	potassium phosphate
LB	Lysogeni Borth medium
LB_{amp}	Lysogeni Borth medium supplemented with ampicillin
LD_{50}	lethal dose 50
LE	late endosome
LF	lethal factor of the anthrax toxin of *B. anthracis*
LF_NDTA	fusion toxin of the N-terminal domain of the anthrax toxin of *B. anthracis* lethal factor conjugated to the enzyme domain of the diphtheria toxin of *C. diphtheriae*
LPS	lipopolysaccharide
LT	lethal toxin of *B. anthracis*
Lys	lysine
M	molar
MAPK	mitogen-activated protein kinase
MEM	Minimum Essential Medium Eagle
MEKs	Mitogen-activated protein kinase kinase
$MgCl_2$	magnesium chloride
min	minute(s)
MT1-MMP	membrane type1-matrix metalloproteinase
mL	milliliter(s)
mM	millimolar

MTS	(3-(4,5-dimethylthiazol-2-yl)-5-(3-carboxymethoxyphenyl)-2-(4-sulfophenyl)-2H-tetrazolium) substrate (CellTiter 96®Aq_{ueous} One Solution Reagence)
MWCO	molecular weight cut-off
Na_2HPO_4-dihydrate	disodium phosphate
NaCl	sodium chloride
NAD	nicotinamide adenine dinucleotide
NaOH	sodium hydroxide
NEAA	non-essential amino acids
NMJ	neuromuscular junction
PA_{20}	cleavage product of the activation of the protective antigen of the anthrax toxin
PA_{63}	activated protective antigen of the anthrax toxin
PA_{83}	full-length protective antigen of the anthrax toxin
PBS	phosphate buffered saline
PDGFR	platelet-derived growth factor receptor
PFT	Pore-forming toxins
PMSF	phenylmethylsulfonyl fluoride
RT	room temperature
SEC	Size exclusion chromatography
SD	standard Deviation
SDS	sodium dodecyl sulfate
SDS-PAGE	sodium dodecyl sulfate polyacrylamide gel electrophoresis
sec	second(s)
STEC	shiga toxigenic *E. coli*
Strep-POD	streptavidin peroxidase
TeNT	tetanus neurotoxin of *C. tetani*
TEM8 or ANTXR1	tumor endothelial marker 8
TEMED	tetramethylethylenediamine
TfR	transferrin receptor
TGN	*trans*-Golgi network

V. cholerae	*Vibrio cholerae*
vATPase	vacuolar H^+-ATPase
WB	Western blot analysis

1. Introduction

1.1. Bacterial Exotoxins

Bacterial toxins are thoroughly investigated since more than a century after they were identified as highly potent virulence factors of many pathogens. They act as causative agents for a large variety of diseases found in humans as well as animals. This group of toxins can be distinguished into two different categories: endotoxins and exotoxins.

Endotoxins as for instance lipopolysaccharides (LPS) are components of the outer membrane of the bacterial cell wall of Gram-negative bacteria. Upon bacterial cell lysis LPS is released, inducing systemic inflammatory responses and pyrogenic effects(GALANOS et al., 1985; Westphal & Lüderitz, 1954). Endotoxins in general are not associated with metabolically active bacteria (Lubran, 1988). In contrast to endotoxins, exotoxins are proteins secreted by Gram-negative as well as Gram-positive bacteria. These soluble proteins act on eukaryotic cells independently from their producing pathogen. Based on their different functionalities, bacterial exotoxins can be further divided into two subgroups.

The first large subgroup of exotoxins are pore-forming toxins (PFT), for example the alpha-toxin produced by *Staphylococcus aureus*. Cytotoxicity of PFTs is mediated by the formation of a pore into the membrane of cells. After binding to specific cell surface receptors, the toxins insert themselves into the cellular membrane which leads to the flux of ions like Ca^{2+} and K^{+}, ATP and other low molecular weight molecules, resulting in necrosis and apoptosis (Berube & Wardenburg, 2013).

The second group of exotoxins are the so-called AB-type toxins. These toxins were identified as causative agents for severe human diseases such as anthrax, cholera and diphtheria, to only name a few (De, 1959; Pappenheimer, 1937; Stanley & Smith, 1961). AB-type toxins are the most toxic substances because of their unique structure and mode of action (Barth & Stiles, 2008). These proteins are composed of various functionally different subunits, which mediate the binding of the toxin to its cellular receptor (B-subunit), the translocation from intracellular vesicles into the host cells cytosol (T-subunit) and the modification of a specific substrate in the cytosol by an enzymatically active subunit (A subunit). (Ernst et al., 2017; W. Liu & Nestorovich, 2021; Stiles et al., 2011). The toxin-catalyzed substrate modification

induces characteristic cellular effects consequently leading to the clinical symptoms that are associated with the respective toxin and toxin-producing bacterium. Taken together, AB-type toxins act inside cells and are extremely potent and substrate specific (Barth et al., 2015; Locht et al., 2011; Schleberger et al., 2006).

1.1.1. Structure, Cellular Uptake and Mode of Action of Bacterial Exotoxins

However, structural organization and composition of the functional subunits of AB-Type toxins can vary. In the case of single-chain AB-type toxins both the A-domain and B-domain are located on a single polypeptide chain. Examples of single-chain AB-type toxins are for instance the diphtheria toxin produced by *Corynebacterium (C.) diphtheriae*, toxin A and toxin B as the large toxins of *Clostridium (C.) difficile* and the clostridial neurotoxins from *Clostridium (C.) botulinum* (botulinum neurotoxins) and *Clostridium (C.) tetani* (tetanus neurotoxin) (Collier, 1975; Goonetilleke & Harris, 2004; Pruitt & Lacy, 2012).

In the case of binary AB-type toxins the A- and B-subunits are localized on two separate proteins. These two functional domains are called components and are individually secreted by the respective bacteria. Cytotoxic effects of the binary AB-type toxins are based on the association of both components into a complex. Only assembled complexes elicit cytotoxicity. Within this group of AB-type toxins, the number of B-subunits can vary and allows further classification. For AB_7-toxins an active B-component consists of seven functional B-subunits organized as a heptamer. This group includes the anthrax toxin from *Bacillus (B.) anthracis* as well as the clostridial toxins CDT from *C. difficile*, C2 toxin from *C. botulinum* and iota toxin from *Clostridium (C.) perfringens*. Notably, all clostridial toxins listed here contain an ADP-ribosylating activity within their respective A-component (Barth, Preiss, et al., 1998; Gülke et al., 2001; Sakurai et al., 2003; Tsuge et al., 2003). Binary AB-type toxins with a pentameric B-component are called AB_5-toxins. These toxins are also called holotoxins since they are released by the bacteria as associated protein complex. This group of binary AB-Type toxins is represented for instance by the cholera toxin of *Vibrio (V.) cholerae*, shiga toxin *of Shigella (S.) dysenteriae,* pertussis toxin of *Bordatella (B.) pertussis* and Shiga toxinogenic *Escherichia (E.) coli* (STEC), heat labile (HL) enterotoxins of enterotoxigenic *E. coli* (ETEC) (Beddoe et al., 2010).

In addition to the classification of AB-type toxins based on their structural organization, they can also be categorized via their different routes of uptake. In general, after specific B-component mediated receptor binding the toxin complex is taken up into the cells via receptor mediated endocytosis. Based on the intracellular route taken afterwards, either “short-trip” or “long-trip” toxins can be categorized (do Vale et al., 2017; Lingwood, 2021; Sandvig et al., 2004). As depicted in Figure 1, “short-trip” toxins are delivered into the cytosol via a pore formed by the B-component. Acidification of the endosomal lumen by the vacuolar H^+-ATPases (vATPase) triggers a conformational change of the B-component which then

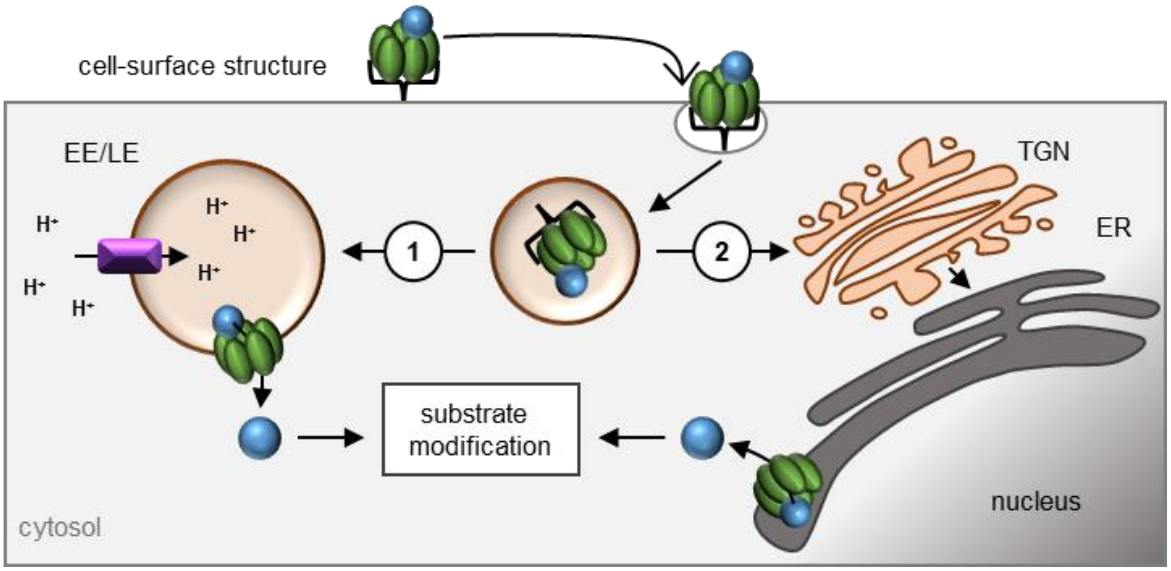


Figure 1:Scheme of the cellular uptake and intracellular trafficking of AB-type protein toxins.
Using an “exemplary” binary toxin the possible routes of uptake and trafficking within a cell are visualized. Following binding of the toxin to its cell surface structure via the B-component (green), receptor mediated endocytosis takes place. From these endosomal vesicles two routes are possible. The A-component (blue) of (1) “short-trip” toxins translocates directly from early (EE) or late (LE) endosomes into the cytosol upon acidification of the compartment. In the case of (2) “long-trip” toxins the protein complex is trafficked via retrograde transport through the *trans*-Golgi network (TGN) to the endoplasmic reticulum (ER). Here, translocation into the cytosol occurs. (Derived from Barth & Stiles, 2010)

integrates into the endosomal membrane enabling translocation of the A-component into the cytosol. Prominent examples for “short- trip” toxins translocating from the early endosome are the binary C2 toxin (Barth et al., 2000) or the single-chain diphtheria toxin (DT) (Sandvig & Olsnes, 1980). The anthrax toxin predominantly shows translocation of its A-components from late endosomes also following endosomal acidification (Abrami et al., 2004). Toxins within the group of “long-trip” toxins such as the pertussis toxin travel farther and undergo retrograde vesicular transport via the *trans*-Golgi network to the endoplasmic reticulum (ER). They translocate across the ER membrane into the cytosol (Plaut & Carbonetti, 2008).

As mentioned above, these sophisticated toxins not only hijack cellular surface structures as receptors for cell binding but also utilize the intracellular vesicle trafficking of the target cells. In addition, most AB-type toxins also rely on other cellular mechanisms after they have reached their first destination - the endosome. For some toxins it is described that host cell chaperones and folding helper enzymes are crucial for the membrane translocation of A-components into the cytosol (for review see Barth, 2011; Ernst, Schnell, et al., 2016). First, the A-component requires partial unfolding to allow translocation through the narrow pore formed by the B-component (Falnes et al., 1994; Falnes & Olsnes, 1995; Haug, Wilde, et al., 2003). This slight conformational change and unfolding of the A-component requires refolding into an active conformation after translocation. Host cell factors involved are for instance chaperones like the heat shock protein 90 (Hsp90) or protein folding enzymes like Cyclophilin A (CypA) (Dmochewitz et al., 2011; Ernst et al., 2015; Haug et al., 2004; Haug, Leemhuis, et al., 2003; Kaiser et al., 2009). Also described are helpers like Cyp40 (Barth et al., 2015; Ernst et al., 2015; Lang et al., 2014) or FK506 binding protein FKBP51 (Kaiser et al., 2012). Furthermore, some toxins like the DT toxin which present an interchain disulfide bond rely on the cytosolic intracellular reductive potential. This potential mediates the release of the A-domain after translocation (Schnell et al., 2016).

After refolding into the active conformation, the AB-type toxins A-components exhibit a variety of different enzymatic activities targeting different yet specific substrate. One large group of AB-type toxins exerts an ADP-ribosyl transferase activity. The textbook example here would be the C2 toxin. The A-component of the C2 toxin C2I transfers an ADP-ribose moiety onto globular actin (Aktories et al., 1986) thereby disrupting the integrity of the actin-cytoskeleton (Aktories et al., 1989). Other examples of ADP-rybosylating toxins are for instance the DT toxin (Collier & Cole, 1969), the cholera toxin (Sánchez & Holmgren, 2008) or the pertussis toxin (Kaslow & Burns, 1992). However, although some of these toxins share the same enzymatic activity they vary in structure, mode of uptake and substrate specificity causing a highly specific cellular effect inducing clinical symptoms and thereby the respective disease.

1.2. Bacterial Toxins as Molecular Tools and Therapeutics – From Basic Research to Scientific and Medical Applications

Even though AB-type toxins show a wide range of structures, mode of uptake and substrate-specificity, their highly sophisticated mechanism regarding cell entry unifies them with respect to their action as virulence factor. The cytotoxic effects manifest in severe human and animal diseases as described above. A lot of research therefore is directed towards unraveling molecular structures in detail and the identification of toxin-substrates to better understand the pathogenicity. Based on this basic research one major focus of the field is directed towards the identification of suitable target-structures for toxin inhibitors. Such targets for instance could be cellular systems necessary for toxin uptake mediating the translocation of the enzymatically active A-domain. The small-molecule gold compound auranofin was found to prevent the translocation of for instance the A-domain of the DT toxin from the acidified endosome into the cytosol. It blocks the cellular thioredoxin reductase (TrxR) necessary for reduction of the disulfide linking the A- to the B-domain (Papini, Rappuoli, et al., 1993). Therefore, the A-domain cannot reach its target in the cytosol and cells were protected from the cytotoxic effects of DT (Schnell et al., 2016). Other small molecules such as Ebselen, myricetin, curcumin, and PX12 that also target the TrxR–Trx system, were recently described to prevent intoxication with clostridial neurotoxins *in vitro* and *in vivo* (Zanetti et al., 2021). These toxins also rely on the TrxR–Trx system to specifically reduce the inter-chain disulfide-bond linking the A- and B-domain to release the catalytically active A-Domain into the cytosol (Kistner & Habermann, 1992; Pirazzini et al., 2014; Zanetti et al., 2015).

The inhibitor bafilomycin A1 (BafA1) on the other hand blocks vATPases and therefore proton uptake into the endosomes, no acidification takes place (Bowman & Bowman, 1986; Werner et al., 1984). Toxins dependent on acidic conditions to translocate into the cytosol such as the C2 toxin can no longer exit the endosome (Barth et al., 2000). Inhibitors like the antibiotic radicicol targeting host cell factors such as Hsp90 and are effective in protecting cells from the cytotoxic effects of toxins like C2 or DT (Haug, Leemhuis, et al., 2003; Schuster et al., 2017).

These examples emphasize the opportunity provided by targeting a central cellular system exploited for cytotoxicity, to inhibit completely different toxins. Such

molecules could serve a parent substance for the development of new therapeutics against toxins.

Another crucial field of research is the development of different approaches to exploit AB-type toxins in a clinical context.

Firstly, the use of native AB-type toxins to selectively modulate cellular functions using the example of botulinum neurotoxins (BoNT). BoNTs are only one type of neurotoxins produced by certain Gram-positive, spore-forming, obligate anaerobic bacteria in the genus *Clostridium (C.)*. Aside from BoNTs, that are mainly secreted by C. botulinum, *C. tetani* is known to secret tetanus neurotoxin (TeNT) (Hatheway, 1990). BoNT as well as TeNT enter motoneurons at neuromuscular junctions (NMJs) after receptor binding. Following receptor mediated endocytosis and acidification of the endosome the A-domain of the toxins is released into the cytosol. Here, the toxins A-domains exert their protease activity and cleave a specific set of proteins (SNARE (soluble N-ethylmaleimide-sensitive factor attachment protein receptor)) that are responsible for neurotransmitter release from nerve terminals. Hence, the neuronal signal-transduction is significantly disturbed (Dong et al., 2019; Rummel, 2016). Both toxins are highly potent and represent the causative agents to the two distinct and severely life-threatening diseases botulism and tetanus in humans, respectively. Tetanus as a results of Intoxication with TeNT typically presents symptoms ranging from trismus, dysphagia, stiffness and reflex spasms during early incubation (Alfery & Rauscher, 1979). If left untreated, these symptoms escalate into spasms and tonic contractions resulting ultimately in respiratory failure and even spinal fractures (Bohrer, 1965; Bunch et al., 2002). Botulism on the other hand is caused by intoxication with BoNTs. The clinical symptoms are caused by flaccid paralysis of the entire body. Early effects of BoNT on the cranial nerve cause impaired vision, difficulty to speak and facial paralysis. A subsequent descending paralysis then result in respiratory arrest (Shapiro et al., 1998).

Notably, both toxins are some of the most toxic substances known to mankind with a LD_{50} in humans for TeNT estimated at 2.5 ng per Kg bodyweight and only 1 ng per Kg bodyweight estimated for BoNT/A (BoNT serotype A) (Gill, 1982), which not only makes them extremely dangerous but also a highly interesting drug-candidate in medicine (for review see Ting & Freiman, 2004). In 1973, BoNT/A was first described as alternative treatment for strabismus, which was usually treated

surgically (Scott & Rosenbaum, 1973). In 1978 this approach was approved by the FDA for testing in humans and in 1989 for clinical use (Klein, 1996). Nowadays also blepharospasm and other conditions of hyperactive extraocular muscles are treated with BoNT/A (Schantz & Johnson, 1997). Aside from the use in ophthalmology, other indication for the use of BoNT/A are involuntary muscle contractions, hemifacial spasms and hyperhydrosis. Today, BoNT/A and BoNT/B are also used in neurology for the treatment of dystonias, tremors, vocal disorders, cerebral palsy in children, tension and migraine headaches, etc. (Binder et al., 2001; Klein & Glogau, 2000; Verheyden et al., 2001). It was also described in a case study that BoNT/A was effective in the treatment of peripheral neuropathic pain (Buonocore et al., 2017). However, the most common use of BoNT/A today is in cosmesis. The toxin is applied locally to reduce glabellar frown lines and wrinkles (Carruthers & Carruthers, 1992; FDA, 2016).

Secondly, the specificity and efficiency of AB-type toxins led to an easily comprehensible idea: manipulate the toxin to generate new approaches to control, rather than cause a disease. Early on, this approach was tested using the DT toxin. In 1960 the LD_{50} for DT after intramuscular injection into human was estimated at approximately 100 ng per kg body weight. Later reports stated that only one molecule of DTA is sufficient to introduce cell death (Gill, 1982; Yamaizumi et al., 1978). After entering the cytosol of target cells DTA ADP-ribosylates the eucaryotic elongation factor 2 (EF-2), thereby inactivating it. Consequently chain elongation during protein translation arrests irreversibly, ultimately resulting in apoptosis and cell death (Collier & Cole, 1969). These properties prompted the field of research to utilize and modify DT for a potential clinical application in cancer treatment. Around 1980 it was already shown that substitution of the receptor binding domain of DT with the α-melanocyte stimulating hormone (α-MSH) sequence results in selective binding to and cytotoxicity for α-MSH receptor-positive malignant human melanoma cells (Murphy et al., 1986). In the following years one prominent example, which was approved by the FDA for the treatment of cutaneous T-cell lymphoma was developed. Here, Interleukin-2 (IL-2) was substituted with the receptor binding domain of DT. This modification resulted in a binding as well as intoxication selective for cells expressing the high-affinity variant of the IL-2 receptor IL-2R such as leukemia and lymphoma cells (Foss, 2000). The chimera was originally created in 1978 as DAB-$_{486}$-IL-2 and later introduced to the market slightly modified as

DAB-$_{389}$-IL-2 under the trade name denileukin diftitox or ONTAK™ in 1999 (FDA, 2008; Williams et al., 1987). Although the drug was able to improve the quality of life for cancer patients significantly, in 2008 the FDA issued a black box warning for ONTAK™ due severe and fatal side effects such as serious infusion reactions, impaired vision and capillary leak syndrome. As a result, the drug was discontinued (FDA, 2008; Lansigan et al., 2010).

Taken together, DT-derivates as well as BoNTs are examples were a toxin-based treatment approach with a modified cell-selectivity was successful and the respective drugs are or were in clinical use. Taking this approach one step further is the exploitation of AB-type toxins (or parts of the toxins) as delivery tools for non-native, foreign cargo. For this purpose, both single-chain and binary toxins have been shown to be able to transport the catalytic domain of one toxin via the transport mechanism of another. However, no clinical application is described so far.

DT as example for a single-chain toxin was fused to the *C. botulinum* C3 toxin. Usually, the C3 toxin is specific for monocytes and macrophages and ADP-ribosylates Rho GTPases when introduced into the cytosol. Thereby, C3 toxin inhibits the Rho-mediated signal transduction. Fusion to DT was now able to provide binding to other cell types which present the DT toxin receptor (Aktories & Frevert, 1987; Boquet et al., 1995). The same approach was applied to binary toxins such as the C2 toxin. For example, the *C. limosum* C3 toxin was fused to the 225 amino acid long N-terminal fragment of the C2 toxins A-component C2I (C2IN). C2IN mediates binding of C2I to the C2 toxins B-component C2IIa. The fusion-protein C2IN-C3 was able to ADP-ribosylate Rho in cells usually sensitive to C2 but not to C3. This C3 cytotoxicity however was only found for cells incubated with the fusion protein C2IN-C3 in combination with C2IIa as transporter, emphasizing the dependency of the delivery of C2IN-C3 on C2IIa (Barth, Hofmann, et al., 1998).

These studies illustrated very convincingly that such toxins are versatile in their use as delivery tool for non-native cargo. The next question now was weather also non-toxin derived foreign cargo could be introduced into cells following the same toxin-mediated route of uptake. Here a system using clostridial toxins like C2 and C3 coupled to streptavidin as a platform was very interesting in particular. On the one hand the transport component C2IIa was used in its native form as transporter but the cargo-proteins were comprised of two different components. One, a fusion-

protein of C2IN and streptavidin and two, a biotinylated cargo. The linkage between biotin-streptavidin is one of the strongest non-covalent interactions known. Streptavidin acts as adapter protein attaching the biotinylated molecules which enables subsequent internalization via C2IIa into the cytosol. Molecules transported with this system are for instance tracer molecules such as biocytin-Alexa 488, biotinylated antitumoral peptide P39 and a biotinylated tumor suppressor P53 (Fahrer et al., 2010, 2011, 2013; Krüger et al., 2016). On the other hand, an enzymatically inactive variant of C3 toxin was coupled to streptavidin via a thioether linkage. Combining this bioconjugate with biotinylated fluorescein as well as biotinylated RNaseA resulted in successful delivery of this cargo into macrophages (Lillich et al., 2012).

One toxin used intensively as a molecular transporter is the *Bacillus (B.) anthracis* anthrax toxin. Its protective antigen PA_{63} is used for many years for the delivery of non-native as well as non-toxin derived cargo. Since PA_{63} is subject of this thesis, its mode of uptake and central role in the delivery of cargo will be explained in more detail in the following chapters 1.2.1. and 1.2.2.

1.2.1. Anthrax Toxin

The binary AB-type anthrax toxin is produced by the Gram-positive, spore-forming bacterium *B. anthracis*. Together with a poly-D glutamic acid capsule the three-component AB_7-toxin represents the main causative agent for the disease anthrax (Bhatnagar & Batra, 2001). *B. anthracis* spores enter a mammalian host via cutaneous, gastrointestinal, or inhalational routes and germinate to produce vegetative bacteria (Rabideau & Pentelute, 2016). Dependent on the route of entry anthrax can manifest in different ways. Cutaneous anthrax is associated with edema and necrosis resulting in the formation of black eschars which are historically associated with the disease. Gastrointestinal and inhalational forms of anthrax manifest in generic flu-like symptoms that can lead to sepsis and shock-like vascular collapse. If the bacteria enter the bloodstream and release anthrax toxin, the disease progresses into lethality (Moayeri et al., 2015).

Anthrax toxin consists of three components forming two different toxins. The protective antigen (PA) as the common receptor binding B-component forms the so-called lethal toxin (LT) together with the lethal factor (LF) or the edema toxin (ET)

together with the edema factor (EF) as A-components, respectively (Friebe et al., 2016).

The structure and functionality of PA is defined by its 4 domains (Figure 2). Domain 1 represents the N-terminal part of PA. It harbors the protease-activation side and mediates binding of the A-components LF and EF. Upon proteolytic activation (cleavage of residues 1–167, domain 1a) and heptamerization/octamerization (Kintzer et al., 2009; J. C. Milne et al., 1994) domain 1b is available for binding of LF and EF (Chauhan & Bhatnagar, 2002; Cunningham et al., 2002). Interaction

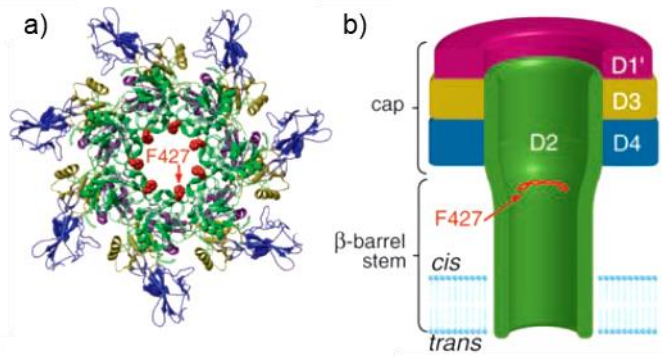


Figure 2: Structural model of PA.
(a) Axial view of the prepore as ribbons rendering. (b) Hypothetical cross section of the pore. Domain 2 forms the channel spanning the membrane as a 14-stranded β-barrel forming. The different domains are colored as follows: D1 in magenta, D2 in green, D3 in yellow and D4 in blue. (Modified from Krantz et al., 2005, reprinted with permission from AAAS).

between the prepore and LF/EF is mediated by an amphipathic cleft termed the α-clamp which also seems to be involved in the unfolding process (Brown et al., 2011). Domain 2 mediates oligomerization and mediates receptor binding but is mainly responsible for membrane insertion via the formation of the PA pore. D2 forms a β-barrel involving amino acids 275–352. Following rearrangement of the heptamer after membrane insertion, the inserted β-barrel extends beyond the bilayer. Residues 337, 342, and 346 were identified to be relevant for binding of the prepore to the cellular receptors (Cao et al., 2009; Lacy et al., 2004; Mourez et al., 2003; Nassi et al., 2002; Petosa et al., 1997; Santelli et al., 2004; Sellman et al., 2001; Singh et al., 2001; Wu et al., 2012). Domain 3 seems to be play a principal role in stabilizing the heptamer (Mogridge et al., 2001; Mourez et al., 2003). Domain 4 represents the C-terminal part of the protein and is crucial for receptor binding. Mutagenesis studies regarding residues 679–693 showed that four residues substituted with alanine decreased toxicity more than 10-fold. Interestingly, residue D683 was shown to be critical based on its interaction with the divalent metal ion in the receptor (Brossier et al., 1999; Rosovitz et al., 2003; Singh et al., 1991; Varughese et al., 1999).

Cell entry (Figure 3) of LT and ET is mediated by the toxins B-component PA. The full-length PA_{83} (83 kDa) binds to two different cell surface receptors, tumor endothelial marker 8 (TEM8 or ANTXR1) or capillary morphogenesis gene 2 (CMG2 or ANTXR2) (Bradley et al., 2001; Scobie et al., 2003). Both receptors are involved in the regulation of angiogenic processes and are expressed on most human cells. TEM8 however shows a higher binding affinity as CMG2 (Abi-Habib et al., 2005; Deuquet et al., 2012; Nanda et al., 2004; Reeves et al., 2010; van der Goot & Young, 2009). The receptor-side essential for PA-binding is a metal ion–dependent adhesion site (MIDAS) within a von Willebrand domain, that is typical for integrins (Bradley et al., 2003; Liu et al., 2007; Rosovitz et al., 2003). After binding PA_{83} is

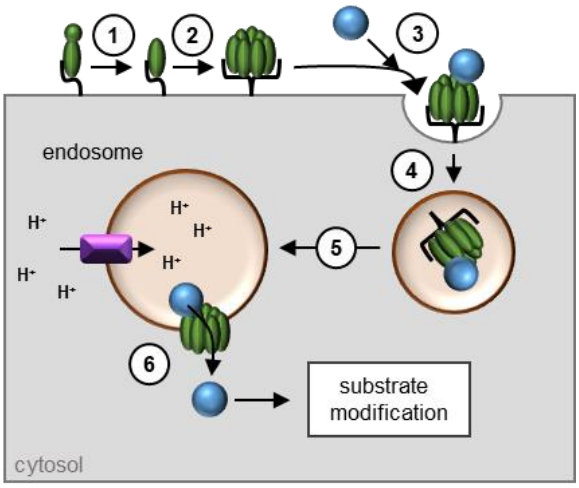


Figure 3: Scheme representing the cytosolic delivery of LF/EF via the central transport protein PA.
Cytosolic delivery of LF/EF is mediated by PA after (1) binding of PA_{83} to the anthrax receptors followed by (2) proteolytic activation to PA_{63} which then self-assembles into the PA prepore as a heptamer/octamer. After (3) LF/EF binding the entire complex enters the cell via (4) receptor mediated endocytosis. (5) Acidification of the endosome now triggers a conformational change and pore-formation enabling (6) translocation of LF/EF into the cytosol where they perform their respective substrate modification. (Derived from Rabideau & Pentelute, 2016)

cleaved by cell surface proteases such as furin (Klimpel et al., 1992) into PA_{63} and PA_{20} (20 kDa) allowing the formation of oligomers (Abrami, Liu, Cosson, Leppla, & Van Der Goot, 2003; Shihui Liu & Leppla, 2003). Rapid movement of the receptor-toxin complex to lipid rafts upon the formation of heptamers/octamers results in clathrin-dependent endocytosis induced by src-like kinase activation. Actin was also identified to play role in heptamerization of TEM8-bound PA_{63} but not CMG2-bound PA_{63} and seems to be relevant for endocytosis (Abrami et al., 2004; Abrami, Bischofberger, et al., 2010; Abrami, Kunz, et al., 2010; Abrami, Liu, Cosson, Leppla, & Van der Goot, 2003; Kintzer et al., 2009). Acidification of these endosomal compartments via vATPase activity triggers a PA prepore-to-pore conversion which leads to the formation of a SDS- and heat-stable pore structure (Shihui Liu & Leppla, 2003; Miller et al., 1999; Jill C. Milne & Collier, 1993). Interestingly, pore formation and subsequent translocation for receptor-bound toxin occurs at different pH

thresholds (TEM8 = pH 6.0-6.5, CMG2 pH=5.2) suggesting different endosomal routes of entry. Pore formation for PA bound to TEM8 is predicted in EE but for PA bound to CMG2 in LE. This is probably due to a higher affinity of CMG2 to PA which requires a more dramatic condition for CMG2 to release PA (Rainey et al., 2005). The translocation of LF and EF into the cytosol now takes place through a syringe-like structure (stem) of the PA pore from late endosomes and is driven by a proton gradient. It was described that translocation of LF preferably occurs from Rab7-associated late endosomal compartments (Abrami et al., 2004; Feld et al., 2012; Krantz et al., 2006).

In more detail, the translocation is initiated by the amino terminus of LF/EF bound to the PA oligomer. Although the amino-termini of LF and EF are different in sequence they contain a high number of charged residues (net-charge zero). Under acidic conditions the negatively charged residues are protonated resulting in a positively net-charged amino-terminus. This positive charge mediates docking of the amino-terminus to the negatively charged, cation-selective PA pore. Additionally, the acidic environment within the endosomes destabilizes the tertiary structure of LF and EF resulting in unfolding of LF and EF to molten globules which allows the proteins to pass the lumen of the PA pore (Figure 2). The translocation of LF and EF is unidirectional following the proton gradient across the endosomal membrane (Brownian ratchet model). The luminal phenylalanine (F427) residues in domain 2 of each PA monomer converge within the lumen, resulting in solvent-exposed aromatic rings. This ‘‘Phe-clamp’’ structure mediates translocation of the A-component by interacting with hydrophobic sequences presented. The PA pore now actively chaperones LF and EF during diffusion via the Phe-clamp as hydrophobic narrow constriction into the cytosol of the target cell. (Krantz et al., 2005, 2006; Zhang et al., 2004)

Alternative to the traditional translocation into the cytosol from endosomes it was described that LF and maybe even EF translocate into the lumen of endosomal intraluminal vesicles. Here LF can persist for days and even be transmitted to daughter cells during cell division before it is released into the cytosol upon vesicle-fusion. Such vesicles can also be delivered to the extracellular medium as exosomes that enable delivery of LF or EF into the cytosol of cells completely independent from the classical trafficking pathway via anthrax toxin receptors. In

both cases, the anthrax toxins are able to circumvent degradation processes mediated by the host (Abrami et al., 2004, 2013).

Even though LF and EF enter the cytosol of target cells the same way, they exert different catalytic activities. LF (90 kDa) is a zinc-dependent metalloprotease that cleaves the amino-terminal region of Mitogen-activated protein kinase kinases (MEKs) thereby disrupting the mitogen-activated protein kinase (MAPK) signaling pathway (Duesbery et al., 1998; Klimpel et al., 1994; Vitale et al., 1998, 2000). EF (93 kDa) on the other hand is a calmodulin-dependent adenylate cyclase. After translocation and refolding EF utilizes cytosolic calmodulin to generate cAMP at the late endosome membrane and perinuclear location. It converts ATP into cAMP and thereby increases the intracellular cAMP levels. (Dal Molin et al., 2006; Leppla, 1982, 1984)

Once they have reached the cytosol of their target cells LT and ET both contribute to the pathogenesis of anthrax. During the early stages of infection ET causes edema and both toxins disable the innate immune response to enable the replication as well as dissemination of the bacterium to the regional lymph nodes and blood stream. During the later and systemic stages LT targets cardiomyocytes and smooth muscle cells whereas ET targets the liver to induce lethality (for review see Moayeri et al., 2015).

1.2.2. PA_{63} as a Molecular Transporter

Due to their significance as virulence factors and the substantial threat regarding the use of anthrax as a bioterrorism weapon (Lane et al., 2001) anthrax toxins have been heavily investigated over the years. The respective fundamental research regarding the understanding of molecular functions and activities and the insides gained led to the use of anthrax toxins as a molecular carrier as already described above for other toxins like C3, C2 or DT. In the early years chimeras of LF were constructed to elucidate the translocation process as well as the potential of LT to mediate the transport of non-native or foreign cargo and the structural requirements for such delivery. One early example is the fusion of the ADP-ribosylation domain of Pseudomonas exotoxin A to either the full-length LF (Arora et al., 1992) or truncated versions of LF. The latter was used to determine the minimum region required for PA binding and the amino-terminal residues 1-254 (LF_N) were identified (Arora & Leppla, 1993). Shortly after, these results were used to generate chimeras

of DTA fused either the amino- or the carboxy-terminus of LF_N. Additionally, the ribosome-inactivating A1 subunit of the shiga toxin was fused to the carboxy-terminus of LF_N. All chimeras were highly toxic when applied in combination with PA_{63} as transporter, indicating that translocation does not necessarily require a free amino-terminus of LF and that LF_N fusion proteins from divers bacterial sources can be introduced into the cytosol of target cells dependent on PA_{63} (Arora & Leppla, 1994; Leppla et al., 1999; J C Milne et al., 1995). Also, LF_N fused to DTA with an artificial disulfide was blocked in its translocation demonstrating nicely the relevance of unfolding for this step of cell entry of cargo proteins (Wesche et al., 1998). A similar approach was used to study the uptake of the LT into different immune cells where LF_N was fused with beta-lactamase (Hu & Leppla, 2009).

PA/LF_N-delivery was also used to elucidate the biological functions of other protein-cargos such as the cytotoxic T lymphocyte epitope of *Listeria monocytogenes* listeriolysin O (LLO) that was introduced regarding its immune response activity (Ballard et al., 1996). Further examples for LF_N-cargos are antibody mimics such as a tandem monobody to Bcr-Abl or an affibody binder that targets hRaf-1 (Liao et al., 2014). Even small molecule drugs like doxorubicin and monomethyl auristatin F have been successfully delivered fused to LF_N via PA_{63}. However, docetaxel and other cyclic peptides did not translocate, most likely due to size and structural rigidity (Rabideau et al., 2015). For a more detailed list of LF_N-linked cargos see also Hirschenberger et al., 2021; Rabideau & Pentelute, 2016.

Taken together, for a long list of highly variably cargo the PA/LF_N-system was successful in translocation and delivery. However, taking into consideration that LF_N as the native binding-partner provides the optimal linker based on its molecular structure it is not surprising that cargos able to unfold and refold under acidic conditions can be introduced into cells with this system. Most interestingly, in 1996 Blanke et al. reported that even a short polycationic tail of lysine, arginine or histidine residues fused to the amino terminus of DTA enables translocation into the cytosol of Chinese hamster ovary (CHO) cells via PA_{63}. It was proposed that the minimal function of LF_N, which is to bind PA_{63} under neutral conditions and allow release under acidic conditions, might also be provided by such short tags. Even though the affinity of the tested peptides was lower compared to LF_N, they provided other advantages like high hydration due to their strong charge as well as the lack of

secondary structures. The latter abolishes the need for folding of the tag for its own functionality and reduces the risk of unwanted interference of the fused cargos´ folding (Blanke et al., 1996). 20 years later this concept was picked up by Neumeyer et al. who showed that fusing a His_6-tag (sequence of six histidine residues) to the amino-terminus of EF increases its affinity to PA_{63} in Lipid Bilayer Experiments (Neumeyer et al., 2006). In 2012 Beitzinger et al. was able to show that also other toxin components such as C2I of C2 as well as the epidermal cell differentiation inhibitor (EDIN) of *Staphylococcus aureus* are delivered into the cytosol of cells via PA_{63} (Beitzinger et al., 2012). The same results were obtained using the ADP-ribosyltransferase domain of TccC3 (His-TccC3hvr) of *Photorhabdus (P.) luminescens* (Lang et al., 2014).

The general theory behind this interaction between His-tagged proteins and PA_{63} is that two structures mediating LF/EF binding and translocation are involved. On the one hand, the α-clamp, an amphipathic cleft at the top of the PA_{63} prepore binds polycationic tails and the Phe-clamp mediates translocation based on rings of negatively charged amino acids lining the lumen of the pore and pull the positively charged tags inwards (Brown et al., 2011; Feld et al., 2012). The benefits listed above regarding His-tags instead of LF_N-tags are obvious in terms of effects of the tag upon the fused cargo. Additionally, if one keeps in mind that nowadays the standard for protein purification in research labs is an immobilized metal affinity chromatography His-tags as linkers seem attractive. His-tagged proteins are isolated from a lysate based on a His-tag cloned to the target protein, expressed from already available expression vectors. Hence, if the transport of toxin-based His-fused cargo is that efficient, is the system transferrable to non-toxin cargo? To this end, the establishment of such cargo is subject of this thesis. The model cargo used is the tumor suppressor protein NME1 which will be explained in more detail in the following chapter 1.2.3.

1.2.3. NDPK-A as Model Cargo for PA-mediated Transport into the Cytosol of Cancer Cells

In 1988 Steeg et al. described the first metastasis suppressor, the human gene *nm23-H1* or *nme1* encoding for the A isoform of the enzyme nucleoside diphosphate kinase (NDPK-A or NME1) (Biggs et al., 1990; Steeg et al., 1988). It was originally described as non-metastatic 23 gene found in mouse carcinoma cells, homologous

to the drosophila *awd* (altered wing disk) protein (Heimann et al., 1998; Steeg et al., 1988). In humans, the *nme* family consists of 10 genes, *NME1–9 and RP2* encoding for multifunctional proteins (Boissan et al., 2009; Desvignes et al., 2009). Regarding metastasis the proteins encoded by *NME1* and *NME2* have been studied in more detail. It could be shown that expression levels of NDPK-A correlate with migratory capabilities of tumor cells. Overexpression of NDPK-A in metastatic tumor cells resulted in reduced metastasis *in vivo* but did not affect the primary tumor size (Salerno et al., 2003). Re-expressing of NDPK-A on the other hand was able to reduce migration of different tumor cells as shown in wound healing assays and Boyden chamber experiments, suggesting a pivotal role of NDPK-A in the regulation of tumor cell motility (Horak et al., 2007; Kantor et al., 1993; Marino et al., 2013). Up

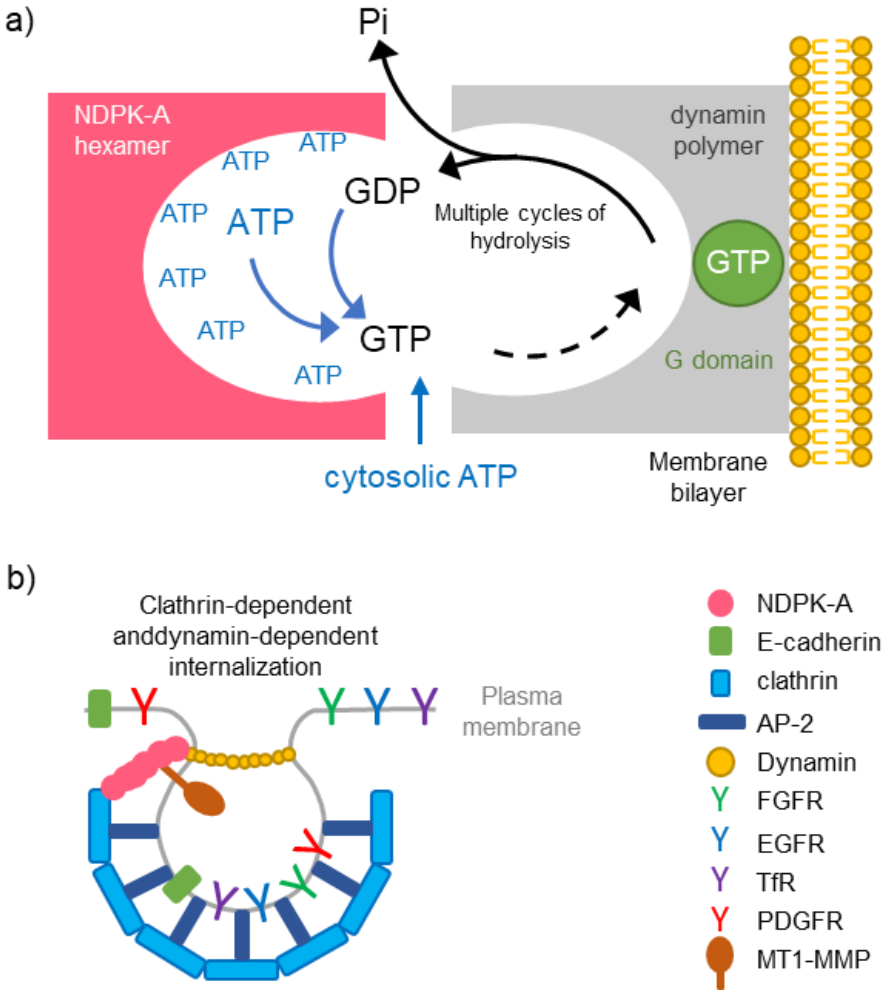


Figure 4: NDPK-A and its multiple functions during endocytosis.
(a) NDPK-A provides GTP for dynamin at clathrin-coated pits during endocytosis.
(b) NDPK-A regulates dynamin-mediated endocytosis. It facilitates clathrin-dependent and dynamin-dependent internalization of E-cadherin, fibroblast growth factor (FGFR), epidermal growth factor receptor (EGFR), transferrin receptor (TfR), and platelet-derived growth factor receptor (PDGFR) as well as endocytic clearance of membrane type1-matrix metalloproteinase (MT1-MMP). (Derived from Boissan et al., 2018; Lodillinsky et al., 2021)

until recently the underlying mechanisms have not been fully understood. A schematic overview over the current model regarding the activity of NDPK-A during endocytosis and its interaction with different cytosolic molecules is given in Figure 4. Data presented by Kahn et al. now suggests a role of NDPK-A in dynamin 2 oligomerization and endocytosis. Overexpression of NDPK/A in breast cancer cells increased the endocytosis of transferrin and EGF receptors simultaneous with a suppression of motility and migration. Inhibition of dynamin however abolished this effect of NDPK-A. It is suggested that an interaction of dynamin and NDPK-A promotes dynamin oligomerization and therefore contributes to the underlying mechanism responsible for the inhibitory effect of NDPK-A on metastasis (Khan et al., 2019). A recent study now clearly demonstrated that increasing NDPK-A expression could prevent or at least interfere with the tissue-invasive behavior of aggressive breast cancers due its modulation of membrane type1-matrix metalloproteinase MT1-MMP (Castro-Castro et al., 2016; Lodillinsky et al., 2021). MT1-MMP is involved in the process of switching from *in situ* carcinoma to invasive cancer (Boissan et al., 2018). These invasive tumor cells now travel through the circulation until they exit and colonize a secondary organ. It was demonstrated that NDPK-A interacts with MT1-MMP and dynamin in clathrin-coated pits. Overexpression of NDPK-A in breast cancer cell lines resulted in increased internalization of MT1-MMP, thereby reducing the surface levels of MT1-MMP. If expression levels of NDPK-A are low (as during the invasive switch), MT1-MMP increases invasion and collagenolysis. These data suggest that NDPK-A negatively regulates MT1-MMP activity and therapies directed towards the increase of NDPK-A levels could be effective in the treatment of aggressive breast cancer (Lodillinsky et al., 2021). However, there is still a black box of unknown factors and regulators of metastasis that has yet to opened.

1.3. Aim of the Thesis

PA_{63} and its capability to mediate transport of a large variety of different cargo molecules into the cytosol of mammalian target cells is one of the best understood systems for intracellular delivery based on a non-toxic component of bacterial AB-type toxins. As already extensively investigated and proven successful for LF_N-fused cargo, also His-tagged cargo proteins can be introduced into target cells via PA. Comparing the two established linkers LF_N and poly-histidine, the latter presents itself highly attractive since potential negative effects on fused cargo are minimal due to its short sequence. Standard-use of His-tagged expression of recombinant proteins generates a large number of potential cargos already available for use. However, delivery of His-tagged cargo via PA_{63} was only shown for toxin-derived molecules so far.

Hence, the major aim of this thesis was to establish the PA63-mediated delivery of recombinant human tumor metastasis suppressor protein His-NDPK-A into the cytosol of human breast cancer cells.

To this aim, the target cell line MDA-MB-231 must be characterized in detail regarding its susceptibility to PA63-based transport using His-DTA as reference cargo. Thereafter, the PA63-mediated transport of His-NDPK-A into MDA-MB-231 cells will be investigated regarding intracellular localization of His-NDPK-A and its potential effect on the cells migratory and metastatic potential.

The vision of this project is to establish this modular system as a starting point for the development of novel pharmacological options for a certain population of patients suffering from cancer types with low expression levels of NDPK-A but high metastasis rates.

2. Materials and Methods

2.1. Materials

2.1.1. Chemicals

Description	Manufacturer
6-biotin-17- NAD (biotin-NAD$^+$), 250 µM	Trevigen, Gaithersburg, MD, USA
Acetic acid glacial	VWR International GmbH, Darmstadt
Acrylamide (Rotiophorese® Gel 30)	Carl Roth GmbH & Co. KG, Karlsruhe
Adenosine diphosphate (ADP)	Sigma-Aldrich Chemie GmbH, Steinheim
Adenosine triphosphate (ATP)	Sigma-Aldrich Chemie GmbH, Steinheim
Ammonium persulfate (APS)	Carl Roth GmbH & Co. KG, Karlsruhe
Ampicillin sodium salt	SERVA Electrophoresis GmbH, Heidelberg
Bacto™ Trypton	Becton, Dickinson and Company, Franklin Lakes, NJ, USA
Bafilomycin A1 (BafA1)	ChemCruz, Santa Cruz Biotechnology, Heidelberg
Bovine serum albumin, fraction V (BSA)	Carl Roth GmbH & Co. KG, Karlsruhe
Bromphenol blue sodium salt	Sigma-Aldrich Chemie GmbH, Steinheim
cOmplete™ Protease Inhibitor Cocktails, EDTA-free	Roche Diagnostics GmbH, Mannheim
Coomassie Brilliant Blue G250	SERVA Electrophoresis GmbH, Heidelberg
Coomassie Brilliant Blue R250	SERVA Electrophoresis GmbH, Heidelberg
Dimethyl sulfoxide (DMSO)	AppliChem GmbH, Darmstadt

Disodium hydrogen phosphate dihydrate (Na_2HPO_4 x 2 H_2O)	AppliChem GmbH, Darmstadt
Dithiothreitol (DTT)	Merck KGaA, Darmstadt
DMEM (1x)+GlutaMAX^{TM}-1	GIBCO® life technologies, Karlsruhe
Ethanol, HPLC grade (EtOH)	Sigma-Aldrich Chemie GmbH, Steinheim
Ethanol denatured (EtOH denat.)	VWR Chemicals, Darmstadt
Ethylenediaminetetraacetic acid disodium salt (EDTA)	Carl Roth GmbH & Co. KG, Karlsruhe
Fetal calve serum (FCS)	GIBCO® life technologies, Karlsruhe
Glacial acetic acid	VWR Chemicals, Darmstadt
Glycerol	Carl Roth GmbH & Co. KG, Karlsruhe
Glycine	AppliChem GmbH, Darmstadt
Guanosine diphosphate (GDP)	Sigma-Aldrich Chemie GmbH, Steinheim
Guanosine triphosphate (GTP)	Sigma-Aldrich Chemie GmbH, Steinheim
Hydrochloric acid (HCl)	Sigma-Aldrich Chemie GmbH, Steinheim
Hydrogen peroxide (H_2O_2)	J.T. Baker, Griesheim
Imidazole	Carl Roth GmbH & Co. KG, Karlsruhe
Isopropanol (2-Propanol)	VWR Chemicals, Darmstadt
Isopropyl-β-D-1-thiogalactopyranoside (IPTG)	AppliChem GmbH, Darmstadt
L-Glutamine	Biochrom AG, Berlin
Luminol	AppliChem GmbH, Darmstadt
Magnesium chloride ($MgCl_2$)	Carl Roth GmbH & Co. KG, Karlsruhe
Magnesium sulfate ($MgSO_4$)	Carl Roth GmbH & Co. KG, Karlsruhe
Methanol, HPLC grade (MetOH)	Sigma-Aldrich Chemie GmbH, Steinheim
Methanol technical grade (MetOH)	VWR Chemicals, Darmstadt

Minimum Essential Medium (MEM)	GIBCO® life technologies, Karlsruhe
Non-essential amino acids (NEAA)	GIBCO® life technologies, Karlsruhe
Ortho-Phosphoric acid (H_3PO_4), 85 %	Carl Roth GmbH & Co. KG, Karlsruhe
p-Coumaric acid	Sigma-Aldrich Chemie GmbH, Steinheim
Phenylmethylsulfonyl fluoride (PMSF)	Fluka Chemie GmbH, Buchs, Switzerland
Ponceau S	AppliChem GmbH, Darmstadt
Potassium chloride (KCl)	Carl Roth GmbH & Co. KG, Karlsruhe
Potassium hydrogen phosphate (KH_2PO_4)	Carl Roth GmbH & Co. KG, Karlsruhe
Skim milk powder	Carl Roth GmbH & Co. KG, Karlsruhe
Sodium chloride (NaCl)	Carl Roth GmbH & Co. KG, Karlsruhe
Sodium dodecyl sulfate (SDS)	Carl Roth GmbH & Co. KG, Karlsruhe
Sodium hydroxide (NaOH)	Merck KGaA, Darmstadt
Sodium pyruvate 100 mM (100x)	GIBCO® life technologies, Karlsruhe
Staurosporine	Sigma-Aldrich Chemie GmbH, Steinheim
Streptavidin-peroxidase (strep-POD)	Roche Diagnostics GmbH, Mannheim
Tris	AppliChem GmbH, Darmstadt
Triton® X-100	Sigma-Aldrich Chemie GmbH, Steinheim
Trypsin	Roche Diagnostics GmbH, Mannheim
Trypsin-inhibitor	Roche Diagnostics GmbH, Mannheim
Tween® 20	Sigma-Aldrich Chemie GmbH, Steinheim
Yeast extract Servabacter® powder	SERVA Electrophoresis GmbH, Heidelberg

2.1.2. Ready-to-use Solutions, Enzymes and Kits

Description	Manufacturer
Amersham Low Molecular Weight Calibration Kit for SDS Electrophoresis “Unstained Protein Ladder”	Cytiva, Marlborough, MA, USA
CellTiter 96® AQ_{ueous} One Solution Reagent, MTS solution for cell viability assay	Promega GmbH, Mannheim
Hoechst33342	Thermo Fisher Scientific Inc., Waltham, MA, USA
Immobilon™ Western Chemiluminescent HRP Substrate	Millipore Corporation, Billerica, MA, USA
Kinase-Glo® Luminescent Kinase Assay	Promega GmbH, Mannheim
Lysozyme	Thermo Fisher Scientific Inc., Waltham, MA, USA
SuperSignal™ Western Blot Enhancer	Thermo Fisher Scientific Inc., Waltham, MA, USA
SuperSignal™ West Femto Maximum Sensitivity Substrate	Thermo Fisher Scientific Inc., Waltham, MA, USA
Ni-NTA-Agarose Beads	Qiagen N.V., Venlo, Netherlands
NucelBond™ Plasmid Preparatin Kit	Macherey-Nagel GmbH & Co.KG, Düren
PageRuler™ Prestained Protein Ladder, 10-180 kDa	Thermo Fisher Scientific Inc., Waltham, MA, USA
Penicillin-Streptomycin-Glutamine	Thermo Fisher Scientific Inc., Waltham, MA, USA
PureCube 100 INDIGO Ni-Agarose	Cube Biotech GmbH, Monheim
ROTI®Block blocking solution	Carl Roth GmbH & Co. KG, Karlsruhe
RTU 60 Developer	Adefo-Chemie GmbH, Neu-Isenburg
RTU 60 Fixer	Adefo-Chemie GmbH, Neu-Isenburg

Trypsin-EDTA solution	Sigma-Aldrich Chemie GmbH, Steinheim

2.1.3. Consumables

Description	**Manufacturer**
µ-slide 8 Well, Ibitreat	Ibidi GmbH, Martinsried
Blotting Paper MN 827 B	Macherey-Nagel GmbH & Co.KG, Düren
Cell scraper 25 cm, 2-position blade	Sarstedt AG & Co. KG, Nümbrecht
CryoPure Tube 1.8 mL white	Sarstedt AG & Co. KG, Nümbrecht
Culture-Inserts 2 Well for self-insertion	Ibidi GmbH, Martinsried
Cuvette 10x4x45 Polystyrol	Sarstedt AG & Co. KG, Nümbrecht
Filtopur S 0.2	Sarstedt AG & Co. KG, Nümbrecht
Filtopur S 0.45	Sarstedt AG & Co. KG, Nümbrecht
Medical X-ray film CX-BL+ (13 x 18 cm, 18 x 24 cm)	AGFA Health Care N.V., Mortsel
Microtiter plates (6-, 12- and 96-well), cell culture dishes	TPP®Techno Plastic Products AG, Trasadingen
Microplate, 96 well, PS, half area, white CELLSTAR®, sterile	Greiner Bio-One GmbH, Frickenhausen
Nitrocellulose Blotting Membrane Amersham™ Protran™ 4.45 µm NC	Cytiva, Marlborough, MA, USA
Parafilm M®	Bemis Company Inc. Neenah, WI, USA
Pasteur glass pipettes	Brand GmbH & Co. KG., Wertheim
PD-10 Desalting Columns, Sephadex G-25	GE Healthcare Europe GmbH, Freiburg
Pipette tips	Sarstedt AG & Co. KG, Nümbrecht
Protino Ni-NTA Columns, 1mL	Macherey-Nagel GmbH & Co.KG, Düren

Reaction tubes (1.5, 2.0 mL)	Sarstedt AG & Co. KG, Nümbrecht
Serological pipettes (5/10/25 mL)	Sarstedt AG & Co. KG, Nümbrecht
Sterican® sterile needles, 26G x 1, size 18	B. Braun, Melsungen
Sterile syringe BD Plastipak™	BD GmbH, Heidelberg
Tissue culture dish 100 (d = 10 cm)	TPP®Techno Plastic Products AG, Trasadingen, Switzerland
Tissue Culture Flasks T25, T25	TPP®Techno Plastic Products AG, Trasadingen, Switzerland
Tissue culture testplates (10/24/96 well)	TPP®Techno Plastic Products AG, Trasadingen, Switzerland
Tube 15 mL 120x17 mm, PP	Sarstedt AG & Co. KG, Nümbrecht
Tube 50 mL 114x28 mm, PP	Sarstedt AG & Co. KG, Nümbrecht
Vivaspin® 20, MWCO 5 kDa, 10 kDa, 30 kDa	Sartorius AG, Göttingen

2.1.4. Devices

Description	**Manufacturer**
ÄKTA Explorer FPLC system	GE Healthcare Life Sciences, Sweden
Centrifuge 5415 D	Eppendorf AG, Hamburg
Centrifuge 5417 R	Eppendorf AG, Hamburg
Centrifuge 5810 R	Eppendorf AG, Hamburg
Centrifuge Avanti J-26S XP	Beckman Coulter™ GmbH, Brea
Centrifuge JS-HS	Beckman Coulter™ GmbH, Brea
Centrifuge Megafuge 1.0	Heraeus Holding GmbH, Hanau
EL 340 Microplate Reader	Bio Tek Instruments GmbH, Bad Friedrichshall
Electrophoresis power supply – EPS 601	Amersham Bioscience GmbH, Freiburg

Glass plate 20 x 10 cm	PEQLAB Biotechnologie GmbH, Erlangen
Glass plate 20 x 10 cm, notched	PEQLAB Biotechnologie GmbH, Erlangen
iMIC digital microscope	FEI, München
Incubation shaker CERTOMAT® BS-1	Sartorius AG, Göttingen
Incubator HERAcell 240i CO_2	Thermo Fisher Scientific, Waltham
Magnetic stirrer IKA® RET basic C	IKA®-Werke GmbH & Co. KG, Staufen
Microcentrifuge Rotilab®	Carl Roth GmbH, Karlsruhe
Micro scales	Sartorius AG, Göttingen
Microscope Axiovert 40 CFL	Carl Zeiss AG, Oberkochen
Microscope-camera ProgRes™ C10 *plus*	Jenoptik, Jena
Multichannel pipette/Transferpipette®-8 (50 – 200 µL)	Brand GmbH & Co. KG, Wertheim
Multimode Microplate Reader TriStar² LB 942	Berthold Technologies GmbH & Co. KG, Bad Wildbad
NanoDrop One©, UV-Vis Spectrophotometer	Thermo Fisher Scientific Inc., Waltham, MA, USA
Overhead shaker Reax 2	Heidolph Instruments GmbH & Co. KG, Schwabach
PerfectBlue™ Double Gel System Twin ExW S	PEQLAB Biotechnologie GmbH, Erlangen
PerfectBlue™ Semi-Dry Electro blotter	PEQLAB Biotechnologie GmbH, Erlangen
pH-meter ino Lab pH 720	WTW GmbH, Weilheim
Pipetboy	INTEGRA Bioscience GmbH, Fernwald
Pipette Reference® (0.5 – 10 µL)	Eppendorf AG, Hamburg

Pipette Research® Plus (0.1 – 2.5 µL, 2 – 20 µL, 20 – 200 µL, 100 – 1000 µL)	Eppendorf AG, Hamburg
Pipettes Pipetman® (2 – 20 µL, 20 – 100 µL, 50 – 100 µL, 200 – 1000 µL)	Gilson Inc., Middelton, WI, USA
Platform shaker Duomax 1030	Heidolph Instruments GmbH & Co. KG., Schwabach
Platform shaker Unimax 2010	Heidolph Instruments GmbH & Co. KG., Schwabach
Safety cabinet HERAsafe	Heraeus Holding GmbH, Hanau
Safety cabinet LaminAir® HA 2448	Heraeus Holding GmbH, Hanau
Sonifier® B-12	Branson, Dietzenbach
Spectrophotometer DU® 640	Beckman Coulter™ GmbH, Brea
Superdex 75 PC 3.2/30, SEC column	Pharmacia Swedeb
Thermomixer comfort	Eppendorf AG, Hamburg
Thermomixer compact	Eppendorf AG, Hamburg
Tube shaker Reax top	Heidolph Instruments GmbH & Co. KG., Schwabach
Vertical electrophoresis system	GE Healthcare Life Sciences, Sweden
Water batch AQUAline AL 18	Lauda Dr. R. Wobser GmbH & Co. KG., Lauda-Königshofen

2.1.5. Buffers and Solutions

All buffers were prepared in Milli-Q® water.

General buffer	
10 x PBS (pH 6.8)	1.37 M NaCl, 27 mM KCl, 80 mM Na_2HPO_4, 18 mM KH_2PO_4
1 x PBS (pH 7.4)	10 x PBS diluted to pH 7.4
PBS-T	1 x PBS supplemented with 0.1 % Tween® 20

Bradford Assay	
Bradford reagent	10 mg Coomassie Brilliant Blue G250, 5 mL EtOH, 10 mL H_3PO_4 (85 %), 100 mL H_2O; stored at 4 °C, light protected

Protein expression	
10 x LB-medium	100 g tryptone, 50 g yeast extract, 100g NaCl, ad. 1 L H_2O; Stored at 4 °C; for use: autoclaved, diluted with H_2O for 1 x, supplemented with antibiotic if applicable
LB-ager	1 L LB-medium, 7.5 g agar; autoclaved, supplemented with antibiotic and plated
1000 x Amp. solution	0.1 g/mL Amp. In H_2O

Protein purification of His-NDPK-A All buffers were filtered for sterility, 0.45 µm.	
Lysis buffer (pH 8)	50 mM NaH_2PO_4, 300 mM NaCl, 10 mM imidazole, 1 M EDTA, 5 % (w/v) glycerol
Equilibration- / washing buffer (pH 8)	50 mM NaH_2PO_4, 300 mM NaCl, 20 mM imidazole, 1 mM EDTA, 5 & (w/v) glycerol
Elution buffer (pH 8)	50 mM NaH_2PO_4, 300 mM NaCl, 250 mM imidazole, 1 mM EDTA
Storage buffer (pH 7.5)	20 mM Tris-HCl, 1 mM DTT, 10 % (w/v) glycerol

Protein purification of His-DTA	
All buffers were filtered for sterility, 0.45 µm.	
Lysis buffer (pH 8)	50 mM NaH_2PO_4, 300 mM NaCl, 10 mM imidazole
Equilibration- / washing buffer (pH 8)	50 mM NaH_2PO_4, 300 mM NaCl, 20 mM imidazole
Elution buffer (pH 8)	50 mM NaH_2PO_4, 300 mM NaCl, 250 mM imidazole
Storage buffer (pH 7.4)	1 x PBS

Purification and preparation of PA_{63}	
All buffers were filtered for sterility, 0.45 µm.	
Lysis buffer	20 mM Tris-HCl (pH 8), 300 mM NaCl, 10 mM imidazole, 0.5 mM EDTA, 10 % (w/v) glycerol Added immediately before use: 1 mM DTT, 1 x cOmplete
Equilibration- / washing buffer	20 mM Tris-HCl (pH 8), 500 mM NaCl, 20 mM imidazole, 5 % (w/v) glycerol, 0.05 % Tween® 20
Elution buffer	20 mM Tris-HCl (pH 8), 500 mM NaCl, 500 mM imidazole, 5 % (w/v) glycerol, 0.05 % Tween® 20
SEC buffer / Storage buffer	20 mM Tris-HCl (pH 8), 100 mM NaCl, 5 % (w/v) glycerol, 0.05 % Tween® 20

SDS-PGE and Western blot analysis

Composition for 10 x 20 cm gels

Resolving gel buffer (RGB)	1.5 M Tris-HCl pH 8.8
Resolving gel composition (12.5 % gels)	8 mL MilliQ H_2O, 6.2 mL RGB, 273 µL 10 % (w/v) SDS solution, 10.4 mL acrylamide solution, 248 µL 10 % (w/v) APS, 25 µL TEMED
Stacking gel buffer (SGB)	0.5 M Tris-HCl, pH 6.8
Stacking gel composition (6 % gels)	8 mL MilliQ H_2O, 3.8 mL SGB, 150 µL 10 % (w/v) SDS solution, 3 mL acrylamide solution, 150 µL 10 % (w/v) APS, 17 µL TEMED

Composition for 13 x 18 cm gels (AP)

Resolving gel buffer (RGB)	1.5 M Tris-HCl pH, 8.8
Resolving gel composition (12.5 % gels)	20.9 mL MilliQ H_2O, 16.5 mL RGB, 726 µL 10 % (w/v) SDS solution, 27.5 mL acrylamide solution, 660 µL 10 % (w/v) APS, 44 µL TEMED
Stacking gel buffer (SGB)	0.5 M Tris-HCl, pH 8.8
Stacking gel composition (6 % gels)	13.35 mL MilliQ H_2O, 6.25 mL SGB, 250 µL 10 % (w/v) SDS solution, 5 mL acrylamide solution, 250 µL 10 % (w/v) APS, 25 µL TEMED

Buffers and Solutions

10 x Tris-glycine buffer	272 mM Tris base, 1.92 M glycine
SDS-running buffer	1 x Tris-glycine buffer, 0.1 % SDS (w/v)
Towbin blotting buffer	10 % 10 x Tris-glycine buffer, 20 % MetOH tech., 70 % H_2O
5 x Laemmli Sample buffer	0.31 M Tris-HCl 1 M (pH 6.8 for standard WB, pH 8.8 for AP), 10 % SDS (w/v), 37.5 % glycerol, 0.25 mg/mL bromphenol blue, 100 mM DTT or 500 mM DTT for AP; dilution with MilliQ H_2O for 2.5 x
Ponceau S solution	0.2 % Ponceau S (w/v), 5 % acetic acid
Blocking solution	5 % (w/v) skim milk powder in 1 x PBS-T

Blocking solution Roti®-Block	Roti®-Block diluted 1:10 with MilliQ
ECL solution A	4.4 mL H_2O, 500 µL 1 M Tris-HCl (pH 9.0), 50 µL 250 mM luminol (in DMSO), 22 µL 90 mM coumaric acid (in DMSO); stored at 4 °C, light protected
ECL solution B	4.5 mL H_2O, 500 µL 1 M Tris-HCl (pH 9.0), 50 µL 30 % H_2O_2; stored at 4 °C, light protected
Coomassie staining solution	2.5 g Coomassie Brilliant Blue R250, 450 mL MetOH tech., 450 mL H_2O, 100 mL acetic acid
Coomassie destaining solution	450 mL MetOH tech., 450 mL H_2O, 100 mL acetic acid
Strip buffer A	0.2 M glycine, 0.5 M NaCL (pH 2.0)
Strip buffer B	0.5 M Tris (pH 11)

Enzyme activity of His-NDPK-A	
Kinase Assay (KA)	
Assay buffer (pH 7.5) (filtered for sterility, 0.45 µm)	50 mM Tris-HCl (pH 8), 2 mM $MgCl_2$, 0.01 % BSA (w/w); immediately before use: 1 mM DTT
Nucleotides	ADP: 50 mg/mL ATP: 50 mg/mL GDP: 100 mg/mL (prepared fresh, no storage possible) GTP: 10 mg/mL (maximal storage: 3-6 month); all nucleotides were dissolved in MilliQ and stored at -20 °C
Autophosphorylation Assay (AP)	
Assay buffer (APB)	50 mM Tris-HCl (pH 8),150 mM NaCl

Sequential ADP-ribosylation	
Sequential ADP-ribosylation buffer (ARB)	20 mM Tris-HCl (pH 7.5), 1 mM EDTA, 1 mM DTT, 5 mM $MgCl_2$; immediately before use: cOmplete protease inhibitor (1:50)

2.1.6. Antibodies and Binding Proteins

Primary

Antigen	**Species**	**Dilution**	**Manufacturer**
Poly histidine, His-tag (HIS.H8)	Mouse	1:1000 (WB), 1:500 (IF)	Invitrogen, Carlsbad, CA, USA
Poly histidine, His-tag (AD1.1.10)	Mouse	1:100 (IF)	SantaCruz Biotechnology, Dallas, TX, USA
Hsp90 α/β (F-8)	Mouse	1:1.000 (WB)	SantaCruz Biotechnology, Dallas, TX, USA
GAPDH (G-9)	Mouse	1:1.000 (WB)	SantaCruz Biotechnology, Dallas, TX, USA
Nm23-H1 (C-8)	Mouse	1:200 (WB)	SantaCruz Biotechnology, Dallas, TX, USA)
N1-Phosphohistidine (1-pHis) (SC1)	Rabbit	1:1.000 (AP)	Millipore Corporation, Billerica, MA, USA
Filamentous actin, Phalloidin-FITC conjugate	-	1:100 (IF)	Sigma-Aldrich Chemie GmbH, Steinheim

Secondary

Antigen	Species	Dilution	Manufacturer
Mouse IgG kappa binding protein (m-IgGκ BP) HRP-conjugate	-	1:2.500 (WB)	SantaCruz Biotechnology, Dallas, TX, USA)
Rabbit IgG, HRP-conjugate	Goat	1:25.000 (AP) 1:40.000 (AP in lysate)	Bio-Rad Laboratories, Inc., Hercules, CA, USA
Rabbit IgG, HRP-conjugate	Goat	1:2.500 (WB)	SantaCruz Biotechnology, Dallas, TX, USA)
Streptavidin, HRP-conjugate	-	1:2.500 (WB)	Roche Diagnostics GmbH, Mannheim
Mouse IgG, Alexa Fluor™ 488 conjugate	Goat	1:750 (IF)	Invitrogen, Carlsbad, CA, USA
Mouse IgG, Alexa Fluor™ 568 conjugate	Goat	1:500 (IF)	Invitrogen, Carlsbad, CA, USA

2.1.7. Mammalian Cell Lines

Type	Species	Tissue	Cell type	Supplier
HeLa	*Homo sapiens*, human	cervix	epithelial	DSMZ, Braunschweig (ATCC: CCL-2)
MDA-MB-231	*Homo sapiens*, human	breast; mammary gland	epithelial	Cell Biolabs, San Diego, CA, USA (HTB-26)

2.1.8. *Escherichia coli* Strains

Strain	Application	Description
DH5α	Plasmid amplification	Recombination deficient (*recA9*, endonuclease I deficient (*endA1*)
BL21 DE3	Protein expression	Protease deficient (*ompT*)
Rosetta	Protein expression	Protease deficient (*lon*, *ompT*), *lacYZ* deleted

2.1.9. Toxins and Plasmids

Toxin	Production organism and plasmid	Source
Diphtheria toxin (DT), 58 kDa	Corynebacterium diphtheriae	Merck KGaA, Darmstadt
His-DTA, 23 kDa	*E. coli* BL21 (DE3), pET-15b	Created by R. John Collier, Harvard Medical School, Boston, MA, USA
PA_{83}, 83 kDa	*E. coli* Rosetta, pET22b	Created and provided by R. John Collier, Harvard Medical School, Boston, MA, USA
NDPK-A, 18 kDa	*E. coli* BL21 (DE3), pD444-NH	Created by P. Attwood, Perth, Australia, provided by T. Wieland, Mannheim, Heidelberg

2.1.10. Software

Software	Source
Microsoft® Office 2016	Microsoft Corporation, Redmond, W, USA
ImageJ 1.52c	National Institute of Health, Bethesda, MD, USA
GraphPad Prism 9.3.0.463	GraphPad Software Inc., La Jolla, CA, USA
Live Acquisition 2.6	FEI, München
AxioVision Rel. 4.7	Carl Zeiss AG, Göttingen

2.2. Methods

2.2.1. Culture of Mammalian Cell Lines

2.2.1.1. Cultivation of HeLa and MDA-MB-231 cells

Towards the goal of a continuous cultivation of immortalized cell lines, regular maintenance measures must be performed. The cells have to be supplied with fresh nutrients on a regular basis and the cell number has to be controlled. Therefore, the cells were subjected to media exchanges and splitting of the cultures. Passaging was performed 20 – 30 times or until undesired properties emerged. All solutions used during the performance of these maintenance steps were prewarmed to 37 °C. To prevent the culture from contamination, media and buffers were sterile filtered (0.45 µm), antibiotics were added to the media and all steps were performed under sterile conditions under a laminar flow cabinet.

HeLa and MDA-MB-231 cells were cultivated in a CO_2 incubator (37 °C, 5 % CO_2, saturated humidity) in 10 cm petri dishes in 10 mL of corresponding serum-containing medium up to 70 - 95 % of confluency. As soon as the cells reached this degree of confluency, they were splitted. Usually splitting was necessary three times a week.

HeLa cells were splitted in a ratio of cell suspension to total volume of 1:3 or 1:4 for two days of intermediate culture and 1:10 for three days of intermediate culture. Therefore, the old medium was removed, the cells were washed with 10 mL PBS and detached with 1 mL trypsin-EDTA solution in the incubator for 5-10 min. (or until detachment was visible). If necessary, the cells were fully detached mechanically by lightly tapping the petri dish on the work top. Afterwards, 9 mL of medium was added (minimum essential medium (MEM) supplemented with 10 % heat-inactivated FCS, 2 mM L-glutamine, 1 mM sodium pyruvate, 0.1 mM NEAA and 1 x penicillin/streptomycin). The cells were resuspended and singularized by carefully pipetting up and down. The cell suspension was now transferred to a new petri dish using the volume corresponding to the respective splitting ratio and fresh medium was added (ad. 10 mL). The petri dish was placed in the incubator as intermediate culture.

MDA-MB-231 cells were maintained and splitted in a similar fashion. However, for MDA-MB-231 cells Dulbecco´s modified eagles medium (DMEM) supplemented

with 10 % heat-inactivated FCS, 2 mM L-glutamine, 1 mM sodium pyruvate, 0.1 mM NEAA and 1 x penicillin/streptomycin was used. The cells were cultured in T75 tissue culture flasks in 15 mL total volume for intermediate cultures. The cells were splitted in a ratio of cell suspension to total volume of 1:4 or 1:5 for two days of intermediate culture and 1:12 or 1:15 for three days of intermediate culture. MDA-MB-231 cells are more sensitive to mechanical and physical manipulation and had to be treated more carefully. Prewarming of all solutions was obligatory, detachment was performed at room temperature for only 2-5 min. and resuspension was performed only very carefully.

2.2.1.2. Freezing and Thawing of cells

HeLa and MDA-MB-231 cells were stored long-term in liquid nitrogen. For the preparation of fresh storage vials, several plates of nearly confluently grown cells of the same cell lines were brought into suspension. Preferred were intermediate cultures with a passage number < 5. After determining the total cell number, the cells were pelleted by centrifugation at 500 rcf for 5 min. The supernatant was replaced with warm PBS (equal volume to previous supernatant) and the cells were resuspended. After pelleting as described above, the PBS was replaced with freezing medium (cultivation medium supplemented with 10 % FCS and 10 % DMSO) for a final cell count of 1 x 10^6 cells/mL (HeLa) or 2 x 10^6 cells/mL (MDA-MB-231), respectively. After resuspending, 1 mL of cell suspension was immediately transferred into CryoPure tubes which were placed into the Mr.Frosty Cryo 1 °C Freezing Container for two days at -80 °C at least. Afterwards, the vials were placed in the liquid nitrogen tank for long-term storage.

For thawing of the cells one cryovial of the respective cell line was placed into a 37 °C water bath. As soon as the solution was melted the cells were transferred into a 15 mL tube already prepared with 10 mL warm culture medium. The cells were carefully resuspended, pelleted as described above and the supernatant was replaced with 10 mL fresh, warm culture medium to remove the DMSO. After resuspension the solution was transferred into a petri dish and placed into the incubator over night. The following day the medium was exchanged.

Thawing of MDA-MB-231 cells was performed similarly. However, the cells were resuspended in 5 mL of the respective culture medium ant transferred into a T25

tissue culture flask. The following day the cells were transferred into a T75 tissue culture flask and first splitting was performed at day three after thawing.

2.2.1.3. Seeding of cells

HeLa and MDA-MB-231 cells were seeded into respective multi-well plates to be used in various experiments (Table 1). Therefore, a cell suspension with a defined cell number/mL was prepared in serum-containing medium as described in 2.2.1.1 and the respective volume was transferred into each well of the plates (Table 1). The cells were seeded one day in advance. The cell number was chosen regarding the desired confluency for the experiment and can therefore vary.

Table 1: Volume per well of multi-well plates

Multi-well plate	**Volume/well [mL]**
2 well	0.07
8 well	0.3
12 well	1
24 well	0.5
96 well	0.1

2.2.2. Preparation of MDA-MB-231 Cell Lysate

MDA-MB-231 cells were grown to a degree of confluence of approximately 90% in a 10 cm culture dish as described above with a total volume of 10 mL and washed once with 10 mL warm PBS. The PBS was aspirated from the cells, the dish was frozen and after thawing on ice 240 µL of APB supplemented with 1x cOmplete™ and 1 mM PMSF were added. The cells were detached from the dish via scraping and the cell suspension was homogenized by pipetting up and down before transfer of the suspension into a 1.5 ml tube. The cells were further lyzed with a needle (26 G) by pipetting up and down. Cell debris was removed by pelleting for 1 min. at 4 °C, max. rcf. and the supernatant was transferred into a new tube. The cleared lysate was aliquoted and stored at – 20 °C for further use.

2.2.3. Bradford Assay

The Bradford assay was used to determine the concentration of proteins after protein purification (Bradford, 1976). Therefore, the protein solution was diluted with MilliQ H_2O to a total volume of 800 µL in a cuvette and 200 µL of Braford reagent were added. The samples were incubated at RT for 5 min. before the absorbance at 595 nm was measured in a spectrophotometer. For quantification of the protein concentration, the results were correlated with a BSA standard (1 µg/mL to 15 µg/mL BSA) curve.

2.2.4. Expression and Purification of Proteins

2.2.4.1. Recombinant Tumor Metastasis Suppressor Protein His-NDPK-A

Heat shock transformation of competent *E. coli*

For the expression of recombinant His-NDPK-A the expression plasmid (kindly provided by T. Wieland, Mannheim) was transformed into chemically competent DH5α *E. coli* via heat shock transformation.

Therefore, a vial with 50 µL of cells (stored at – 80 °C, provided by AG Barth) was thawed for 5-10 min. on ice. Afterwards, 20-40 ng of plasmid were added to the cells which were further incubated for 20-30 min. on ice before a heat shock transformation was performed. Here, the cells were incubated for 90 sec. at 42 °C, followed by 120 sec. on ice. All following steps were performed under sterile conditions. First, 450 µL LB-medium without antibiotic were added to the cells which was followed by an incubation for 30-60 min. at 37 °C and 180 rpm. A fraction of 100 µL of the cell suspension was then plated on prewarmed LB-agar plates with ampicillin. The plates were then incubated over night at 37 °C or until colonies were present. The following plasmid preparation was performed following the manufacturer´s instructions using the ready-to-use NucleoBond™ midi prep kit from Macherey-Nagel GmbH & Co.KG (Düren). DNA elution was performed with MilliQ H_2O and the final solution was stored at -20 °C. DNA concentration was measured with the NanoDrop One©, UV-Vis Spectrophotometer, MilliQ H_2O was used as blank.

For long-term storage of the transformed cells, glycerol stocks of DH5α_ pD444-NH_His_6-nm23-H1 were prepared. The saturated bacterial suspension was mixed

in a ratio of 1:1 with 85 % glycerol and the final solution was aliquoted in 1.5 mL tubes with 1 mL each. Stocks were stored at -80 °C.

Expression in BL21 *E. coli*

A preculture was prepared using one vial of transformed competent cells. The vial of cells was thawn and added to 175 mL prewarm (37 °C) LB-medium supplemented with 100 µg/mL ampicillin (LB_{amp}) in a 500 mL Erlenmeyer flask. The culture was incubated over night at 37 °C, 180 rpm. The following day 40 mL of preculture were used to inoculate 1 L LB_{amp} main culture in a 2 L Erlenmeyer flask. The cells were incubated at 37 °C, 180 rpm until an optical density (OD_{600}) of 0.6 – 0.8 was reached. At this point the expression was induced with IPTG (final concentration of 500 µM). Expression was performed for 3 h at 37 °C, 180 rpm followed by harvesting. The cells were harvested and pelleted via centrifugation of the complete culture at 6.000 rcf for 15 min. at 4 °C. The supernatant was discarded, and the pellet was stored at -20 °C until further processed.

Protein purification

For purification of His-NDPK-A the cell pellet was thawn and resuspended in 10 mL lysis buffer per liter main culture on ice. Cell lysis was performed via pipetting up and down, a subsequent incubation with 1 mg/ml lysozyme for 30 min. on ice and 10 cycles of sonification (40% intensity, 30 s per burst, halted for 30 s on ice). The generated cell lysate was cleared via centrifugation at 10,000 rcf for 30 min. at 4 °C, filtered (0.45 and 0.2 µm) and subsequently subjected to immobilized metal affinity chromatography (IMAC) using a Ni^{2+}-NTA resin.

IMAC allows purification of His-tagged proteins based on the high affinity of the immobilized Ni^{2+} and the His-tag of the protein. With this method the target His-tagged protein can be isolated very efficiently.

Fast protein liquid chromatography (FPLC) was performed using the ÄKTA™ explorer FPLC system from GE Healthcare Life Sciences, Sweden. The system as well as the installed column were prepared via equilibration with 10-15 column volumes (CV, 1 mL) equilibration- / washing buffer at a flow rate of 1 mL/min. (as for all the following steps as well). After the sample was loaded, the system was washed with 10 CV equilibration- / washing buffer. Elution was performed via a 5 CV gradient to 100 % elution buffer and was followed by another 20 CV of flushing with elution

buffer to retrieve as much protein as possible. The elution was collected in fractions of 0.5 mL, analyzed via SDS-PAGE and kept on ice until further processed.

Buffer exchange and protein storage

The elution buffer was exchanged to a physiological storage buffer via diafiltration using the Vivaspin® 20 centrifugal concentrators with a molecular weight cut-off (MWCO) of 5 kDa. Therefore, the eluate was pooled, sterile filtered (0.2 µM) and transferred into the concentrator. The protein solution was concentrated via centrifugation to 15-20 % of the starting volume and re-diluted with storge buffer to 20 mL. This step was repeated 4 times, the final product was stored on ice and the protein concentration was determined via SDS-PAGE and Bradford assay. Finally, the protein solution was concentrated via ultrafiltration in the same Vivaspin® concentrators used before to a final concentration of approximately 1 mg/mL. The protein concentration was again determined via SDS-PAGE and Bradford assay, before the protein was aliquoted and subjected to shock-freezing in liquid nitrogen before storage at -80 °C.

2.2.4.2. Recombinant Catalytic Domain of DT - His-DTA

Expression and purification of His-DTA were performed by Dr. S. Carle or M. Fellermann (AG Barth). The process is described in short.

Expression in BL21 *E. coli*

In contrast to the expression of His-NDPK-A, for the expression of His-DTA competent BL21 *E. coli* were freshly transformed via heat shock transformation (see His-NDPK-A) and plated. The plates were incubated over night at 37 °C or until colonies were present. One colony was used to inoculate 5 mL of prewarm (37 °C) LB_{amp} in a culture tube. The culture was incubated for ~5 h at 37 °C, 180 rpm. That evening the 5 mL culture is transferred into 100 mL of LB_{amp}, incubated over night (37 °C, 180 rpm) and used the following day to inoculate the main culture (see above). At an OD_{600} of 0.6 – 0.8 the expression was induced with IPTG (final concentration of 250 µM). Expression was performed for 4-5 h at 37 °C, 180 rpm followed by harvesting and pelleting. The pellet was resuspended in 10 mL lysis buffer per L main culture and stored at -20 °C until further processed.

Protein purification

Cell lysis was performed via pipetting up and down on ice and 10 cycles of sonification (50% intensity, 30 s per burst, halted for 30 s on ice). The lysate was cleared and filtered and subjected to immobilized metal affinity chromatography (IMAC) using a Ni^{2+}-NTA resin.

FPLC was performed as described for His-NDPK-A with the respective buffers for His-DTA. Also, elution was performed via a 10-20 CV gradient to 100 % elution buffer. The elution fractions were analyzed via SDS-PAGE and kept on ice until further processinf.

Buffer exchange and protein storage

Buffer exchange was performed as described above, however a concentrator with a MWCO of 10 kDa was used. The step of dilution after concentration during diafiltration was performed twice. Protein concentration was determined again with SDS-PAGE and Bradford assay before the protein was aliquoted and subjected to shock-freezing in liquid nitrogen before storage at -80 °C.

2.2.4.3. Recombinant Protective Antigen – PA

The described expression-protocol (Ost et al., 2019) for His-PA_{83} was adjusted and optimized towards maximum yield and purity. The procedure is explained in the following chapters.

For the expression of His-PA_{83} the plasmid (11.5 ng) was transformed into Rosetta *E. coli*, followed by plating and subsequent inoculation of 5 mL prewarmed LB_{amp} with one colony. This culture was again incubated for ~ 5 h and transferred into 200 mL of prewarmed LB_{amp}. After over-night incubation at 37 °C, 180 rpm, 40 mL of preculture were used to inoculate 1 L LB_{amp} main culture in a 2 L Erlenmeyer flask. The culture was incubated at 37 °C, 180 rpm and induced for expression at an optical density (OD_{600}) of 0.6 – 0.8 with IPTG (final concentration of 500 µM). The culture was now shifted to 16 °C, 180 rpm and expression was performed over night. Harvest and pelleting were performed as described for His-NDPK-A and the pellet was immediately processed.

Protein purification

For purification the pellet was resuspended in 10 mL lysis buffer per liter main culture on ice. Cell lysis was performed via pipetting up and down and 10 cycles of sonification (80% intensity, 20 s per burst, halted for 30 s on ice). The generated cell lysate was cleared via centrifugation at 15,000 rcf for 45 min. at 4 °C, filtered (0.45 and 0.2 µm) and subsequently subjected to IMAC using a Ni^{2+}-NTA resin.

Fast protein liquid chromatography (FPLC) was performed as described for His-NDPK-A. In short, equilibration with 10-15 CV equilibration- / washing buffer, sample-loading, washing with 10 CV equilibration- / washing buffer and elution via a 5 CV gradient to 100 % elution buffer, followed by 20 CV elution buffer. The collected elution fractions of 0.5 mL were analyzed via SDS-PAGE and stored on ice until further processed.

Buffer exchange and Size exclusion chromatography (SEC)

The elution buffer was exchanged to a physiological storage buffer via PD-10 Desalting Columns (Sephadex G-25) according to the manufacturer´s instructions.

The SDS-PAGE performed after the IMAC via FPLC revealed a large number of impurities as well as large aggregates. To remove these unknown proteins, a size exclusion chromatography (SEC) using a Superdex 75 column (bed volume of 83 mL) was performed. With this method all components (but mainly proteins) present in the preparation are separated based on their size. Comparison of the generated chromatogram to a chromatogram gained after a SEC performed with proteins of known size for calibration, allows the association of a peak fraction to the target protein.

To this end, the elution fractions of the previous IMAC were pooled, concentrated via a Vivaspin® concentrator (MWCO 30 kDa) to ~ 2 mL and subjected to the SEC. The SEC was performed with a flow rate of 0.8 mL/min., the column was equilibrated with 0.1 CV SEC buffer and the loop used for sample-loading was emptied with 10 mL. The flow-through was collected in fractions of 0.2 CV. Afterwards, the collected fractions were analyzed using SDS-PAGE and the chromatogram from the calibration SEC. The identified PA_{83}-fractions were now pooled, the protein concentration was determined via SDS-PAGE and the protein was subjected to proteolytic activation.

Proteolytic activation of PA_{83} via trypsin to PA_{63}

The cytotoxicity of LT and ET are dependent on PA_{63}-mediated binding of LF and EF as well as translocation of the A-components into the cells´ cytosol. Therefore, the full-length PA_{83} is proteolytically cleaved at the amino-terminus after receptor-binding by cellular proteases like furin which can be recreated *in vitro* using trypsin (Singh et al., 1989).

To this end, the purified protein was incubated with trypsin in a 500:1 ratio (w/w) of PA_{83} to trypsin for 60 min. on ice. After 60 min., a sample was tested via SDS-PAGE for successful cleavage. When the band shift confirmed the PA_{83} to PA_{63} activation trypsin inhibitor was added in a 10:1 ratio of trypsin inhibitor to trypsin followed by another incubation for 60 min. on ice. Protein concentration was determined again with SDS-PAGE before the protein was aliquoted and subjected to shock-freezing in liquid nitrogen before storage at -80 °C.

2.2.5. Protein analysis

2.2.5.1. Sodium Dodecyl Sulfate Polyacrylamide Gel Electrophoresis (SDS-PAGE)

For the separation of proteins based on their molecular weight, SDS-PAGEs after the method of Laemmli (Laemmli, 1970) were performed. The polymerized acrylamide acts as a molecular net. SDS is added as ionic detergent to the gel as well as the protein samples (via Laemmli buffer). It leads to protein denaturation and a negative net charge of the proteins, which is necessary for their separation within the electric field. DTT is added as reduction agent for disulfide bonds. The samples were prepared by adding Laemmli buffer supplemented with DTT and boiling for 10 min. at 95 °C. Additionally to the samples, molecular weight standards were loaded to the gel in parallel. Here dependent on the assay performed subsequently, either an unstained ladder (Coomassie staining) or a prestained ladder (WB) was used, 5 µL each. After subjecting all samples, the gel was run at 37 mA/gel at variable voltage for 45-60 min. (or until a sufficient separation was visible) with 1x SDS-running buffer. Large gels were usually run for about 3 h.

Following the SDS-PAGE the gels were either stained immediately with Coomassie staining or used for WB analysis.

In case of a densitometric determination of protein concentrations based on SDS-PAGEs, the protein samples (typically from protein purification) were subjected to

the SDS-gel alongside with a BSA concentration series (200 ng to 1000 ng). The gels were then stained with Coomassie staining and analyzed with ImageJ. The protein concentration was estimated using the BSA standard curve.

2.2.5.2. Coomassie Staining

Staining of SDS-PAGE gels with Coomassie staining allows the visualization of proteins. Therefore, the gels were unmounted from the chamber and glass-plates used for casting and running and placed in Coomassie staining solution for at least 30 min. under constant shaking on a rocking shaker at RT. Afterwards, the staining solution was poured back in the storage flask, the gel was rinsed with tap-water to remove excess staining solution and placed in Coomassie on a rocking shaker at RT. The destaining solution was exchange (and recycled over activated charcoal) on a regular basis until the bands were clearly visible. Heating of the solutions considerably reduced the incubation times and was typically performed. After sufficient destaining, the gels were rinsed again with tap water, placed between two plastic foils, and documented via scanning.

2.2.5.3. Western Blot Analysis

For the immunodetection of specific proteins, they have to be transferred from the SDS-gel onto a nitrocellulose membrane. The gel was placed on top of the membrane which was placed on 3 layers of blotting paper itself. This stack was placed on the anode of the semi-dry blotter, gel-side up. Afterwards, the gel was covered with another 3 layers of blotting paper before the cathode of the semi-dry blotter was placed on top to close the blotting chamber. All layers of the entire stack were soaked in Towbin buffer prior to mounting. Before placing the cathode on top, potential air pockets were removed by rolling a 15 mL tube over the stack and a small amount of Towbin buffer was poured over the stack again. Blotting was performed by applying a constant current of 1.5 mA/cm^2 for ~ 80 min., large gels were blotted for 110 min.. In the following, the gel was stained with Coomassie staining for remaining protein and the membrane was stained with PonceauS solution. PonceauS staining allows the visualization of proteins via unspecific protein-binding. Therefore, the membrane was rinsed once with tap water and placed in PonceauS solution at RT until bands were visible. The membrane was then rinsed again with tap water to remove excess staining solution and documented

via scanning. The membrane was now rinsed repeatedly with tap water to remove all staining solution before it was placed in the blocking solution at RT for at least 60 min. (or optionally over night at 4 °C). This step is performed to block unspecific protein binding of the antibodies used later on. Before the primary antibody dilution was added, the membrane was rinsed with 1 x PBS-T until the washing solution was clear. The membrane was incubated with the primary antibody diluted in 1x PBS-T at RT for at least 60 min. (or optionally over night at 4 °C). Afterwards, the primary antibody was poured back in its storage tube for later re-use and the membrane was washed three times with 1x PBS-T for 5 min.. The secondary antibody was diluted in 1 x PST-T and incubated for 60 min. at RT. The membrane was washed again three times with 1x PBS-T for 5 min. before it was placed between plastic foils for the detection with X-ray films in the darkroom. To this end, the membrane was incubated (within the foil) with a 1:1 mixture of either self-made or commercial ECL (Immobilon™ Western Chemiluminescent HRP Substrate), the X-ray films were placed on top of the membrane and exposed for varying time periods. The exposed films were now placed in developer (until bands appeared) followed by a wash in tap water. Afterwards, the films were placed in fixer for a few minutes and finally placed in a tap water-bath. After drying, the ladder bands were transferred onto the film from the membrane before documentation via scanning of the films.

2.2.6. His-NDPK-A Kinase Assays

For the analysis of the kinase activity of His-NDPK-A after purification, the protein was subjected to the following two assays. Both are based on the inherent histidine kinase activity of the protein (Figure 5).



Figure 5: Exemplary nucleoside diphosphate activity of NDPK-A *in vitro*.
His-NDPK-A dephosphorylates GTP, is thereby phosphorylated at 1N-His itself before transferring that phosphate group onto ADP, thereby generating ATP. (Derived from Attwood & Muimo, 2018)

2.2.6.1. Autophosphorylation Assay

During its nucleoside diphosphate kinase activity, His-NDPK-A is autophosphorylated itself. As a consequence, a 1N-phosphohistidine enzyme intermediate is formed that can be detected during Western blot analysis with a

specific antibody (Fuhs et al., 2015). The assay described here was performed in assay buffer as well as in MDA-MB-231 cell lysate.

His-NDPK-A was diluted in assay buffer (APB) or added to MDA-MB-231 cell lysate (diluted 1:10 in APB), respectively. To initiate the reaction, 1 mM ATP and 2 mM $MgCl_2$ were pipetted into the tube and the samples were incubated for 5 min. at RT. The reaction was terminated by the addition of 5 mM EDTA (pH 8) and incubation for 5 min. at RT. As preparation for WB analysis, 2.5 x Laemmli (prepared with Tris-HCl pH8.8) supplemented with 500 mM DTT were added to the samples. In contrast to the preparation of samples for standard WB analysis, these sample must be incubated cold and must not be heated, otherwise the phosphorylation is lost. Therefore, the samples were subjected to 30 min. incubation at RT followed by a freeze-thaw cycle prior to the SDS-PAGE. For SDS-PAGE, a gel prepared with a stacking-gel composition with Tris-HCl pH 8.8 was used. SDS-PAGE was performed as described in chapter 2.2.5.1 and was followed by WB analysis.

Immunostaining was adjusted as follows for optimal results. The membrane was stained with PonceauS as described in chapter 2.2.5.3. Afterwards, the membrane was washed with MilliQ H_2O for 2 min. at RT on the rotary shaker and rinsed twice with MilliQ H_2O. The membrane was then incubated with antigen pretreatment solution (SuperSignal™ Western Blot Enhancer, Thermo Fisher Scientific Inc., Waltham, MA, USA) for 1 min. at RT before it was rinsed with MilliQ H_2O five times. Blocking was performed with Roti®-Block blocking solution diluted 1:10 with MilliQ H_2O for 60 min. at RT. The membrane was rinsed three times and washed once for 5 min. on the rotary shaker with 1x TBS-T. The primary anti-N1-phosphohistidine antibody was diluted in primary antibody diluent (SuperSignal™ Western Blot Enhancer, Thermo Fisher Scientific Inc., Waltham, MA, USA). It was incubated with the membrane over night at 4 °C. The following day, the membrane was washed four times with 1x TBS-T for 5 min. on the rotary shaker. The secondary antibody was diluted in Roti®-Block blocking solution (diluted 1:10 with MilliQ H_2O). The membrane was incubated for 30 min. at RT, before it was washed four times with 1x TBS-T for 5 min. on the rotary shaker. Afterwards, the membrane was placed between plastic foils and detected with X-ray films as described in chapter 2.2.5.3. However, SuperSignal™ West Femto Maximum Sensitivity Substrate (Thermo Fisher Scientific Inc., Waltham, MA, USA) was used.

For samples prepared in MDA-MB-231 cell lysate, Hsp90 was detected in addition to the N1-phosphohistidine-detection. The membrane-incubation with the primary and secondary antibodies as well as the detection was performed as described in chapter 2.2.5.3.

2.2.6.2. Kinase Activity Assay

When exhibiting its diphosphate kinase activity, NDPK-A transfers a phosphate group from a nucleoside triphosphate to a nucleoside diphosphate, generating ew triphosphates (Figure 5). This enzymatic activity was now used in the kinase activity assay.

His-NDPK-A was incubated *in vitro* with a substrate mix containing ADP and GTP in assay buffer. Therefore, His-NDPK-A was diluted in assay buffer for a final concentration of 22.5 – 360 pM. 4 µL of His-NDPK-A dilution were combined with 4 µL of substrate mix containing 50 µM ADP and 50 µM GTP and 4 µL assay buffer in one well of a white, half-area 96 well plate. Assay buffer only, substrate mix only and His-NDPK-A only were used as controls. Triplicates were performed for each condition. In addition, a standard with defined di-/triphosphate ratios (Table 2) was added to the plate. The plate was incubated for 30 min. at RT before the reaction was terminated by the addition of 12 µl of Kinase-Glo® Luminescent Kinase Assay mix. The plate was again incubated at RT for 5-12 min., light protected.

Table 2: Formulation of Standard Solutions

ADP and GTP [µM]	ATP and GDP [µM]
50	0
49,5	0,5
49	1
48	2
46	4
44	6
42	8
40	10

Afterwards, the luminescence at 560 nm was measured. The amount of generated ATP was determined by correlating the measured luminescence signal of the samples to the luminescence signal of the standards.

2.2.7. Overview of the Performed Assays

To investigate the potential delivery of His-tagged proteins into MDA-MB-231 as well as HeLa cells, a serious of different assays were performed. A short overview is depicted in Table 3, listing which assay was performed with which cell line to what end. Also, the number of cells per well and the total duration of the experiment from the addition of the proteins to the defined respective endpoint are listed.

The treatment procedure for each assay will be explained in detail in the following chapters. In general, the cells were seeded one day prior to the experiment in serum-containing medium. After treatment, the cells were placed back into the incubator for incubation at 37°C, 5 % CO_2 and saturated humidity. Triplicates for all conditions tested have been performed. The progress of the different treatments was recorded using a Zeiss Axiovert 40CFL microscope with a Jenoptik progress C10 CCD camera. The quantification of rounded cells was performed for each picture taken separately via the ImageJ software. The total number is displayed as mean ± standard deviation.

Table 3: Overview over the performed assays

Assay	Cell line	His-tagged protein	Well plate	Cells/ well	Duration of treatment	Analysis of
Intoxication	HeLa	His-DTA	96 well	10.000	24 h	Cell rounding
Uptake	HeLa	His-DTA	96 well	10.000	24 h	Susceptibility to PA_{63}-mediated delivery
	MDA-MB-231					
Binding	HeLa	His-NDPK-A	12 well	100.000	30 min.	Binding (WB)
	MDA-MB-231			150.000	30 min.	
Uptake	HeLa	His-DTA	8 well	2.000	3 h	Morphological changes (IF)
			24 well	50.000	24 h	Uptake (WB)
			24 well	10.000	12 h	Uptake (EF-2-status)
			96 well	2.000	48 h	Cell viability (MTS)

Uptake	MDA-MB-231	His-DTA	8 well	2.500*	48 h	Morphological changes (IF)
			24 well	150.000	12 h	Uptake (WB)
			24 well	150.000	12 h	Uptake (EF-2-status)
			96 well	10.000	24 h	Cell viability (MTS)
Uptake	HeLa	His-NDPK-A	8 well	2.000	3 h	Morphological changes (IF)
			24 well	50.000	24 h	Uptake (WB)
			24 well	10.000	12 h	Uptake (EF-2-status)
			96 well	2.000	48 h	Cell viability (MTS)
Uptake	MDA-MB-231	His-NDPK-A	8 well	2.500*	48 h	Morphological changes (IF)
			24 well	50.000	48 h	Uptake (WB)
			24 well	150.000	12 h	Uptake (EF-2-status)
			96 well	2.500	48 h	Cell viability (MTS)
Migration	MDA-MB-231	His-NDPK-A	2 well-insert	25.000	48 h	Scratch assay

* Equals the number of cells at the start of the experiment. Actual number seeded was only have the given amount. Cells were seeded 48 h prior to the experiment.

2.2.8. Cell Binding Assay

The binding of His-NDPK-A to HeLa and MDA-MB-231 cells was analyzed by performing a cell binding assay. Therefore, the cells (seeded as given) were adjusted to 4 °C on ice for 30 min. to reduce membrane flexibility and washed once with cold PBS to remove detached cells and remaining culture medium. This step is crucial since remaining FCS from the culture medium could interfere with the assay and bind to the later added proteins. The proteins were added at concentrations of 3 µg/mL for PA_{63} and 30 µg/mL for His-NDPK-A in serum-free cell culture medium. As controls, cells were either left untreated or were treated with His-NDPK-A alone. The cells were incubated for 30 min. on ice, the protein solution was removed, and the cells were washed twice with cold PBS. The PBS was aspirated completely, and the cells were frozen at -20 °C over night before they were lyzed in hot 2.5x Laemmli

buffer supplemented with 100 mM DTT. The cells were scraped with a cell-scraper and transferred into a 1.5 mL tube for boiling at 95 °C for 10 min. followed by transfer of the sample into the pockets of an SDS-gel and a SDS-PAGE. Subsequently, a WB analysis was performed for the detection of His-NDPK-A (anti-His antibody) and Hsp90 (anti-Hsp90). The amount of His-NDPK-A taken up into the cells was determined densitometrically using the ImageJ software. The band intensity for the detection with the anti-His antibody was quantified against the band intensity for the detection with the anti-Hsp90 antibody.

2.2.9. Uptake Assays

2.2.9.1. Intoxication assay After Protein Purification

For the analysis of the proteins´ biological activity after protein purification, cells were seeded as given and incubated with the following toxins for up to 48 h. For treatment, 5 µg/mL His-DTA alone or plus 1 µg/mL PA_{63} were added, controls were left untreated. The progress of the intoxication was recorded via a bright-field microscope and the acquisition of pictures. The endpoint of intoxication was cell rounding. An occurrence of this morphological change would confirm biological activity of the toxins (Blumenthal et al., 2007; Schnell et al., 2016).

2.2.9.2. For the Analysis of the Selectivity of cells for PA_{63}-mediated Delivery of the His-tagged Proteins His-DTA and His-NDPK-a

Pretreatment with BafA1

To investigate the role of PA_{63} during delivery of recombinant His-tagged NDPK-A and DTA, the inhibitor BafA1 was applied to some of the cells. It inhibits the vATPase activity and prevents acidification of endosomes. Therefore, the PA_{63}-translocation pore cannot be formed. To this end, the culture medium of all wells was replaced with fresh serum-containing culture medium supplemented with 30 nM BafA1 or without BafA1, respectively. After 30 min. at 37 °C, the medium was again replaced, this time with the respective intoxication mixes. For each combination of proteins one set of triplicates with and without BafA1 was performed. The inhibitor was present during the entire time frame of the experiment.

Uptake assay for His-DTA and His-NDPK-A

To analyze whether HeLa and MDA-MB-231 cells are susceptible to the PA_{63}-mediated delivery of His-DTA and His-NDPK-A, the cells were seeded as given, pretreated with 30 nM BafA1 as described and incubated with the respective protein-combinations. As control, cells were left untreated or were treated with the His-protein only. The cells were incubated for the indicated time frames at 37 °C and the number of rounded cells was quantified. In addition, different approaches were used to determine the cytosolic localization of the His-proteins. The cells were either lyzed and subjected to WB analysis to directly detect the His-proteins using specific antibodies or were subjected to sequential ADP-ribosylation of EF-2 (for His-DTA-treated cells). Further, a cell viability assay was performed.

Immunofluorescence Microscopy

As a different approach to analyze changes in cell-morphology upon treatment with His-tagged proteins and PA_{63}, the cells were subjected to immunofluorescence microscopy. The cells were seeded into 8-well µ-slide plates and incubated with various treatments. Since MD-MB-231 cells responded more sensitive to the following treatment, the cells were seeded 48 h prior to the assay so they would adhere more tightly. Afterwards, the plate was placed on ice and washed with 300 µL (used as standard volume for alle following steps if not indicated differently) cold PBS-T three times (further referred to as “wash”). The cells were then fixated with prewarmed (37 °C) 4 % PFA for 20 min. at 37 °C before washing. The cells were now permeabilized for 5 min. at RT with 0.4 Triton® X-100 in PBS, light protected. After washing, the samples were quenched with warm 100 mM glycine for 2 min. at RT followed by washing and blocking with 5 % skim-milk powder in PBS-T (IF blocking solution) for at least 45 min. at 37 °C. For all following steps, the dilutions were performed using IF blocking solution. The samples were washed before adding the respective primary antibodies diluted in IF blocking solution for 45 min. at 37 °C. The samples were washed four times with 300 µL warm PBS-T before adding the corresponding secondary antibodies for either 30 min. at 37 °C, 60 min. at RT or over night at 4 °C. The different combinations are listed in Table 4.

Table 4: List of antibodies and conjugates used per His-protein and cell line

Cell line	His-tagged protein	Primary antibody	Secondary antibody
MDA-MB-231	His-DTA	anti-His (Invitrogen, Carlsbad, CA, USA), 1:500	Goat-anti-mouse Alexa Fluor™ 488, 1:750
	His-NDPK-A	anti-His (Invitrogen, Carlsbad, CA, USA), 1:500	Goat-anti-mouse Alexa Fluor™ 488, 1:750
HeLa	His-DTA	anti-His (SantaCruz Biotechnology, Dallas, TX, USA,) 1:100	Goat-anti-mouse Alexa Fluor™ 488, 1:750; Goat-anti-mouse Alexa Fluor™ 568*, 1:500
	f-actin	Phalloidin-FITC conjugate, 1:100	-
	His-NDPK-A	anti-His (SantaCruz Biotechnology, Dallas, TX, USA), 1:100	Goat-anti-mouse Alexa Fluor™ 488, 1:750

* if samples were incubated with Phalloidin-FITC additionally

After incubation, the samples were washed five times with 300 µL warm PBS-T. In case of f-actin staining, the respective 1:100 Phalloidin-FITC dilution was added, and the samples were incubated for 1 h at RT before washing. The nuclei staining with Hoechst33342 was performed with a dilution of 1:10.000 for 5 min. at RT, light protected. After the last time of washing, fresh PBS-T was added and the plates were stored at 4 °C, light protected. The iMIC digital microscope was used to acquire multi-channel images, which were processed with the imageJ software. They were adjusted to the same levels of brightness and contrast and were exported as multi-color images.

In vitro sequential ADP-ribosylation of EF-2

This assay was used to determine whether His-DTA enters the cytosol of HeLa and MDA-MB-231 cells enzymatically active. Therefore, after treatment of the cells as indicated, they were placed on ice and washed once with cold PBS. The PBS was aspirated, and the plate was frozen for at least 60 min. at – 20°C. All following steps were performed on ice. The cells were detached by adding 30 µL cold ARB and

scraping with the pipette tip. The samples were transferred into a 1.5 mL tube and additionally lyzed with a needle (26 G) by pipetting up and down. After collection of the sample in the tube-tip (short centrifugation), the tubes were opened. 100 ng of recombinant His-DTA and 1 µL of biotinylated NAD^+ (250 pmol) in ARB were added into the lid. The enzyme reaction was initiated synchronized by shortly centrifuging the tubes. The samples were incubated for 30 min. at 37 °C before the reaction as terminated by adding 7 µL of hot 5 x Laemmli + DTT and incubation for 10 min. at 95 °C. The samples were then subjected to an SDS-PAGE with subsequent WB analysis and detection of substrate modification using strep-POD. To determine equal protein loading, GAPDH was detected as well.

Cell viability assay

The cell viability of HeLa and MDA-MB-231 cells was estimated after treatment with the His-proteins and PA_{63}. Therefore, 10 µL of MTS solution were added into the treatment medium of each well of the 96 well plates. The plates were incubated for 90 min. at 37 °C before the absorbance at 490 nm was measured in a plate reader. Statistical analysis was performed with GraphPad Prism. The absorbance values of treated cells were compared to untreated negative controls. As positive control, either staurosporine (Tamaoki et al., 1986) or DMSO (Holzer & Maier, 1987) were used and added to the respective wells at the start of the experiment.

For the cell viability assay performed after the migration assay, the treatment medium was removed and replaced with 450 µL fresh culture medium plus 50 µL of MTS solution per well of the 24 well plate. The incubation and absorbance measurement were performed as described above.

2.2.10. Migration Assay

To determine the effects of treatment with His-NDPAK-A plus PA_{63} on the migratory behavior of MDA-MB-231 cells, they were subjected to a wound-healing/scratch

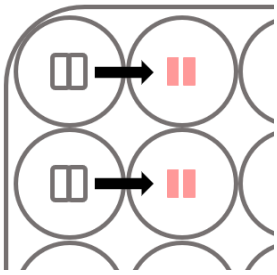


Figure 6: Migration assay set-up using the Ibidi® culture-insert 2 well.
The culture inserts are placed in the wells of a 24 well plate. Cells were seeded into the two wells. Removal of the insert (black arrow) creates a wound/scratch area in between the two patches of attached cells that can be monitored (based on Ibidi, 2020).

assay. To this end, 2 well culture-inserts were placed in wells of 24 well plates (Figure 6). 25.000 cells per insert-well were seeded and the surrounding plate-well was filled with 250 µL PBS to prevent the cells from drying out. After adherence over night at 37 °C, 5 % CO_2, saturated humidity, the inserts were carefully removed using sterile tweezers. This step creates a wound/scratch are between the two patches of cells. Detached cells removed by washing twice carefully with prewarmed PBS before 250 µL of protein solutions were added. Three technical replicates were performed. The cells were incubated at 37 °C for up to 48 h and the progress of cell-migration into the wound area was monitored and recorded via a microscope with camera. Pictures were taken every for 4 h at three different areas of the scratch. After 48 h of incubation, a cell viability assay was performed. Quantitative analysis of the total wound area was performed using the MRI tool (ImageJ software) and the relative wound area was determined in relation to the initial scratch (immediately after the addition of the treatment solutions).

2.2.11. Reproducibility and Statistics

All experiments presented in this thesis were conducted independently at least two times. Figures are generated from representative experiments, technical triplicates were performed, and calculated values are given as average ± SD. Significance was tested using either the One-Way ANOVA followed by Dunnett´s multiple comparison test with a 99.9 % confidence interval or the modified t-test using the two-stage step-up method of Benjamini, Krieger and Yekutieli, which does not assume equal distribution. For presentation of immunoblots, sections of larger membrane parts are given but the protein bands were always detected originally on the same membrane.

3. Results

3.1. Purification and Characterization of Recombinantly Expressed Proteins

The molecular transporter consists of two components, the His-tagged tumor metastasis suppressor protein His-NDPK-A tested as potential cargo molecule and the transport component PA_{63}. Both proteins were recombinantly expressed in *E. coli* with subsequent purification and characterization to determine protein identity as well as biological activity.

3.1.1. Purification and Characterization of His-NDPK-A

The cargo molecule His-NDPK-A (Figure 7a) was expressed in *E. coli* BL21 followed by immobilized metal affinity chromatography (IMAC) for protein isolation. Via Western blotting the protein identity was confirmed (Figure 7b) using an anti-His antibody directed against the N-terminal His-tag of the recombinant His-NDPK-A. The blot shows a distinct band on the expected molecular weight of 18 kDa, which corresponds to the predicted molecular weight of the His-NDPK-A construct.

The inherent nucleoside diphosphate kinase activity of His-NDPK-A was confirmed using two different approaches. Due to its diphosphate kinase activity, NDPK-A transfers a phosphate group from a nucleoside triphosphate to a nucleoside diphosphate (Figure 5). Consequently, a 1N-phosphohistidine enzyme intermediate is formed that can be detected with a specific antibody (Fuhs et al., 2015). On the one hand the purified His-NDPK-A was subjected to an autophosphorylation assay, and the generated enzyme intermediate was confirmed via Western blotting using a 1-phosphohistidine-specific antibody (Figure 7c). The band-intensity is correlates with the amount of protein added to the sample. The higher amount of His-NDPK-A also results in a stronger band intensity. The same assay was performed in MDA-MB-231 cell lysate (Figure 7d). WB analysis and subsequent detection again presented a clearly visible band at 18 kDa for the samples with the highest amount of His-NPDK-A added. Two additional bands appeared, which most likely represent the phosphorylated enzyme intermediates of the two native proteins NDPK-A (17.1 kDa) and NDPK-B (17.3 kDa), which are abundantly present in cells such as MDA-MB-231. The band shift for the purified His-NDPK-A can be explained based on the additional His-tagged and linkers added during cloning of the construct.

With a kinase activity assay the conversion efficiency of His-NDPK-A (Figure 5) was determined. The amount of ATP generated during incubation by the ADP to ATP conversion catalyzed by His-NDPK-A, was quantified via the Kinase-Glo® Luminescent Kinase Assay and the luminescence signal at 560 nm was measured. An increase in luminescence signal indicates enzymatic activity, which is the case here. The higher the amount of His-NDPK-A added to the samples, the higher the luminescence signal (Figure 7e).

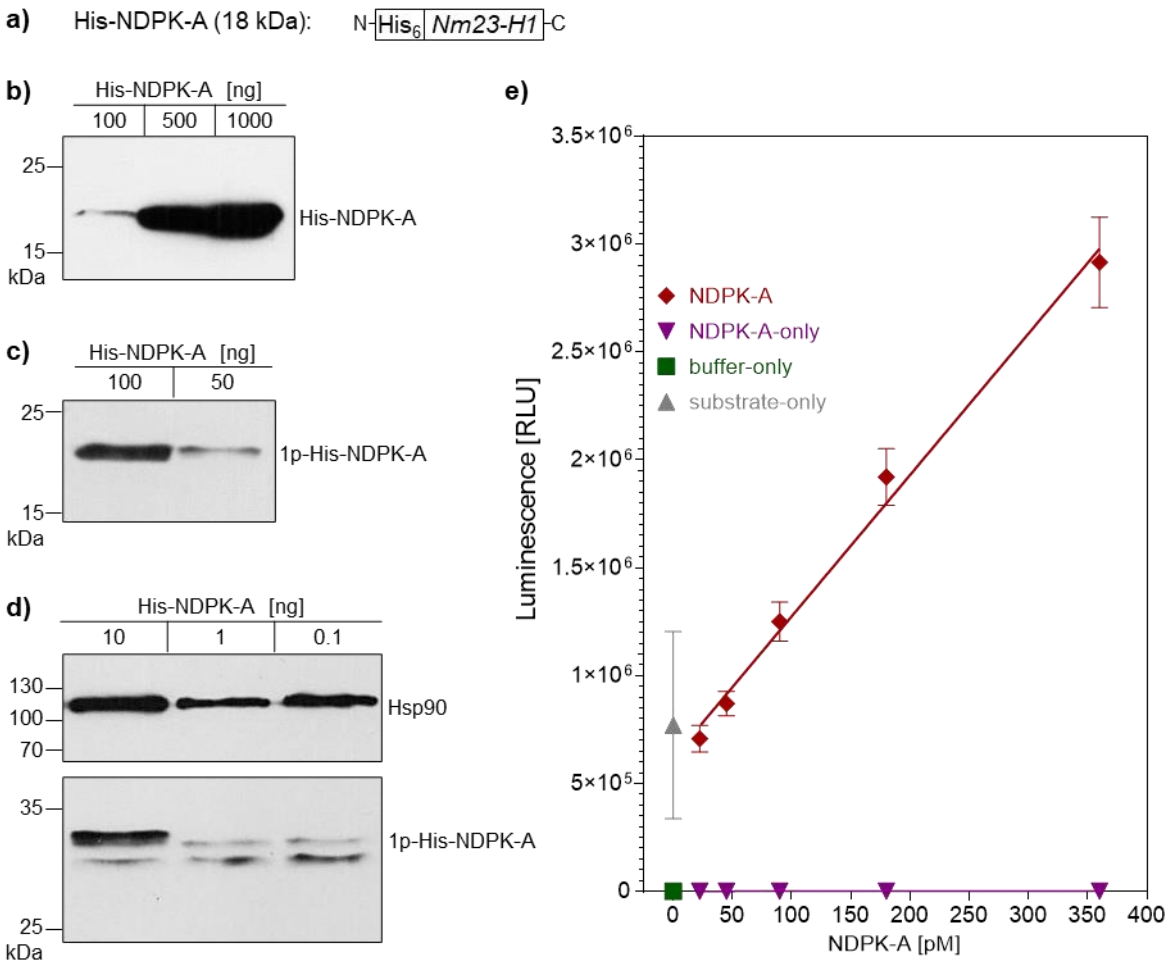


Figure 7: Characterization of the cargo protein His-NDPK-A.
The cargo protein His-NDPK-A was recombinantly expressed in *E. coli*, followed by purification via affinity chromatography and Western blotting to confirm protein identity using a (b) anti-His antibody. To analyze the proteins intrinsic kinase activity, its autophosphorylation activity was measured. During the autophosphorylation assay His-NDPK-A was incubated with ATP (1 mM) and $MgCl_2$ (2 mM) at room temperature for 5 min in assay buffer (c) or MDA-MB-231 cell lysate (d), EDTA (5 mM) was added to stop the reaction. Western blotting was performed to detect the phosphorylated His-NDPK-A intermediate with an anti-N1-phosphohistidine (1-pHis) antibody. For determination of the kinase activity of His-NDPK-A the substrate conversion status after incubation at room temperature for 30 min was measured in a concentration dependent manner (His-NDPK-A at 22.5 pM, 45 pM, 90 pM, 180 pM and 360 pM). As controls His-NDPK-A only, substrate only and buffer only were used. Via the Kinase-Glo® Luminescent Kinase Assay the ATP conversion was quantified. (Figure derived from Felix et al., 2020; permission from CC BY 4.0.)

In conclusion, the recombinant His-NDPK-A was successfully expressed and enzymatically active. Therefore, it could be used in the following experiments as a model cargo to test the hypothesis of a PA_{63}-mediated delivery of non-toxin derived His-tagged cargo into cells.

3.1.2. Purification and Characterization of PA_{63}

The transport component PA_{63} was expressed recombinantly in *E. coli* Rosetta. In general, the expression and purification protocols were based on a protocol previously described (Ost et al., 2019). The process was adjusted for maximum yield and purity, accordingly. After protein expression and purification (FPLC using the ÄKTA™ system) the full-length PA_{83} was subjected to proteolytic cleavage using trypsin. Proteolytic cleavage of the full-length protein PA_{83} results in the cleavage products PA_{63} and the cleaved amino terminus of PA_{83}, PA_{20}. This proteolytic activation usually occurs on the cell surface after receptor binding and is performed by cellular proteases like furin. This was mimicked *in vitro* with trypsin. SDS-PAGE and Coomassie staining of the gel (Figure 8a) reveal successful cleavage. A band-shift and a second band at a lower molecular weight of ~20 kDa was visible. This represents the proteins´ amino-terminal 20-kDa domain PA_{20}.

To confirm biological activity of the purified protein, HeLa cells were incubated with PA_{63} and an established cargo molecule, His-DTA. DTA as the catalytically active domain of the diphtheria toxin (DT) is delivered into cells via PA_{63} when recombinantly expressed with an amino-terminal His-tag. It induces a drastic morphological change (cell rounding), that can be monitored via a microscope with a camera. Cell rounding is induced by intracellular substrate modification. DTA ADP-ribosylates the eucaryotic elongation factor 2 (EF-2), which halters protein synthesis and results in reduced cell viability. It therefore is a very suitable choice of cargo to monitor cytosolic localization of enzymatic activity. As shown in Figure 8, incubation of HeLa cells with PA_{63} and His-DTA in combination resulted in cell rounding (Figure 8b) after 4 h, which was still present after 24 h. In addition, the cell viability (Figure 8c) was significantly reduced after 24 h. Comparing the results for the treatment with His-DTA plus PA_{63} to the treatment with DT (which was used as positive control), cell rounding as well as cell viability were comparably affected. After 4 h, all cells incubated with His-DTA plus PA_{63} or DT are completely rounded. After 24 h the cell viability was reduced to under 20 % compared to the untreated control.

Taken together, recombinant PA_{63} was successfully expressed, purified and proteolytically activated. The adjusted purification process did not affect the final protein negatively. Hence, this protein was used in the following experiments as transport molecule for the delivery of His-DTA and His-NDPK-A.

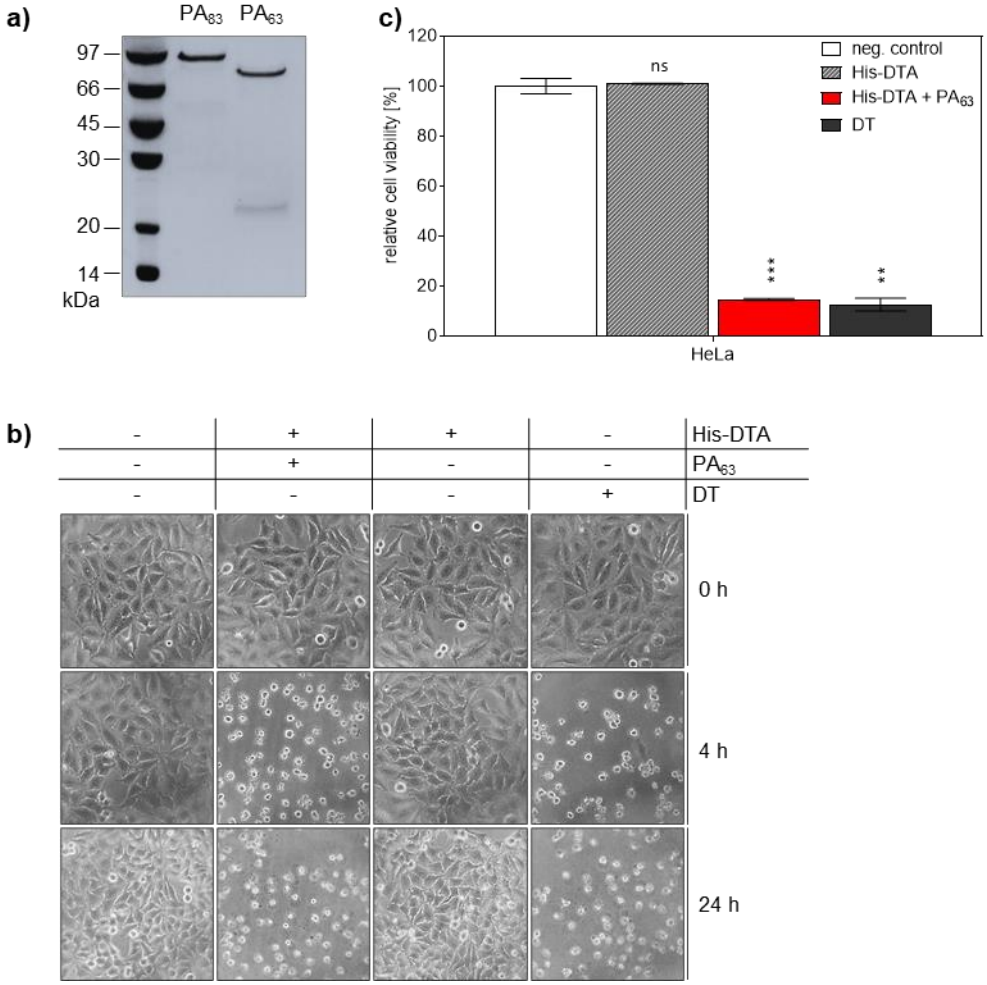


Figure 8: Characterization of the transporter protein PA_{63}:
PA_{63} was recombinantly expressed in *E. coli* and purified via a two-step chromatography. Affinity chromatography was followed by size-exclusion chromatography and proteolytic cleavage of the full-length protein PA_{83} to PA_{63}. For cleavage PA_{83} was incubated for 60 min. on ice with a 1:500 trypsin to PA_{83} ratio [µg], the reaction was terminated by adding trypsin inhibitor (10:1 inhibitor to trypsin ratio [µg]) and incubation for 60 min. on ice. Cleavage of PA_{83} to PA_{63} was determined via SDS-PAGE and (a) Coomassie staining of the proteins. Protein activity was qualified with an intoxication assay. (b) HeLa cells were seeded into a 96-well plate and were left untreated or incubated with 5µg/mL His-DTA (as enzymatically active cargo) and 1 µg/mL PA_{63} in combination or His-DTA only in shMEM for up to 24 h at 37 °C. DT was used as positive control at a concentration of 1µg/mL. Pictures were taken shortly before adding the proteins as well as after 4 h and 24 h of incubation. Representative pictures are shown for the indicated timepoints. (c) After 24 h the cell viability was assessed using the MTS assay. Results are given as average ± SD (n=3), significance was tested using the One-Way ANOVA followed by Dunnett´s multiple comparison test with a 99.9 % confidence interval, referring to the untreated negative control, **p≤0.01, ***p≤0.001.

3.2. Susceptibility of Human cells to PA_{63}-mediated Delivery of His-tagged DTA

As already described in the literature, PA_{63} is able to deliver his-tagged, toxin-derived cargo into the cytosol of different mammalian cell lines. Proof-of-concept was performed (3.1.2) for HeLa cells. The aim of this study now is to exploit this system to deliver a non-toxin derived cargo – the tumor metastasis suppressor NDPK-A. To investigate the effects of the delivery of His-NDPK-A into cells via PA_{63}, the breast cancer cell line MDA-MB-231 was chosen. It resembles the situation in patients and allows analysis of anti-metastatic effects since these cells harbor present a migratory behavior. The prerequisite of such experiments is a susceptibility of the MDA-MB-231 cells towards the delivery of cargo via PA_{63}. To this end, MDA-MB-231 cells were subjected to a serious of experiments with the reference-cargo His-DTA where a direct read-out of cellular effect upon treatment with His-DTA and PA_{63} are possible.

3.2.1. MDA-MB-231 cells are Susceptible to His-DTA Delivery via PA_{63}

MDA-MB-231 cells were subjected to an intoxication assay. The cells were incubated with His-DTA in the absence or presence of PA_{63}. Changes in cell morphology were monitored using a microscope with a camera and the number of rounded cells was quantified.

After 4 h of incubation with His-DTA plus PA_{63} only 30 % of cells showed morphological changes compared to the untreated controls (Figure 9b). However, after 24 h of incubation almost all cells treated with both components in parallel were rounded (Figure 9c). The treatment with His-DTA only however, did not result in morphological changes, even after 24 h of incubation. The induced morphological changes in MDA-MB-231 could be prevented by pretreatment of the cells with BafA1. This pharmacological inhibition of vATPase activity protected the cells from cytotoxic effects of the treatment with His-DTA plus PA_{63}.

In conclusion, MDA-MB-231 cells respond to treatment with His-DTA plus PA_{63} with a specific change in cell morphology, cell rounding. MDA-MB-231 cells are susceptible to PA_{63}-mediated delivery of His-DTA and therefore a promising candidate for the investigation of His-NDPK-A transport via PA_{63}.

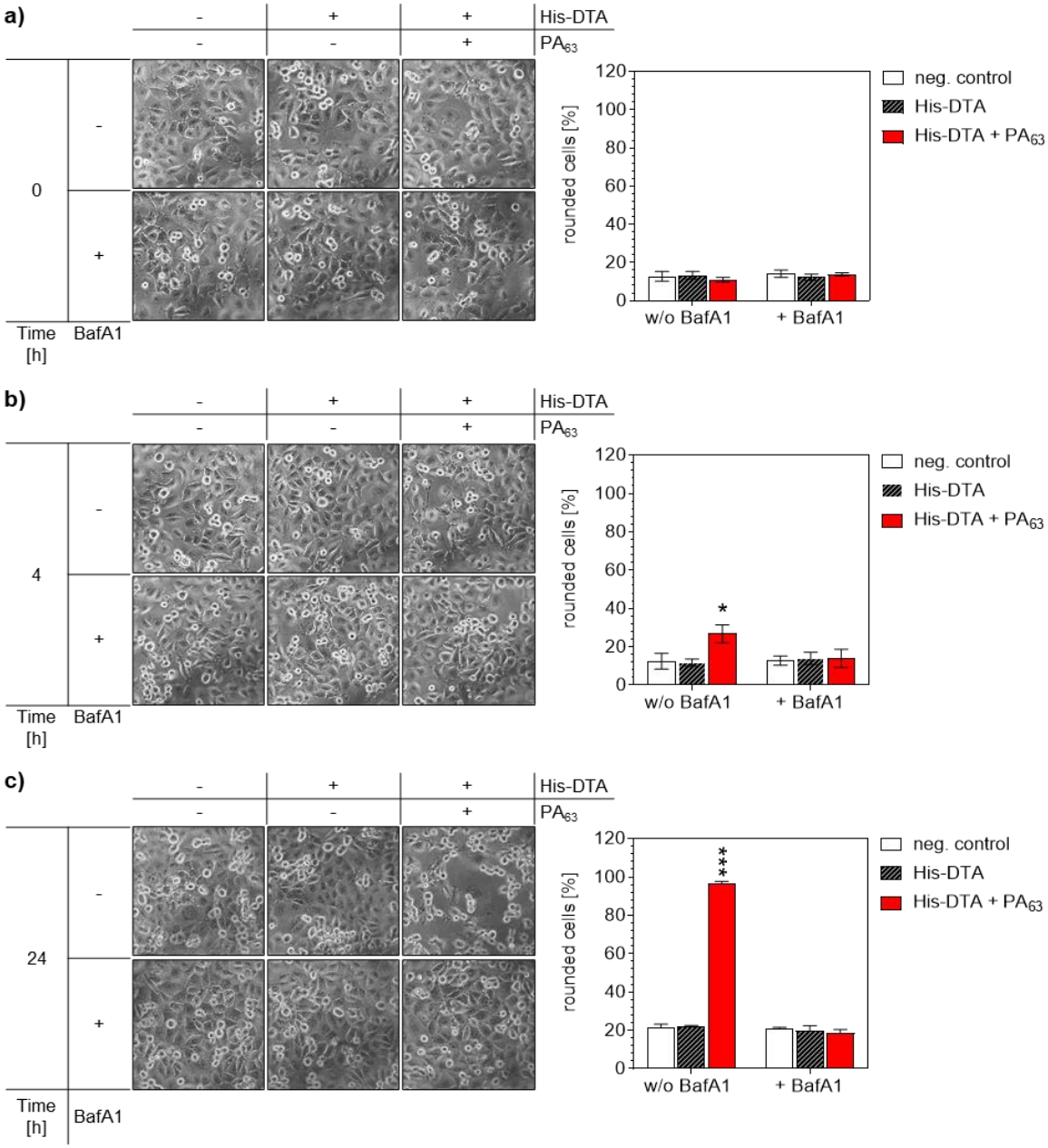


Figure 9: PA_{63} mediates delivery of His-DTA into MDA-MB-231 cells.
MDA-MB-231 cells were seeded into a 96-well plate and incubated with BafA1 (30 nM) for 30 min. at 37 °C prior to protein addition. After pretreatment cells were either left untreated or incubated with 5µg/mL His-DTA and 1 µg/mL PA_{63} in combination or His-DTA only in shDMEM at 37 °C. Morphological changes were investigated and pictures taken at the depicted timepoints. Representative pictures are shown before treatment with the proteins (a) as well as (b) after 4 h and (c) 24 h of incubation. For all timepoints the number of rounded cells was determined using the imageJ software, results are given as average ± SD (n=3), significance was tested using the One-Way ANOVA followed by Dunnett´s multiple comparison test with a 99.9 % confidence interval, referring to the untreated negative control, *p≤0.05, ***p≤0.001. (Figure derived from Felix et al., 2020; permission from CC BY 4.0.)

3.2.2. HeLa cells are Susceptible to His-DTA Delivery via PA_{63}

HeLa cells were used as reference cell line for the following experiments to analyze the changes in MDA-MB-231 cells and exclude a cell-line specific effect.

As for MDA-MB-231 cells, HeLa cells were subjected to an intoxication assay with His-DTA and PA_{63}. As endpoint for the intoxication the morphological changes were monitored and analyzed as described for MDA-MB-231 cells. As shown in Figure 10, cell rounding was already pronounced after 4 h of incubation (Figure 10b) with His-DTA and PA_{63}. The number of rounded cells was at almost 100 %. In contrast

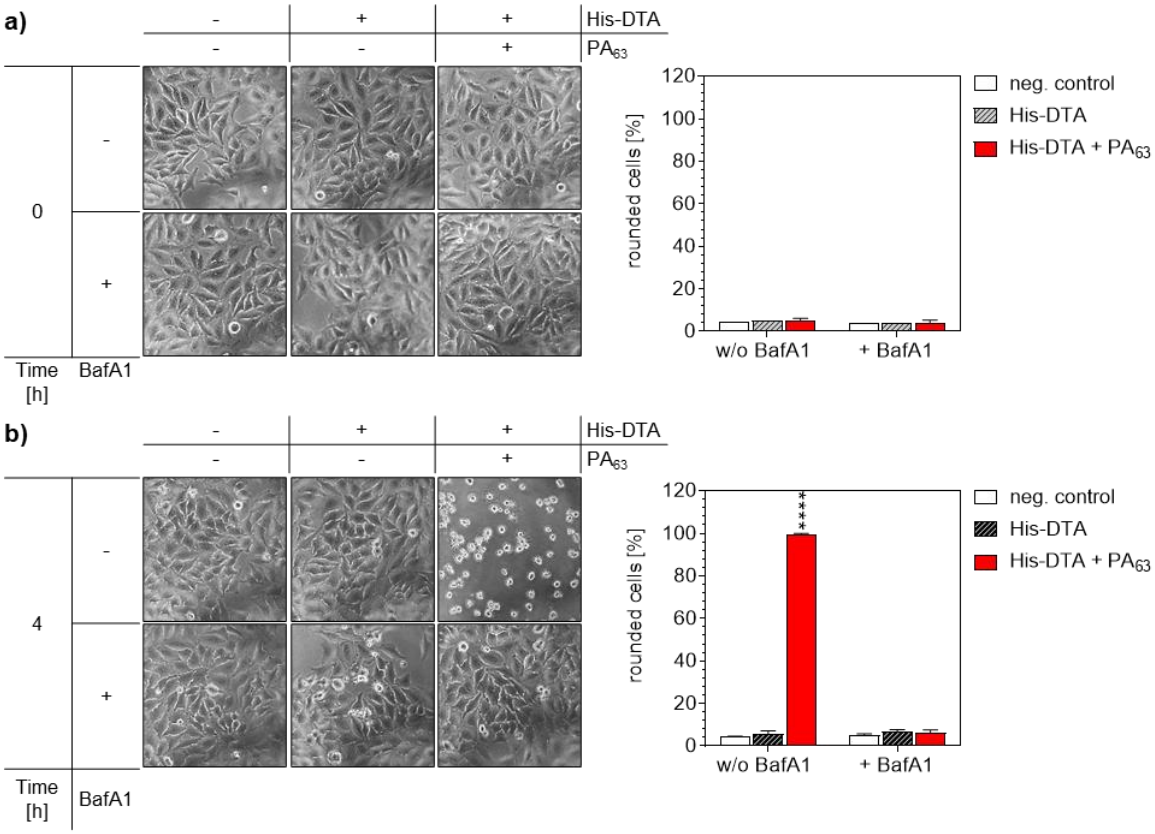


Figure 10: PA_{63} mediates delivery of His-DTA into HeLa cells.
HeLa cells were seeded into a 96-well plate and incubated with BafA1 (30 nM) for 30 min. at 37 °C prior to protein addition. Cells were either left untreated or incubated with 5µg/mL His-DTA and 1 µg/mL PA_{63} in combination or His-DTA only in shMEM at 37 °C. Morphological changes were investigated and pictures taken at the depicted timepoints. Representative pictures are shown before treatment with the proteins (a) as well as (b) after 4 h of incubation. For both timepoints the number of rounded cells was determined using the imageJ software, results are given as average ± SD (n=3), significance was tested using the One-Way ANOVA followed by Dunnett´s multiple comparison test with a 99.9 % confidence interval, referring to the untreated negative control, ****p≤0.0001. (Figure derived from Felix et al., 2020; permission from CC BY 4.0.)

to that, treatment with His-DTA only did not result in changes in cell morphology. The same inhibitory effect of the pretreatment with BafA1 as for MDA-MB-231 cells

was observed. The number of rounded cells was almost up to the level of untreated cells.

In conclusion. MDA-MB-231 cells are susceptible to the intoxication with His-DTA by PA_{63} and respond with a change in morphology. However, compared to HeLa cells the induced changes occurred later on, which suggests a higher sensitivity of HeLa cells to PA_{63}-mediated delivery of His-DTA.

3.3. PA_{63} mediates Delivery of His-DTA into Human cells

After establishing the intoxication assay for PA_{63}-mediated delivery of His-DTA into HeLa as well as MDA-MB-231 cells, cytosolic localization of the reference-cargo His-DTA was further investigated using different biochemical approaches. The endpoints chosen were cell rounding as well as EF-2-modification after treatment as well as cell viability.

3.3.1. PA_{63} mediates Delivery of His-DTA into MDA-MB-231 cells

In parallel to the reference cell line HeLa, the intended breast cancer model cell line MDA-MB-231 was investigated regarding cytosolic localization of His-DTA. Immunofluorescence microscopy of the cells after 48 h of incubation with the different protein treatments (Figure 11a) revealed a drastic increase in signal for His-DTA (green) when present in combination with PA_{63}. Signals for cells incubated with His-DTA only were comparable to the untreated controls. This was in line with results found after incubating MDA-MB-231 cells in the same manner for 12 h, followed by Western blot analysis (Figure 11b). Immunoblotting using an anti-His antibody resulted in a band corresponding to the same molecular weight as purified His-DTA (far right lane) for cells treated with His-DTA plus PA_{63}. Pretreatment of the MDA-MB-231 cells with BafA1 resulted in a lack of signal and therefore no delivery of His-DTA into the cells. Also, treatment with His-DTA only did not result in any His-DTA uptake. The same findings occurred when analyzing the EF-2-modification status of MDA-MB-231 cells after 12 h of incubation (Figure 11c). The band corresponding to post-ADP-ribosylated EF-2 (during the *in vitro* ADP-ribosylation) for cells treated with His-DTA in the presence of PA_{63} was completely diminished compared to the other conditions. Here, all EF-2 was already ribosylated during the incubation before cell lysis. No EF-2 was available for ribosylation with biotinylated NAD^+ during the *in vitro* assay.

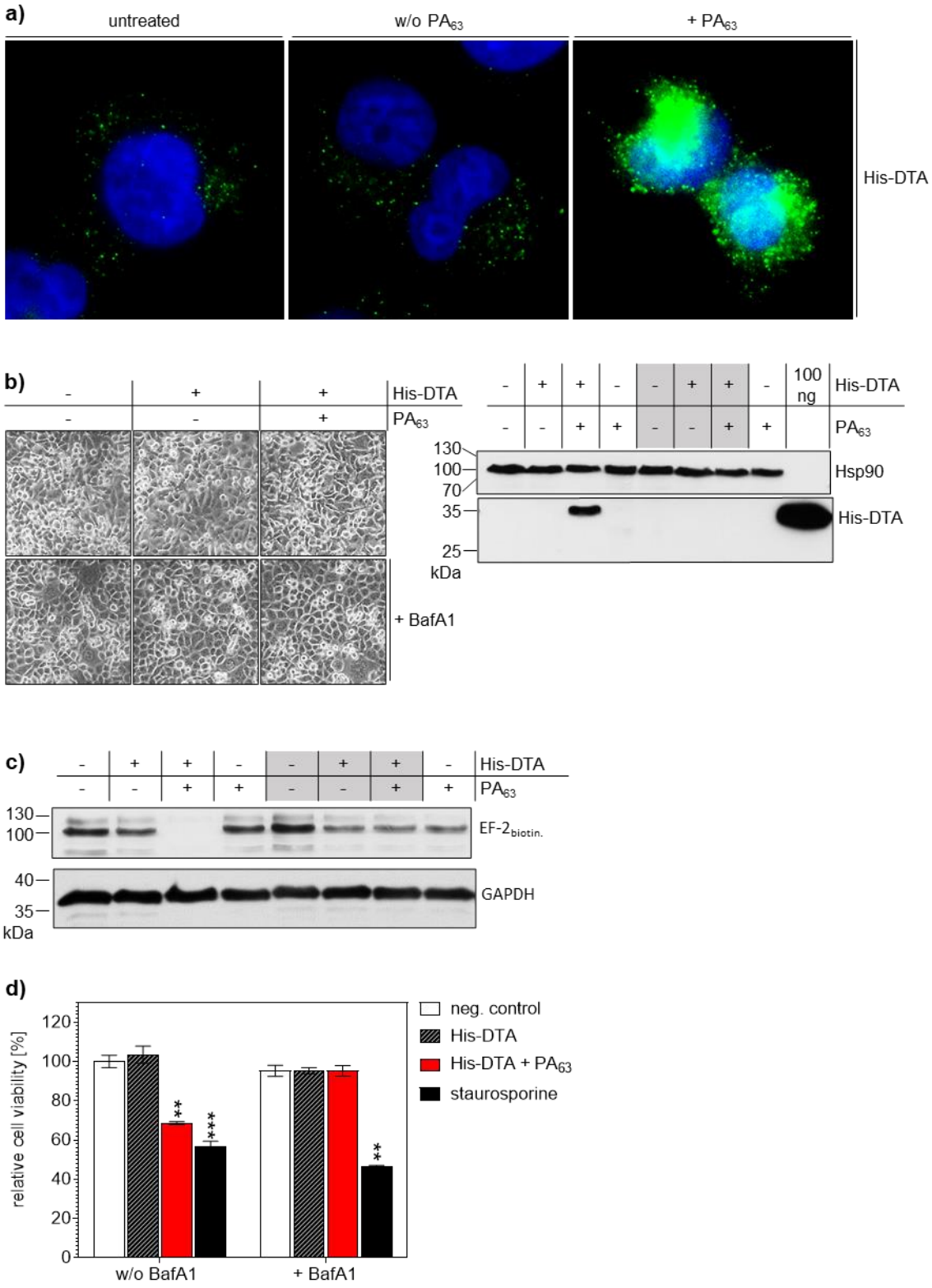

a)
untreated
w/o PA63
+ PA63
His-DTA
b)
His-DTA
PA63
+ BafA1
100 ng
130
100
70
35
25
kDa
Hsp90
His-DTA
c)
EF-2biotin.
GAPDH
d)
relative cell viability [%]
neg. control
His-DTA
His-DTA + PA63
staurosporine
w/o BafA1
+ BafA1

Figure 11: His-DTA is delivered via PA_{63} into MDA-MB-231 breast cancer cells.
a) PA_{63} mediates His-DTA-delivery into MDA-MB-231 cells and induces cell rounding. MDA-MB-231 cells were seeded into a 8-well µ-slide and incubated with His-DTA (5 µg/mL) in the presence or absence of PA_{63} (1 µg/mL) in shDMEM at 37 °C for 48 h. Proteins were visualized via fluorescence microscopy. His-DTA (green) was targeted using an anti-His antibody with subsequent immunostaining via a goat anti-mouse-Alexa Fluor568 antibody. Nuclei were stained with Hoechst 333342 (blue).
(b) BafA1 blocks the PA_{63}-mediated uptake of His-DTA into the cytosol MDA-MB-231. After seeding the cells into a 24-well plate they were incubated with BafA1 (30 nM) for 30 min. at 37 °C prior to protein addition (shaded in grey). Cells were either left untreated or were incubated with 5µg/mL His-DTA in the presence or absence of 1 µg/mL PA_{63} in shDMEM at 37 °C for 12 h. Morphological changes were investigated, and pictures taken at the depicted timepoints. After incubation the cells were washed, frozen, and lyzed in hot 2.5x Laemmli buffer with DTT. The samples were than subjected to SDS-PAGE with subsequent Western blotting. Purified His-DTA loaded to the far-right lane was used as control. Using an anti-His antibody His-DTA was detected and for comparison of equal protein loading Hsp90 was detected.
(c) PA_{63} mediates delivery of His-DTA into the cytosol of MDA-MB-231 cells. Prior to the addition of the proteins the cells were incubated with BafA1 (30 nM, shaded in grey) for 30 min. at 37 °C. Afterwards, incubation with His-DTA (5 µg/mL) in the presence or absence of PA_{63} (1 µg/mL) in shDMEM at 37 °C took place for 12 h. The cells were washed, lyzed and a sequential ADP-ribosylation of EF-2 was performed. Biotinylated NAD^+ (10 mM) was used as substrate allowing precipitation of modified proteins via Strep-POD after the samples were subjected to Western blotting. Biotinylated EF-2 was detected by immunoblotting, GAPDH served as loading control.
(d) PA_{63}-mediated delivery reduces MDA-MB-231 cell-viability. MDA-MB-231 cells were seeded into a 96-well plate and left untreated or were incubated with 5 µg/mL His-DTA in the presence or absence of 1 µg/mL PA_{63} in shDMEM for 24 h at 37 °C. Staurosporine was used as positive control at a concentration of 1µM. The cell viability was assessed using the MTS assay. Results are given as average ± SD (n=3), significance was tested using the One-Way ANOVA followed by Dunnett´s multiple comparison test with a 99.9 % confidence interval, referring to the untreated negative control, **p≤0.01, ***p≤0.001. (Figure derived from Felix et al., 2020; permission from CC BY 4.0.)

This effect was reversed when pretreating the cells with BafA1 prior to the incubation with the proteins. These findings correlate with the significant reduction of cell viability (Figure 11d) after 24 h of incubation with His-DTA and PA_{63} in combination. The MTS assay showed a reduction to almost the level of the positive control staurosporine. His-DTA alone did not affect the cells viability negatively.

3.3.2. PA_{63} mediates Delivery of His-DTA into HeLa cells

HeLa cells were subjected to the same set of experiments as MDA-MB-231 cells. After intoxication for 3 h, the cells were immunostained and immunofluorescence microscopy was performed. As shown in Figure 12a, in the presence of PA_{63} the number of signals for His-DTA (green) was clearly increased compared to untreated or His-DTA only treated cells. In addition, co-staining of F-actin (red) clearly showed cell rounding. Furthermore, analyzing intracellular His-DTA via Western blot analysis revealed a band at the same height as purified His-DTA loaded into the far-right lane.

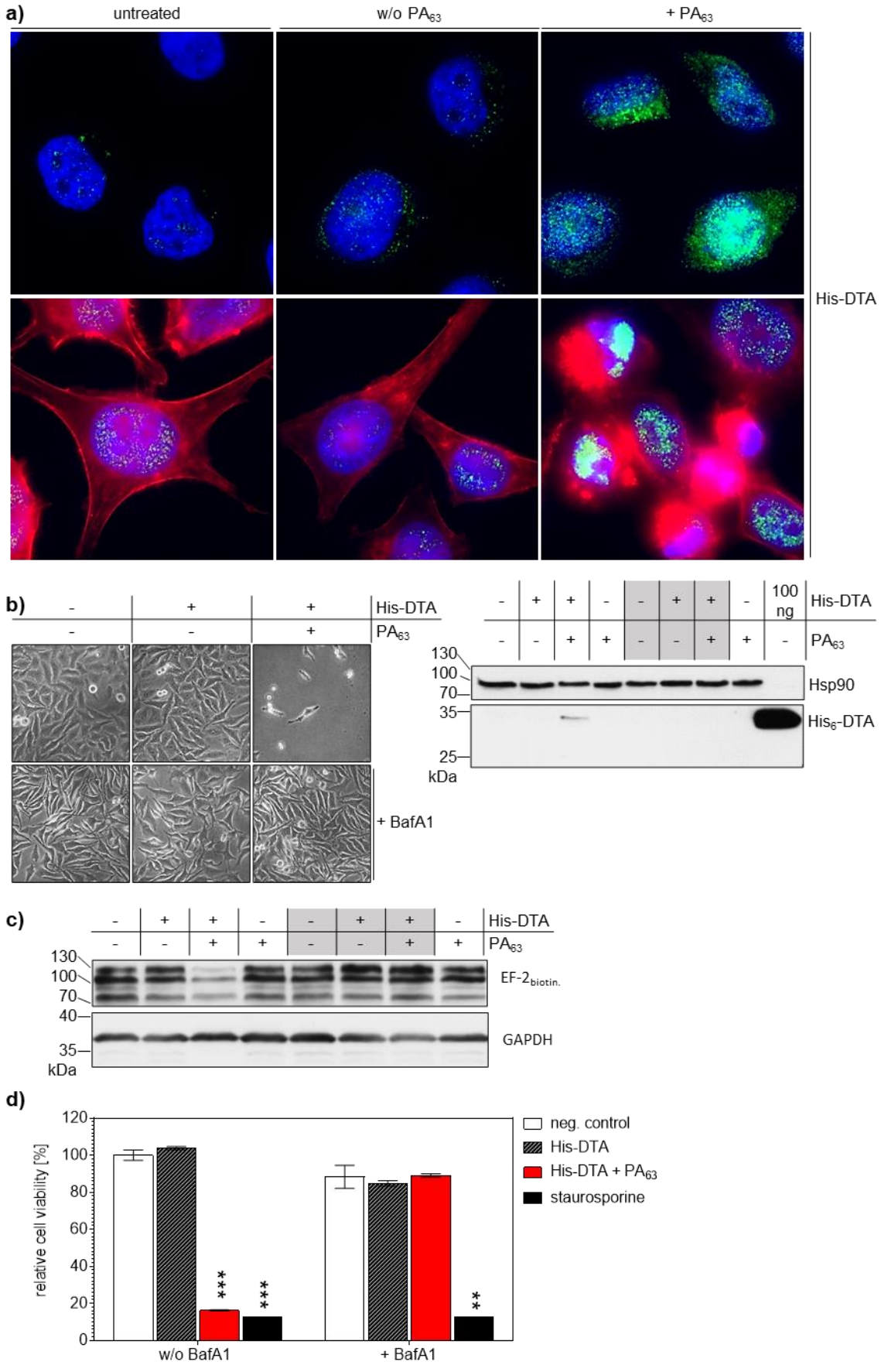

a)
untreated
w/o PA63
+ PA63
His-DTA
b)
His-DTA
PA63
+ BafA1
100 ng
130
100
70
35
25
kDa
Hsp90
His6-DTA
c)
His-DTA
PA63
130
100
70
40
35
kDa
EF-2biotin.
GAPDH
d)
relative cell viability [%]
120
100
80
60
40
20
0
***
***
**
w/o BafA1
+ BafA1
neg. control
His-DTA
His-DTA + PA63
staurosporine

Figure 12: His-DTA delivered via PA_{63} reaches the cytosol HeLa cells as enzymatically active protein.
(a) PA_{63} mediates His-DTA-delivery into HeLa cells and induces morphological changes. HeLa cells were seeded into an 8-well µ-slide and incubated with His-DTA (5 µg/mL) in the presence or absence of PA_{63} (1 µg/mL) in sfMEM at 37 °C for 3 h. Proteins were visualized via fluorescence microscopy. His-DTA (green) was targeted using an anti-His antibody with subsequent immunostaining with a goat anti-mouse-Alexa Fluor568 antibody. F-actin cytoskeleton was stained using Phalloidin-FITC (red), Nuclei were stained with Hoechst 333342 (blue). Phalloidin-staining was used to visualize cell rounding induced by His-DTA.
(b) BafA1 blocks the PA_{63}-mediated uptake of His-DTA into HeLa cells. HeLa cells were seeded into a 24-well plate and incubated with BafA1 (30 nM) for 30 min. at 37 °C prior to protein addition (shaded in grey). Cells were either left untreated or incubated with 5µg/mL His-DTA and 1 µg/mL PA_{63} in combination or His-DTA only in shMEM at 37 °C for 24 h. Morphological changes were investigated, and pictures taken at the depicted timepoints. After incubation the cells were washed, frozen, and lyzed in hot 2.5x Laemmli buffer with DTT. The samples were than subjected to SDS-PAGE with subsequent Western blotting. Purified His-DTA (100 ng) was loaded to the lane on the far right and used as control. His-DTA was detected using an anti-His antibody. For comparison of equal protein loading Hsp90 was detected.
(c) PA_{63} mediates delivery of His-DTA into the cytosol of HeLa cells. Prior to the addition of the proteins the cells were incubated with BafA1 (30 nM, shaded in grey) for 30 min. at 37 °C. Afterwards, incubation with His-DTA (5 µg/mL) in the presence or absence of PA_{63} (1 µg/mL) in shMEM at 37 °C took place for 12 h. The cells were washed, lyzed and a sequential ADP-ribosylation of EF-2 was performed. Biotinylated NAD+ (10 mM) was used as substrate allowing precipitation of modified proteins via Strep-POD after the samples were subjected to Western blotting. Biotinylated EF-2 was detected by immunoblotting, GAPDH served as loading control.
(d) PA_{63}-mediated delivery reduces HeLa cell-viability. HeLa cells were seeded into a 96-well plate and left untreated or were incubated with 5µg/mL His-DTA alone or in combination with 1 µg/mL PA_{63} in shMEM for 24 h at 37 °C. Staurosporine was used as positive control at a concentration of 1µM. The cell viability was assessed using the MTS assay. Results are given as average ± SD (n=3), significance was tested using the One-Way ANOVA followed by Dunnett´s multiple comparison test with a 99.9 % confidence interval, referring to the untreated negative control, **p≤0.01, ***p≤0.001. (Figure derived from Felix et al., 2020; permission from CC BY 4.0.)

These results are in line with the corresponding cell rounding. Pretreatment with BafA1 before incubation with His-DTA in the presence of PA_{63} for 24 h (Figure 12b) presented a clear lack of signal. BafA1-treatment prevented His-DTA uptake into HeLa cells. The results were in line with the results of the analysis of the EF-2-riboslyation status (Figure 12c). Only His-DTA plus PA_{63} reduced the band intensity drastically and pretreatment with BafA1 reversed this effect. The cell viability assay (Figure 12d) performed after 24 h of incubation presented the same trend. Treatment with His-DTA plus PA63 reduced the viability of HeLa cells to almost the level of the positive control and pretreatment with BafA1 protected the cells from intoxication with His-DTA.

In conclusion, the results for MDA-MB-231 cells are not only comparable to the results for HeLa cells but confirm the PA_{63}-specific delivery of enzymatically active His-DTA into the cytosol of MDA-MB-231 cells. However, the specific changes in

morphology (cell rounding) upon treatment with His-DTA plus PA_{63} found for HeLa cells were not as pronounced in MDA-MB-231 cells as in HeLa cells.

Taken together, these different approaches confirmed that the changes in morphology, EF-2-ribosylation status and the drastic reduction in cell viability after treatment of HeLa cells with His-DTA plus PA_{63} are due to cytosolic localization of enzymatically active His-DTA, which was delivered into the cytosol by PA_{63}.

3.4. PA_{63} mediates the Binding of His-NDPK-A to MDA-MB-231 and HeLa cells

Encouraged by the finding that PA_{63} successfully delivered the reference cargo His-DTA into the cytosol of HeLa as well as MDA-MB-231 cells, the same approach

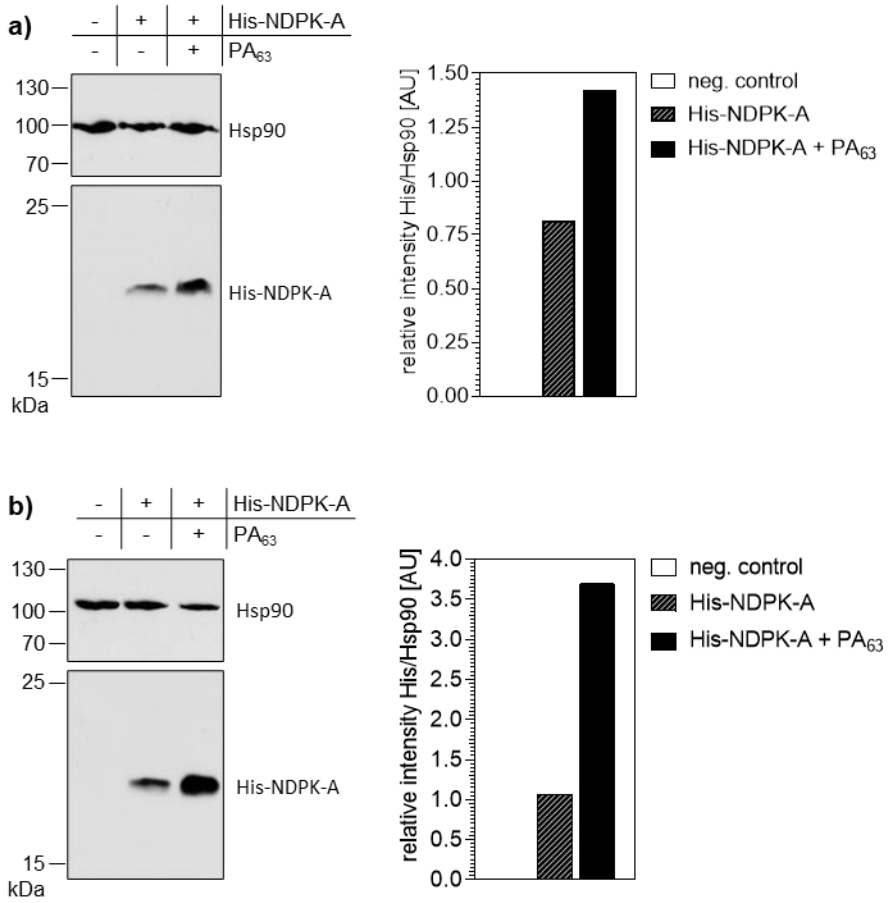


Figure 13: PA_{63} mediates the binding of His-NDPK-A to HeLa and MDA-MB-231 cells.
(a) MDA-MB-231 cells and (b) HeLa cells were seeded into a 12-well plate and adjusted to 4 °C for 15 min. prior to the experiment. After washing the cells with cold PBS the proteins (30 µg/mL His-NDPK-A in the presence or absence of 3 µg/mL PA_{63}) were added in sfMEM (HeLa) or sfDMEM (MDA-MB-231) and incubated on ice for 30 min.. To stop the binding process via removal of the proteins the cells were washed with cold PBS again and frozen. After cell lysis with 2.5x Laemmli the samples were subjected to Western blotting to determine the amount of His-NDPK-A bound to the cells with an anti-His antibody, Hsp90 was detected for the comparison of equal protein loading. Densitometric analysis to quantify of the signal intensity of His-NDPK-A against the signal intensity of Hsp90 was performed with the ImageJ software. (Figure derived from Felix et al., 2020; permission from CC BY 4.0.)

was used for the delivery of the model cargo His-NDPK-A. First it was investigated whether PA_{63} is able to bind His-NDPK-A to the cell surface of MDA-MB-231 (Figure 13a) as well as HeLa cells (Figure 13b). Therefore, the cells were incubated with His-NDPK-A in the presence or absence of PA_{63} at 4 °C. This low temperature allows binding but prevents uptake due to a reduced membrane flexibility. Here, the proteins were prepared in serum-free medium to prevent any interference of FCS components during the binding process. Western blot analysis was then used to determine the amount of cell-bound His-NDPK-A. For both cell lines, immunoblotting with an anti-His antibody revealed some unspecific binding of His-NDPK-A without the transporter present. However, both cell lines also showed a clear increase in band intensity when PA_{63} was present, suggesting a PA_{63}-specificity for binding. Densitometric analysis revealed that the amount of His-NDPK-A specifically bound via PA_{63} to MDA-MB-231 cells was higher compared to HeLa cells. This could be due to different availability or expression levels of the anthrax toxin receptors in MDA-MB-231 cells. In conclusion, both cell lines were susceptible to binding of His-NDPK-A via PA_{63}.

3.5. PA_{63} Mediates Delivery of His-NDPK-A into the Cytosol of MDA-MB-231 and HeLa cells

After confirming PA_{63}-specific cell-binding to the reference cell line HeLa as well as to the model cell line MDA-MB-231, several approaches were tested to analyze the uptake of the target-cargo His-NDPK-A into both cell lines.

3.5.1. PA_{63} Mediates Delivery of His-NDPK-A into MDA-MB-231 cells

MDA-MB-231 cells were incubated with His-NDPK-A in different concentrations comparably to an intoxication assay. The cellular response regarding changes in cell morphology and cell viability over the course of a total of 48 h were investigated.

After incubation of the cells with either the low or the high concentrations of His-NDPK-A with or without PA_{63} present for 48 h (Figure 14a), no changes in cell morphology or negative effects on cell viability could be found. Only cells treated with DMSO as positive control for the MTS assay showed clear changes in morphology and a reduction of cell viability to around 40 %. Applying the lower concentration to MDA-MB-231 cells for 48 h prior to performing fluorescence microscopy resulted in the same pattern of PA_{63}-mediated delivery of His-DTA

(Figure 14b). Some unspecific signals for all conditions were present when treating only with His-NDPK-A, under the presence of PA_{63} the number of signals for His-NDPK-A however were markedly increased. This PA_{63}-specific uptake was also present when analyzing MDA-MB-231 cells after treatment with His-NDPK-A in the presence or absence of PA_{63} via Western blotting (Figure 14c). Immunostaining with an anti-nm23-H1 antibody allowed the distinguishment between endogenous NDPK-A in the cell lysate (17 kDa) and introduced recombinant His-NDPK-A

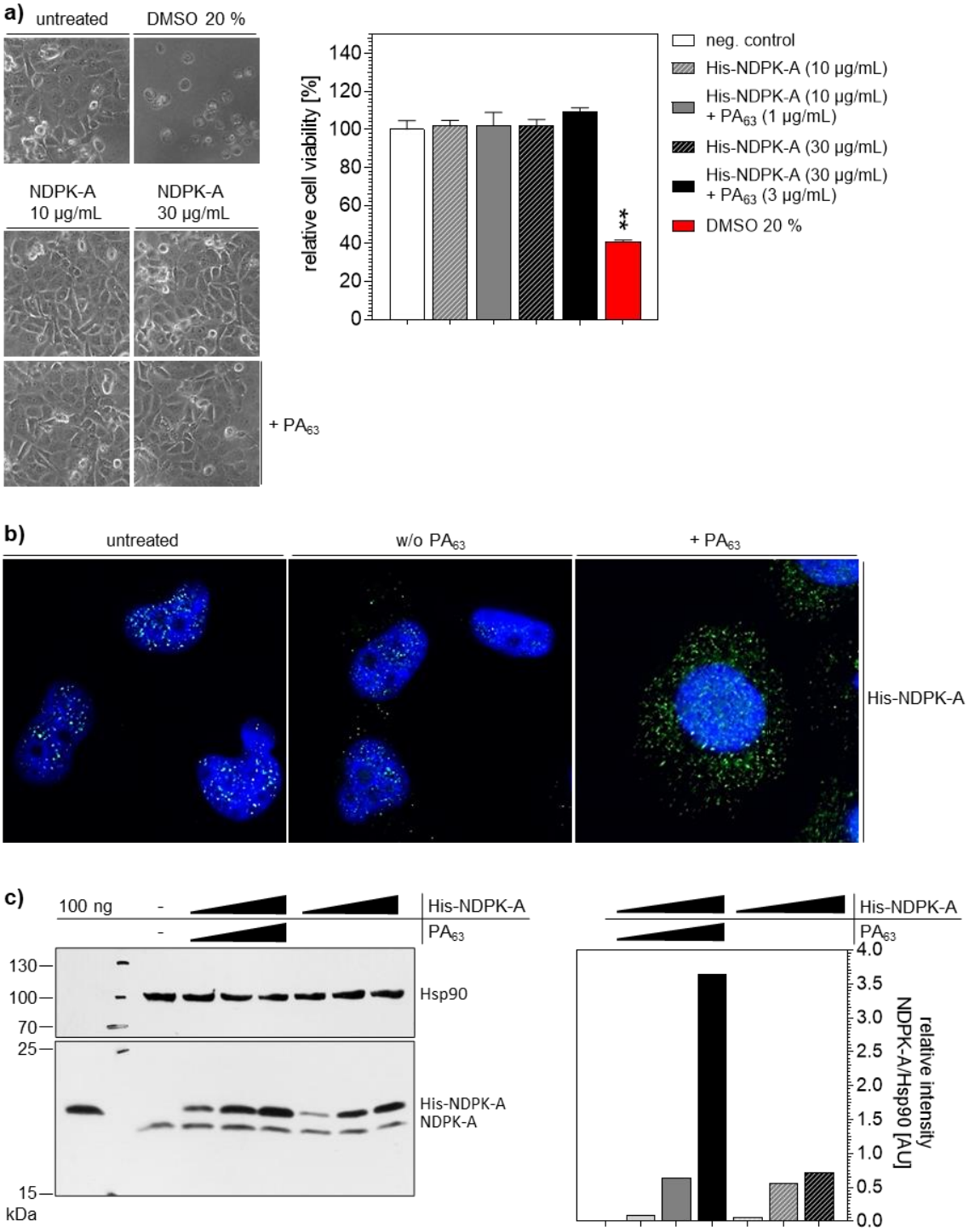


Figure 14: PA_{63} delivers His-NDPK-A into MDA-MB-231 cells.
a) Treatment with His-NDPK-A does neither effect cell morphology nor cell-viability of MDA-MB-231 cells. After seeding of MDA-MB-231 into a 96-well plate they were incubated with 10 µg/mL or 30 µg/mL His-NDPK-A in the presence or absence of 1 µg/mL or 3 µg/mL PA_{63} in shDMEM at 37 °C for 48 h. DMSO 20 % was used as positive control for the subsequent MTS assay to assesses cell viability. Results are given as average ± SD (n=3), significance was tested using the One-Way ANOVA followed by Dunnett´s multiple comparison test with a 99.9 % confidence interval, referring to the untreated negative control, **p≤0.01.
PA_{63} mediates delivery of His-NDPK-A into MDA-MB-231 cells.
(b) For fluorescence microscopy MDA-MB-231 cells were seeded into an 8-well µ-slide and incubated with His-NDPK-A (10 µg/mL) in the presence or absence of PA_{63} (1 µg/mL) in shMEM at 37 °C for 48 h. Proteins were visualized via immunostainig. His-NDPK-A (green) was targeted using an anti-His antibody with subsequent immunostaining via a goat anti-mouse-Alexa Fluor568 antibody. Nuclei were stained with Hoechst 333342 (blue). (Figure derived from Felix et al., 2020; permission from CC BY 4.0.)
(c) Delivery of His-NDPK-A into the cytosol of MDA-MB-231 cells is concentration-dependent. MDA-MB-231 cells were seeded into a 12-well plate and incubated with His-NDPK-A with or without PA_{63} present in shDMEM for 6 h at 37 °C. Concentrations of His-NDPK-A and PA_{63} used were 10+1, 18+6 or 30+3 µg/mL, respectively. Cells were lyzed in hot 2.5x Laemmli buffer with DTT and a SDS-PAGE with subsequent Western blotting was performed to determine the amount of His-NDPK-A delivered. For His-NDPK-A detection a specific anti-nm23-H1 antibody was used. Purified His-NDPK-A was loaded to the lane on the far left as control to distinguish between endogenous NDPK-A (17 kDa) from the cell-lysate and delivered His-NDPK-A (18 kDa). For comparison of equal protein loading Hsp90 was detected. For the quantification of His-NDPK-A a densitometric analysis of the signal intensity of the upper band (His-NDPK-A, 18 kDa) against the signal intensity of Hsp90 was performed with the ImageJ software.

(18 kDa). After 12 h of incubation a concentration-dependent uptake of His-NDPK-A was detected when PA_{63} was applied in combination with the tumor metastasis suppressor protein. However, MDA-MB-231 cells again presented some unspecific uptake of His-NDPK-A. Via densitometric analysis the PA_{63}-specificity could be confirmed. For the highest concentration used (30 µg/mL His-NDPK-A plus 3 µg/mL PA_{63}) a clear increase in signal intensity was present when PA_{63} was used during the incubation. The amount of endogenous NDPK-A however, was not affected by the treatment.

3.5.2. PA_{63} Mediates Delivery of His-NDPK-A into HeLa cells

HeLa cells were incubated with His-NDPK-A as described for MDA-MB-231 cells. In short, the cellular response regarding changes in cell morphology and cell viability over the course of a total of 48 h after treatment were investigated (Figure 15a). Monitoring the cells via bright-field microscopy presented no changes in cell morphology of HeLa cells for the low as well as the high concentration of His-NDPK-A either with or without PA_{63} present. The cells appeared comparable to the untreated controls. Only cells treated with DMSO (20 %) as positive control for the following MTS assay showed the expected changes. The findings for changes in cell viability upon treatment were in line with these findings. None of the treatments with His-NDPK-A affected HeLa cell viability. Only DMSO as positive

control reduced cell viability to around 30 % compared to untreated controls. To confirm uptake of His-NDPK-A and its localization HeLa cells were treated with His-NDPK-A in the presence or absence of PA_{63} and after immunostaining immunofluorescence microscopy was performed (Figure 15b). Already after 3 h of incubation of HeLa cells with the proteins in the lower concentration the signal for His-NDPK-A was strongly increased when the transporter was presented. His-NDPK-A only treatment however was comparable in signal to the negative control, here for all samples low unspecific signal was found. With Western blotting as alternative approach the His-NDPK-A delivery was further analyzed (Figure 15c).

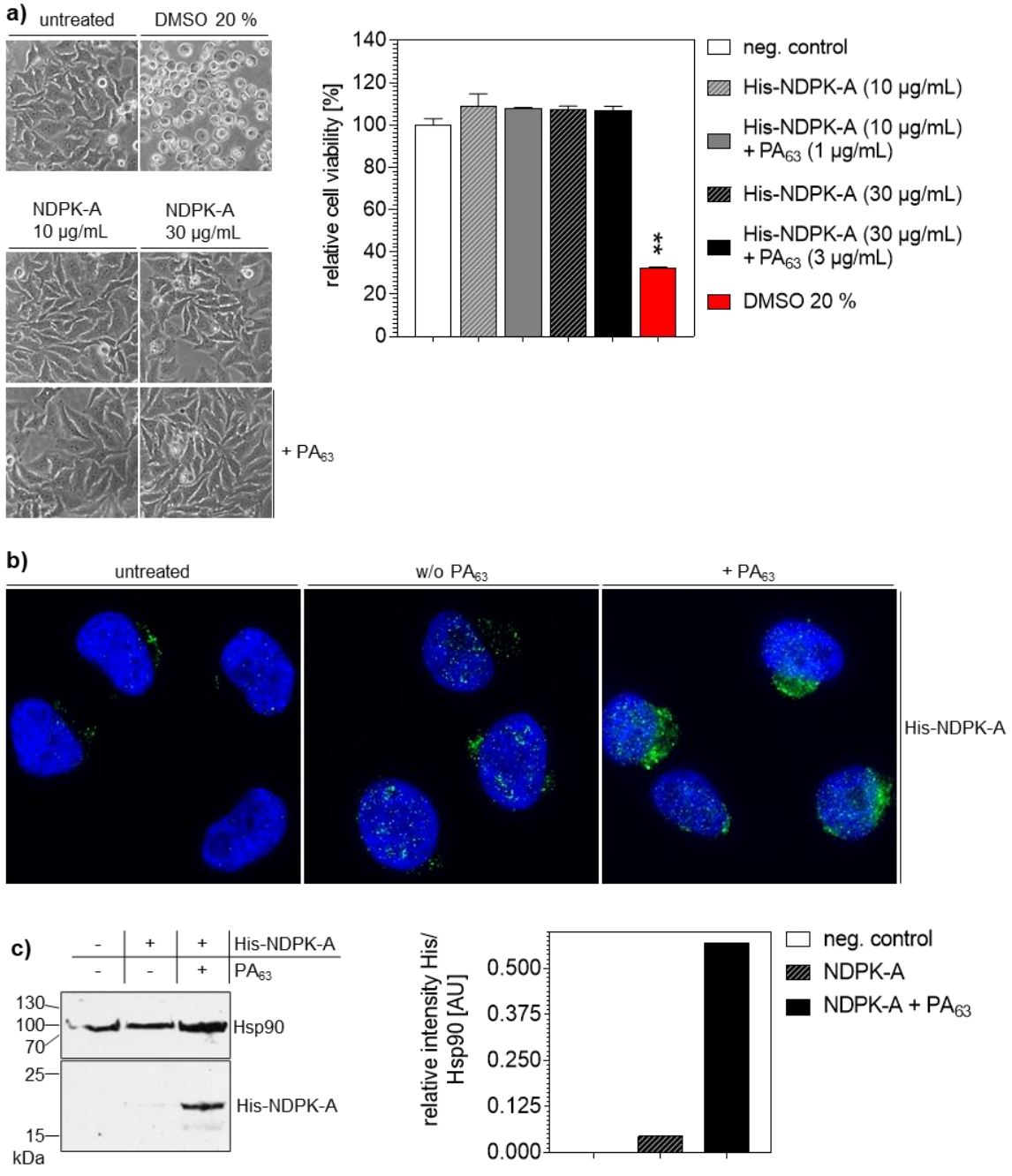


Figure 15: PA_{63} delivers His-NDPK-A into HeLa cells.
a) Treatment of HeLa cells with His-NDPK-A does neither effect cell morphology nor cell-viability. HeLa cells were seeded into a 96-well plate and incubated with 10 µg/mL or 30 µg/mL His-NDPK-A in the presence or absence of 1 µg/mL or 3 µg/mL PA_{63} in shMEM at 37 °C for 48 h. DMSO 20 % was used as positive control for the subsequent MTS assay to assesses cell viability. Results are given as average ± SD (n=3), significance was tested using the One-Way ANOVA followed by Dunnett´s multiple comparison test with a 99.9 % confidence interval, referring to the untreated negative control, **p≤0.01.
PA_{63} mediates delivery of His-NDPK-A into the cytosol of HeLa cells.
(b) For fluorescence microscopy HeLa cells were seeded into an 8-well µ-slide and incubated with His-NDPK-A (10 µg/mL) in the presence or absence of PA_{63} (1 µg/mL) in sfMEM at 37 °C for 3 h. Proteins were visualized via immunostainig. His-NDPK-A (green) was targeted using an anti-His antibody with subsequent immunostaining via a goat anti-mouse-Alexa Fluor568 antibody. Nuclei were stained with Hoechst 333342 (blue). (Figure derived from Felix et al., 2020; permission from CC BY 4.0.)
(c) HeLa cells were seeded into a 12-well plate and incubated with 10 µg/mL His-NDPK-A with or without 1 µg/mL PA_{63} present in sfMEM for 6 h at 37 °C. After cell lysis in hot 2.5x Laemmli buffer with DTT the samples were subjected to Immunoblotting. The delivered His-NDPK-A was detected via an anti-His antibody. For comparison of equal protein loading Hsp90 was detected. For the quantification of His-NDPK-A a densitometric analysis of the signal intensity of His-NDPK-A against the signal intensity of Hsp90 was performed with the ImageJ software.

Immunostaining of His-NDPK-A with the anti-His antibody resulted in the detection of a clearly visible band present only, when PA_{63} was used during incubation. This was even more obvious after densitometric analysis of the blot. Compared to the approach using fluorescence microscopy, an incubation time of 6 h was applied. Tthis was due to the methods lower sensitivity of Western blotting compared to fluorescence microscopy.

Taken together, MDA-MB-231 cells respond to treatment with His-NDPK-A and PA_{63} in a comparable manner as HeLa cells. A clear dependency of PA_{63} for the delivery and therefore uptake of His-NDPK-A into both cell lines was found. No adverse effects on cell morphology or cell viability could be observed.

3.6. Treatment of MDA-MB-231 cells with His-NDPK-A plus PA_{63} Decreased Migration

Prompted by the results regarding transport of His-NDPK-A as tumor metastasis suppressor protein into the cytosol of MDA-MB-231 cells, the effect of this introduced protein the migration of these breast cancer cells was investigated.

For this purpose, a wound-healing assay was performed. MDA-MB-231 cells were seeded into a two-well insert which was placed in a 24-well plate. Via detachment of the insert after adherence of the cells a wound was created allowing the monitoring of cellular behavior upon treatment. Any detached cells were removed by washing of the wells before the application of the proteins. Tested was a

combination of the target cargo His-NDPK-A as well as His-DTA as reference cargo in the presence or absence of PA_{63}. His-DTA was used as positive control in this assay. The cells were incubated for up to 24 h, the wound area was monitored via microscopic analysis and a relative scratch-area was determined based on the

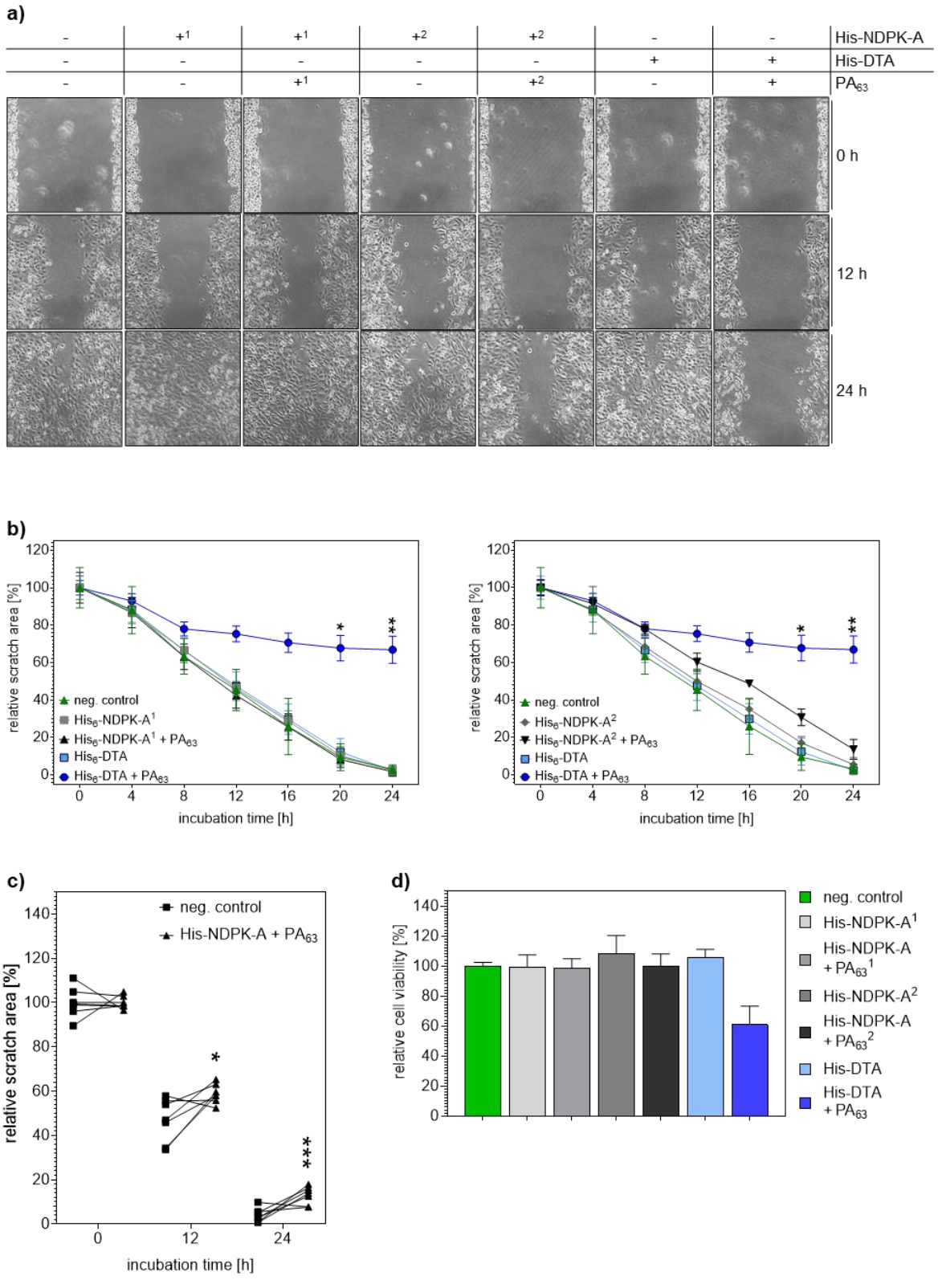


Figure 16: His-NDPK-A delivered by PA_{63} reduces cell-migration of MDA-MB-231 cells in vitro.
(a) For the wound-healing assay MDA-MB-231 cells were seeded into 2-well ibidi culture inserts 24 h prior to the treatment. Right before adding the proteins the insert was removed leaving an area without cells, thereby creating the wound (scratch). For treatment His-NDPK-A (^{1}10 µg/mL as low concentration, ^{2}30 µg/mL as high concentration) was applied to the cells in the presence or absence of PA_{63} (^{1}1 µg/mL as low concentration, ^{2}3 µg/mL as high concentration) in shDMEM. As controls cells were either left untreated or treated with His-DTA (5 µg/mL) with or without of PA_{63} (1 µg/mL). Morphological changes of the scratch area of all assay triplicates were monitored via the acquisition of pictures at 3 different areas per scratch at the indicated timepoints, representative pictures are shown.
(b) Reduction of MDA-MB-231 migration is concentration-dependent. The relative surface of the wound area was quantitatively analyzed via the ImageJ software. Data for the low concentration is shown on the right, data for the high concentration is shown on he left. For each timepoint before and after treatment (every 4 hours) the significance was tested by One-Way-ANOVA followed by Dunnett´s multiple comparison test with a 99.9 % confidence interval, referring to the untreated negative control, * $p \leq 0.05$, ** $p \leq 0.01$ referring to untreated controls, n = 3. (c) Data from three independent experiments after 12 and 24 h of treatment were analyzed and are depicted as scatter plots. Seven replicates in total are used to visualize the statistical significance of each replicate. Significance was tested via a modified t-test using the two-stage step-up method of Benjamini, Krieger and Yekutieli, which does not assume equal distribution. * $p \leq 0.05$, *** $p \leq 0.001$ referring to untreated controls, n = 7.
(d) Cell viability is not negatively affected after 48 h of treatment with His-NDPK-A and PA_{63}. Cell viability was tested via MTS assay. Results are given as average ± SD (n=3), significance was tested using the One-Way ANOVA followed by Dunnett´s multiple comparison test with a 99.9 % confidence interval, referring to the untreated negative control. No conditions affected the cell viability significantly. (Figure derived from Felix et al., 2020; permission from CC BY 4.0.)

photo-documentation. Representative pictures show a concentration dependent reduction in closure of the scratch area over time when PA_{63} was present (Figure 16a) with both His-tagged proteins.

The low concentration of His-NDPK-A used (marked with ^{1}) was not able to block cellular intrusion into the wound area whereas the high concentration used (marked with ^{2}) reduced the number of the cells in the wound area after 12 h markedly. His-NDPK-A only-treatment did not produce such an effect. Only when PA_{63} was present in combination with His-NDPK-A the scratch-area remained more open compared to the untreated controls. After 24 h of incubation this effect was still clearly visible. However, only the positive control His-DTA in combination with PA_{63} was able to reduce scratch-closure significantly. The automated determination of the relative scratch area confirmed these results suggesting a reduced migration of these MDA-MB-231 cells. The change in wound-area was correlated to the area before treatment (Figure 16b) showing clearly that treatment with the high concentration of His-NDPK-A plus PA_{63} reduced migration in a sustained way from 8 h up to 24 h of incubation. As already visible in the representative pictures, His-DTA plus PA_{63} reduced migration as the positive control as expected. After 8 h the maximum migration of cells was reached and sustained over the course of the experiment. In

addition, after 24 h cell rounding was visible. As shown in the scatter plots of Figure 16c data from three independent experiments corroborate the result of the single experiment. The relative scratch area of cells treated with His-NDPK-A plus PA_{63} after 12 h and 24 h was significantly larger compared to untreated cells. In line with these findings and especially the cell rounding present for the positive control are the results of the cell viability assay performed after 48 h of treatment (Figure 16d). Only His-DTA in the presence of PA_{63} reduced the cell viability compared to untreated controls.

In summary, these results implicate a delivery of His-NDPK-A into the cytosol of MDA-MB-231 cells, which reduces the migratory behavior of these breast cancer cells *in vitro*.

4. Discussion

Anthrax toxins are the causative agents for the severe disease anthrax. Reports of first documented cases of anthrax date back to literature of the Greeks. The disease was more specifically described in 1752 by Moret (Bhatnagar & Batra, 2001). It continuous to be a disease of health importance today with occasional outbreaks reported for humans and animals such as a case of human anthrax in Zimbabwe in 2013/2014 following a lethal anthrax outbreak in cattle (Makurumidze et al., 2021), two human outbreaks in Hungary in 2019 (European Centre for Disease Prevention and Control (ECDC), 2019) or the outbreak in the US in white-tailed deer just recently in august this year (Texas Animal Health Commssion, 2021).

The anthrax toxins are produced by *B. anthracis* and are the result of an evolutionary arms race between hosts and pathogens where the bacteria has created a niche for itself to replicate and disseminate via disabling cells of the mammalian immune system (Young & Collier, 2007). Anthrax toxins are one of the most prominent examples of AB_7-toxins and are of binary nature. They consist of an A- and B-component. For the B-component seven monomers oligomerize to form a heptameric prepore structure, hence AB_7. To elicit its cytotoxic potential the catalytic A-component must be introduced into the cytosol of cells. Although the three-component anthrax toxin presents two different catalytic components, the lethal and the edema factor, both rely on the common transport B-component PA for cell-entry. PA hereby singularly mediates this crucial step by providing receptor binding as well as the mediation of translocation into the cytosol of target cells. To this end, the toxins exploit cellular trafficking systems and host-cell factors. This highly specific mode of cell entry results in the high potency and efficiency of these toxins.

Excitingly, it was discovered that PA was able to not only serve as a molecular delivery tool for its native cargo LF and EF but was also able to introduce a large variety of other non-native (Arora & Leppla, 1994) and foreign molecules (Rabideau & Pentelute, 2016) into the cytosol of cells when fused to the PA-binding domain LF_N of LF. This PA_{63}-LF_N system has its limitations and is associated with the generation of new constructs, cloning, expression, purification and characterization of new chimeras. The fused LF_N-sequence could potentially have an impact on all the steps of protein production mentioned before and in the worst-case result in an

incorrectly or unfolded fusion-protein due to steric hindrance. Conveniently, it was also described that a polycationic tail fused to non-native toxin components instead of LF_N is sufficient for delivery via PA_{63} (Blanke et al., 1996). This could be explained by the comparable molecular properties of polycationic tails such as a His_6-tag and LF_N. The presented positively charged residues of the linkers interacts with the negatively charged amino acids lining the lumen of the PA pore and thereby allow translocation into the cytosol (Brown et al., 2011; Feld et al., 2012). Compared to LF_N-fusion, the His-tag-PA_{63} system was only described for toxin-derived cargo so far.

Therefore, this thesis aimed towards a proof-of-concept that also non-toxin derived cargo such as the human tumor metastasis suppressor protein NDPK-A can be delivered into the cytosol of cells via PA_{63}.

Firstly, both components of the transport system were expressed and purified for further characterization and utilization in this thesis (see Figure 7 and Figure 8). Expression-protocols of both proteins required adjustments for maximum yield and purity.

In case of PA_{63} the expression and following purification was performed as previously described (Ost et al., 2019). However, PA_{63} for this thesis was expressed in Rosetta instead of BL21 *E. coli*, purified via Ni^{2+}-NTA resin instead of Ni^{2+}-IDA resin and the finale storage buffer was supplemented with glycerol and polysorbate. Additionally, an additional size-exclusion chromatography via the ÄKTA explorer FPLC system was included for diafiltration to exchange the buffer as well as to separate large aggregates and other impurities observed from the target protein. Since these changes could have affected the biological activity of PA_{63}, an intoxication assay was performed on HeLa cells that confirmed full functionality as transport component. The used cargo His-DTA efficiently induced cytotoxicity resulting in the typical cell rounding. The effects found for the treatment with His-DTA plus PA_{63} were comparable to the results for the full-length DT toxin. DT (single-chain AB-type toxin) however delivers its DTA-domain, most likely via a trans-membrane pore formed by its T-domain in endosomal membranes into the cytosol (Lemichez et al., 1997; Papini, Cabrini, et al., 1993; Papini, Rappuoli, et al., 1993). Cell rounding was also further used as a specific and highly sensitive

endpoint for cytosolic localization of His-DTA, as described earlier (Blumenthal et al., 2007; Schnell et al., 2016).

The recombinantly produced human His-NDPK-A was also tested upon biological activity. For NDPK-A a mammalian histidine kinases (Attwood, 2013) and 3′-5′-exonuclease activity relevant in DNA repair (Kaetzel et al., 2006) were described. The protein also harbors a nucleoside diphosphate kinase activity, where NDPK-A transfers a phosphate group from ATP to nucleoside diphosphates (Lacombe et al., 2000; Lascu & Gonin, 2000). The latter was used to confirm enzymatic activity *in vitro* with two different methods. Both, the autophosphorylation assay as well as the kinase activity assay confirmed full enzymatic activity after purification.

4.1. The Human Breast Cancer Cell line MDA-MB-231 is Susceptible to the Delivery of His-tagged Cargo Proteins via PA_{63}

The underlying mechanisms resulting in the anti-metastatic properties of NDPK-A are not fully understood but may be due to a wide range of activities. Described is for instance the formation of complexes with proteins such as nucleotide exchange factors, transcriptional regulators, cell growth regulators, and cytoskeletal components (Marino et al., 2011). Controversially, numerous clinical studies reported an inverse correlation between NDPK-A expression and the metastatic potential of epithelial tumors like breast, liver, colon, ovarian, lung and skin. Here, a NDPK-A expression correlates with poor clinical outcome. A direct correlation was however found for hematopoietic malignancies, neuroblastoma, and osteosarcoma (Lacombe & Boissan, 2013; Marino et al., 2012). These findings emphasize that the cellular context in which NDPK-A can be investigated regarding a potentially inhibitory effect on migration and metastasis is crucial. To this end, the breast cancer cell line MDA-MB-231 was used in this thesis for which a reduction of migration and motility was induced by restoring expression of NDPK-A (Horak et al., 2007; Kantor et al., 1993; Marino et al., 2013). To exclude however, that any potential uptake of His-NDPK-A found is based on an unexpected cell-type selectivity for MDA-MB-231 cells, HeLa cells were tested in parallel as a reference cell line. As established cell line for assays with PA_{63} as transporter for toxin-derived cargo, the cell lines specific endpoints for the treatment with His-DTA plus PA_{63} were predictable and served as reference points for the treatment of MDA-MB-231 cells. Since there is no direct

approach to determine delivery of His-NDPK-A into the cytosol, His-DTA was used as reference cargo during the investigation of PA_{63}-sensitivity of MDA-MB-231 cells.

Intoxication of both HeLa (Figure 10) and MDA-MB-231 (Figure 9) cells with His-DTA plus PA_{63} resulted in an obvious change in morphology. Microscopic analysis allowed direct correlation of the cell rounding and the presence of enzymatically active His-DTA in the cytosol of cells. These effects were only present when the transporter PA_{63} was applied in parallel. In line with these findings was that the inhibition of endosomal acidification with BafA1 blocked this effect in both cell lines. With this it was confirmed for the first time that MDA-MB-231 cells are susceptible to the delivery of His-DTA with PA_{63}. Immunofluorescence microscopy confirmed the localization of His-DTA in the cytosol. Western blotting verified that the observed cell-rounding and reduced cell viability was due to cytosolic EF-2-ribosylation via His-DTA in HeLa and MDA-MB-231 cells.

Based on these promising results the same approaches were applied to analyze the delivery of His-NDPK-A as cargo. Here it was shown that PA_{63} mediates not only binding (Figure 13) but also uptake of His-NDPK-A into either HeLa (Figure 15) or MDA-MB-231 (Figure 14) cells. However, it has be noted here that both cell lines did present some unspecific binding of His-NDPK-A without the transporter PA_{63} present. As soon as the transporter was present, the binding was drastically increased in a two-fold fashion for MDA-MB-231 cells and almost tripled for HeLa cells.

However, MDA-MB-231 cells seemed to be less sensitive to PA_{63}-mediated binding and delivery of His-cargo in general compared to HeLa cells. This could be due to a reduced availability of the PA receptors TEM8/CMG2 based on a different distribution or expression.

4.2. Delivery of His-NDPK-A into the Cytosol of MDA-MB-231 cells via PA_{63} Decreases Cellular Migration

Since there is no direct way to monitor the delivery of His-NDPK-A into the cytosol of cells, an indirect approach was applied to analyze whether the cargo reaches its destination enzymatically active. This functional analysis has already been described for after transfection-based overexpression of NDPK-A (Khan et al., 2019). For that purpose, the cells were subjected to a wound healing assay and

monitored over time regarding migration. The number of cells migrating into the wound area after treatment with the combination of His-NDPK-A and PA_{63} was less compared to His-NDPK-A only or untreated cells. With this it could be excluded that the unspecific binding of His-NDPK-A alone observed earlier contributes to effects on cellular migration of MDA-MB-231 cells. The protein most likely binds to cell surface structures and might be endocytosed non-specifically in very low amounts, if at all. The reduced migratory behavior when His-NDPK-A and PA_{63} were present however was not based on a cytotoxic effects or reduced cell-division since only His-DTA plus PA_{63}-treated cells presented less cell viability.

4.3. Conclusions

The data from the experiments performed in this study indicate that PA_{63} can be exploited for the delivery of non-toxin derived, His-linked cargo proteins such as the human tumor metastasis suppressor His-NDPK-A. Here it was shown for the first time that PA_{63} is able to mediate binding and uptake of such “foreign” cargo into the cytosol of human MDA-MB-231 breast cancer cells. The reduction in cell migration

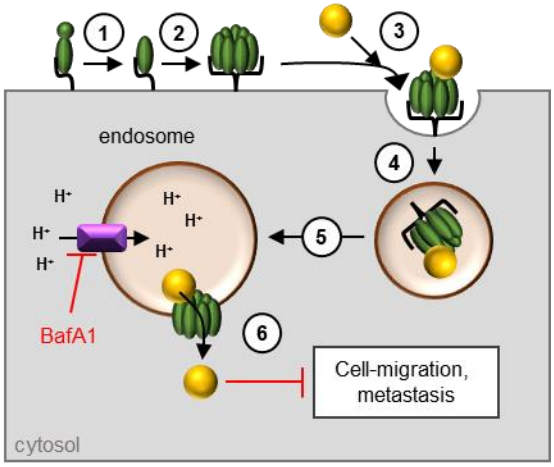


Figure 17: Schematic proposed route of uptake of His-NDPK-A via PA_{63}.
After (1) binding of PA (green) to TEM8/CMG2 and (2) proteolytic activation the oligomerized transporter PA_{63} (3) binds the recombinant His-NDPK-A (yellow) and delivers it into the cytosol of cells via (4) receptor mediated endocytosis. After acidification of the endosome PA_{63} specifically (since BafA1-induced inhibition of the acidification blocks this uptake) mediates (6) translocation of His-NDPK.A into the cytosol where it acts induces reduced cell migration and therefore blocks metastasis (derived from Felix et al., 2020).

was prove for the translocation and cytosolic localization of His-NDPK-A in its active form. Thus, PA_{63} was able to overcome a bottle neck of cellular transport systems such as cell-penetrating peptides, i.e. the efficient translocation from endosomes to the cytosol. The fact that inhibition of endosomal acidification via BafA1 prevents the delivery of the cargo protein into the cytosol, confirms the specific PA_{63}-mediated transport for His-NDPK-A (Figure 17).

4.4. Perspective and Outlook

Optimization of the PA_{63}-mediated Delivery of Recombinant Tumor Metastasis Suppressor Protein NDPK-A into the Cytosol of Certain Cancer Cells

Beyond this thesis the next step towards a clinical application must be the optimization of the transport-system.

One focus should be on a system optimized towards the selective targeting of HER2-positive cells with a highly efficient delivery of recombinant, tagged NDPK-A. HER2-overexpressing cells occur in 20–25% of breast, gastric and ovarian carcinomas (Arteaga et al., 2011; Berchuck et al., 1990; Gravalos & Jimeno, 2008; Slamon et al., 1989) and increased expression of HER2 is associated with an aggressive form of breast cancer with a low rate of patient survival (Arteaga et al., 2011).

Since almost all cells express the anthrax toxin receptors TEM8 and CMG2, our current system cannot be used to target only one selective cell-type. To achieve this goal, PA must be retargeted. Such retargeting of PA_{63} was already described to be effective for targeting matrix metalloprotease (MMPs)-overexpressing tumor cells selectively. Here the furin protease cleavage site of PA_{63} was substituted with sequences selectively cleaved by MMPs. Cytotoxicity was induced via the fusion of LF_N to the ADP-ribosylation domain of Pseudomonas exotoxin A (S. Liu et al., 2000). A promising PA mutant generated by Mechaly et al. mPA, lacks affinity to its native PA receptors due to two single amino acid exchanges (N682A and D683A) within the receptor binding domain (Mechaly et al., 2012). This mutant was fused to the epidermal growth factor (EGF) to generate PA-EGF which delivered LF, EF and LF_N-DTA into EGF-expressing cells. The same mutant mPA was also used shortly after to target HER2-positive cells. The ligand for HER2, ZHER2 was fused to mPA resulting in mPA-ZHER2 which delivered different LF_N-fusion proteins into HER2-positive cells (McCluskey et al., 2013). Another elegant approach was to couple either one of two HER2-recognition proteins (single-chain antibody fragment/ affibody) via a Sortase reaction to mPA. LF_N-DTA as cargo induced selective cytotoxicity in HER2-positive cells (McCluskey & Collier, 2013). Other *in vitro, in vivo and ex vivo* studies did not present indications for obvious immunological reactions upon such treatment (Jack et al., 2020). Therefore, the use of a respectively

modified PA-variant is highly interesting regarding the delivery of His-NDPK-A into for instance HER2-positive breast cancer cells that also show low levels of NDPK-A and high metastasis rates.

Aside from cell-type selectivity, improvement of the efficiency of the system should be in focus as well. Within the first report introducing polycationic tails as an alternative structure for PA binding and cargo-delivery, Blanke et al. also stated that other sequences and especially LF_N were far more efficient in delivery then the His_6-tag used by us and many others (Blanke et al., 1996). In fact, their efficiency was determined as follows: LF_N>Lys_8>Lys_6>Lys_3 whereas His_6 was found to be approximately 100x less efficient compared to Lys_6. For our system exchanging the His_6-tag with other amino acid-tags (Rabideau & Pentelute, 2016; Sharma & Collier, 2014) or LF_N (Arora & Leppla, 1993, 1994; Lang et al., 2014; Leppla et al., 1999) might improve efficiency drastically.

We observed a reduced binding and uptake of His-NDPK-A via PA_{63} for MDA-MB-231 cells compared to HeLa cells. To further elucidate whether the amount of anthrax toxin receptor available on the cell surface is responsible, the system should also be tested on other breast cancer cell lines as well as primary human breast cancer cells that may express larger amounts of TEM8/CMG2. Here, both His-NDPK-A as well as for example LF_N-NDPK-A should be tested to analyze the cells selectivity towards the (optimized) system.

In conclusion, optimization of the PA_{63} protein delivery system for recombinant and tagged human NDPK-A could be a starting point for the development of therapies directed towards the increase of NDPK-A levels in particular cancer cells with low NDPK-A expression. An approach based on the introduction of active NDPK-A into the cytosol of such cancer cells should be effective in the treatment of aggressive forms of breast cancer with high metastatic activity due to lack of this suppressor protein. Such approaches however have to be intensively verified and analyzed regrading toxicology and pharmacokinetics in adequate *in vitro* and *in vivo* models for metastasis to verify and validate their feasibility and efficacy.

Based on the proof-of-concept provided by this study, the Group around P. Papatheodorou was able to replicate these findings just recently. The idea was to transfect a plasmid encoding the target guide RNA into cells, followed by introduction of Cas9 into the same cells via PA. Consequently, Cas9-dependent

cleavage of the target gene results in the knock-out of the respective gene. They could show successful knock-out of the lipolysis-stimulated lipoprotein receptor (LSR) in the human colon cancer cell line HCT116 as well as of green-fluorescent protein (GFP) in human embryonic kidney 293T cells stably expressing GFP (Hirschenberger et al., 2021).

5. Summary

Bacterial AB-type protein toxins are the most toxic substances known and cause a variety of severe diseases. The binary lethal toxin (LT) and edema toxin (ET) are AB-type toxins from *Bacillus (B.). anthracis* causing the potentially lethal disease anthrax in humans and animals. Recurring cases of anthrax every year and the latent threat of anthrax being used as biological weapon led to sustained research of the anthrax toxins regarding better understanding of their mode of action and their use as molecular tools in basic and clinical research.

One inherent feature of anthrax toxins is the highly sophisticated delivery of their enzyme subunits lethal factor (LF) and edema factor (EF) into the cytosol of target cells mediated by their central B subunit protective antigen (PA). For cell entry, the A-components interact with receptor-bound PA to form a complex that enters cells via receptor-mediated endocytosis. Due to the acidification of endosomal vesicles PA forms trans-membrane pores in endosomal membranes, which serve for the transport of LF and EF from the endosomal lumen into the cytosol. This sophisticated transport system was exploited for the delivery of proteins and a variety of “foreign” cargo-molecules into the cytosol of cells. The positively charged amino terminus of LF mediates binding of LF to PA and is necessary for translocation. Therefore, the N-terminal domain of LF (LF_N) was fused to different cargo-molecules and such fusion-proteins were successfully delivered into target cells mediated by PA_{63}. Replacement of LF_N by a polycationic His-tag also enabled delivery of toxins via PA_{63}.

In this project, the PA_{63}-dependent delivery of His-tagged mammalian proteins was analyzed using recombinant human tumor metastasis suppressor protein NDPK-A as model-cargo. Different approaches were applied to investigate cytosolic localization of His-NDPK-A in HeLa cells and the metastatic human breast cancer cell line MDA-MB-231. At first, it was demonstrated that the breast cancer cell line MDA-MB-231 is sensitive to PA_{63}-mediated transport as well as intoxication with His-DTA via PA_{63}. After introduction into the cells, His-DTA ADP-ribosylated its specific substrate EF-2, thereby reducing cell-viability and inducing cell rounding in MDA-MB-231 cells. Moreover, it was confirmed that His-NDPK-A binds to both cell lines and enters their cytosol via PA_{63}. No adverse effects on cell-viability were

observed. However, in contrast to HeLa cells, MDA-MB-231 cells were less sensitive towards PA_{63}-mediated transport. The introduction of His-NDPK-A via PA_{63} into the metastatic MDA-MB-231 cells reduced their migration in a wound-healing assay.

In conclusion, the successful transport of a recombinant human tumor metastasis suppressor protein into human breast cancer cells via PA_{63} was established and the consequences for these cells described *in vitro*. To develop this basic approach for potential therapeutic applications, the transport-system should be optimized towards enhanced cell-selectivity and transport efficiency to enable the targeted delivery of this suppressor protein into cancer cells with low NDPK-A levels and high metastatic activity.

List of References

Abi-Habib, R. J., Urieto, J. O., Liu, S., Leppla, S. H., Duesbery, N. S., & Frankel, A. E. (2005). BRAF status and mitogen-activated protein/extracellular signal-regulated kinase kinase 1/2 activity indicate sensitivity of melanoma cells to anthrax lethal toxin. *Molecular Cancer Therapeutics*, *4*(9), 1303–1310. https://doi.org/10.1158/1535-7163.MCT-05-0145

Abrami, L., Bischofberger, M., Kunz, B., Groux, R., & Van Der Goot, F. G. (2010). Endocytosis of the anthrax toxin is mediated by clathrin, actin and unconventional adaptors. *PLoS Pathogens*, *6*(3). https://doi.org/10.1371/JOURNAL.PPAT.1000792

Abrami, L., Brandi, L., Moayeri, M., Brown, M. J., Krantz, B. A., Leppla, S. H., & VanderGoot, F. G. (2013). Hijacking multivesicular bodies enables long-term and exosome-mediated long-distance action of anthrax toxin. *Cell Reports*, *5*(4), 986–996. https://doi.org/10.1016/J.CELREP.2013.10.019

Abrami, L., Kunz, B., & Van Der Goot, F. G. (2010). Anthrax toxin triggers the activation of src-like kinases to mediate its own uptake. *Proceedings of the National Academy of Sciences of the United States of America*, *107*(4), 1420–1424. https://doi.org/10.1073/PNAS.0910782107

Abrami, L., Lindsay, M., Parton, R. G., Leppla, S. H., & Van Der Goot, F. G. (2004). Membrane insertion of anthrax protective antigen and cytoplasmic delivery of lethal factor occur at different stages of the endocytic pathway. *The Journal of Cell Biology*, *166*(5), 645–651. https://doi.org/10.1083/JCB.200312072

Abrami, L., Liu, S., Cosson, P., Leppla, S. H., & Van Der Goot, F. G. (2003). Anthrax toxin triggers endocytosis of its receptor via a lipid raft-mediated clathrin-dependent process. *The Journal of Cell Biology JCB The Journal of Cell Biology*, *160*(3), 321–328. https://doi.org/10.1083/jcb.200211018

Abrami, L., Liu, S., Cosson, P., Leppla, S. H., & Van der Goot, G. F. (2003). Anthrax toxin triggers endocytosis of its receptor via a lipid raft-mediated clathrin-dependent process. *The Journal of Cell Biology*, *160*(3), 321–328. https://doi.org/10.1083/JCB.200211018

Aktories, K., Bärmann, M., Ohishi, I., Tsuyama, S., Jakobs, K. H., & Habermann, E. (1986). Botulinum C2 toxin ADP-ribosylates actin. *Nature*, *322*(6077), 390–392. https://doi.org/10.1038/322390a0

Aktories, K., & Frevert, J. (1987). ADP-ribosylation of a 21-24 kDa eukaryotic protein(s) by C3, a novel botulinum ADP-ribosyltransferase, is regulated by guanine nucleotide. *The Biochemical Journal*, *247*(2), 363–368. https://doi.org/10.1042/BJ2470363

Aktories, K., Reuner, K. H., Presek, P., & Bärmann, M. (1989). Botulinum C2 toxin treatment increases the G-actin pool in intact chicken cells: a model for the cytopathic action of actin-ADP-ribosylating toxins. *Toxicon : Official Journal of the International Society on Toxinology*, *27*(9), 989–993. http://www.ncbi.nlm.nih.gov/pubmed/2508273

Alfery, D. D., & Rauscher, L. A. (1979). Tetanus: a review. *Critical Care Medicine*, *7*(4), 176–181. https://doi.org/10.1097/00003246-197904000-00007

Arora, N., Klimpel, K. R., Singh, Y., & Leppla, S. H. (1992). Fusions of anthrax toxin lethal factor to the ADP-ribosylation domain of Pseudomonas exotoxin A are potent cytotoxins which are translocated to the cytosol of mammalian cells - PubMed. *J Biol Chem*, *267*(22), 15542–15548. https://pubmed.ncbi.nlm.nih.gov/1639793/

Arora, N., & Leppla, S. H. (1993). Residues 1-254 of anthrax toxin lethal factor are sufficient to cause cellular uptake of fused polypeptides. *The Journal of Biological Chemistry*, *268*(5), 3334–3341. http://www.ncbi.nlm.nih.gov/pubmed/8429009

Arora, N., & Leppla, S. H. (1994). Fusions of anthrax toxin lethal factor with Shiga toxin and diphtheria toxin enzymatic domains are toxic to mammalian cells. *Infection and Immunity*, *62*(11), 4955–4961. https://doi.org/10.1128/IAI.62.11.4955-4961.1994

Arteaga, C. L., Sliwkowski, M. X., Osborne, C. K., Perez, E. A., Puglisi, F., & Gianni, L. (2011). Treatment of HER2-positive breast cancer: current status and future perspectives. *Nature Reviews. Clinical Oncology*, *9*(1), 16–32. https://doi.org/10.1038/NRCLINONC.2011.177

Attwood, P. V. (2013). Histidine kinases from bacteria to humans. *Biochemical Society Transactions*, *41*(4), 1023–1028. https://doi.org/10.1042/BST20130019

Attwood, P. V., & Muimo, R. (2018). The actions of NME1/NDPK-A and NME2/NDPK-B as protein kinases. *Laboratory Investigation; a Journal of Technical Methods and Pathology*, *98*(3), 283–290. https://doi.org/10.1038/LABINVEST.2017.125

Ballard, J. D., Collier, R. J., & Starnbach, M. N. (1996). Anthrax toxin-mediated delivery of a cytotoxic T-cell epitope in vivo. *Proceedings of the National Academy of Sciences of the United States of America*, *93*(22), 12531–12534. https://doi.org/10.1073/PNAS.93.22.12531

Barth, H. (2011). Exploring the role of host cell chaperones/PPIases during cellular up-take of bacterial ADP-ribosylating toxins as basis for novel pharmacological strategies to protect mammalian cells against these virulence factors. *Naunyn-Schmiedeberg's Archives of Pharmacology*, *383*(3), 237–245. https://doi.org/10.1007/S00210-010-0581-Y

Barth, H., Blöcker, D., Behlke, J., Bergsma-Schutter, W., Brisson, A., Benz, R., & Aktories, K. (2000). Cellular uptake of Clostridium botulinum C2 toxin requires oligomerization and acidification. *Journal of Biological Chemistry*. https://doi.org/10.1074/jbc.M000596200

Barth, H., Hofmann, F., Olenik, C., Just, I., & Aktories, K. (1998). The N-terminal part of the enzyme component (C2I) of the binary Clostridium botulinum C2 toxin interacts with the binding component C2II and functions as a carrier system for a Rho ADP-ribosylating C3-like fusion toxin. *Infection and Immunity*, *66*(4), 1364–1369. http://www.ncbi.nlm.nih.gov/pubmed/9529054

Barth, H., Preiss, J. C., Hofmann, F., & Aktories, K. (1998). Characterization of the

catalytic site of the ADP-ribosyltransferase Clostridium botulinum C2 toxin by site-directed mutagenesis. *The Journal of Biological Chemistry*, *273*(45), 29506–29511. http://www.ncbi.nlm.nih.gov/pubmed/9792657

Barth, H., & Stiles, B. G. (2008). Binary actin-ADP-ribosylating toxins and their use as molecular Trojan horses for drug delivery into eukaryotic cells. *Current Medicinal Chemistry*, *15*(5), 459–469. http://www.ncbi.nlm.nih.gov/pubmed/18289001

Barth, H., Stiles, B., & Popoff, M. (2015). *The comprehensive sourcebook of bacterial protein toxins* (J. Alouf, D. Adant, & M. Popoff (eds.); 4th ed.). Academic.

Beddoe, T., Paton, A. W., Le Nours, J., Rossjohn, J., & Paton, J. C. (2010). Structure, biological functions and applications of the AB5 toxins. In *Trends in Biochemical Sciences*. https://doi.org/10.1016/j.tibs.2010.02.003

Beitzinger, C., Stefani, C., Kronhardt, A., Rolando, M., Flatau, G., Lemichez, E., & Benz, R. (2012). Role of N-terminal His6-Tags in binding and efficient translocation of polypeptides into cells using anthrax protective antigen (PA). *PloS One*, *7*(10), e46964. https://doi.org/10.1371/journal.pone.0046964

Berchuck, A., Kamel, A., Whitaker, R., Kerns, B., Olt, G., Kinney, R., Soper, J. T., Dodge, R., Clarke-Pearson, D. L., Marks, P., McKenzie, S., Yin, S., & Bast, R. C. (1990). Overexpression of HER-2/neu Is Associated with Poor Survival in Advanced Epithelial Ovarian Cancer. *Cancer Research*, *50*(13).

Berube, B. J., & Wardenburg, J. B. (2013). Staphylococcus aureus α-Toxin: Nearly a Century of Intrigue. *Toxins*, *5*(6), 1140. https://doi.org/10.3390/TOXINS5061140

Bhatnagar, R., & Batra, S. (2001). Anthrax Toxin. *Critical Reviews in Microbiology*, *27*(3), 167–200. https://doi.org/10.1080/20014091096738

Biggs, J., Hersperger, E., Steeg, P. S., Liotta, L. A., & Shearn, A. (1990). A Drosophila gene that is homologous to a mammalian gene associated with tumor metastasis codes for a nucleoside diphosphate kinase. *Cell*, *63*(5), 933–940. https://doi.org/10.1016/0092-8674(90)90496-2

Binder, W. J., Brin, M. F., Blitzer, A., & Pogoda, J. M. (2001). Botulinum toxin type A (BOTOX) for treatment of migraine. *Seminars in Cutaneous Medicine and Surgery*, *20*(2), 93–100. https://doi.org/10.1053/SDER.2001.24423

Blanke, S. R., Milne, J. C., Benson, E. L., & Collier, R. J. (1996). Fused polycationic peptide mediates delivery of diphtheria toxin A chain to the cytosol in the presence of anthrax protective antigen. *Proceedings of the National Academy of Sciences of the United States of America*, *93*(16), 8437–8442. http://www.ncbi.nlm.nih.gov/pubmed/8710889

Blumenthal, B., Hoffmann, C., Aktories, K., Backert, S., & Schmidt, G. (2007). The cytotoxic necrotizing factors from Yersinia pseudotuberculosis and from Escherichia coli bind to different cellular receptors but take the same route to the cytosol. *Infection and Immunity*, *75*(7), 3344–3353. https://doi.org/10.1128/IAI.01937-06

Bohrer, S. P. (1965). Spinal fractures in tetanus. *Radiology*, *85*(6), 1111–1116.

https://doi.org/10.1148/85.6.1111

Boissan, M., Dabernat, S., Peuchant, E., Schlattner, U., Lascu, I., & Lacombe, M. L. (2009). The mammalian Nm23/NDPK family: From metastasis control to cilia movement. *Molecular and Cellular Biochemistry*, *329*(1–2), 51–62. https://doi.org/10.1007/s11010-009-0120-7

Boissan, M., Schlattner, U., & Lacombe, M. L. (2018). The NDPK/NME superfamily: State of the art. In *Laboratory Investigation*. https://doi.org/10.1038/labinvest.2017.137

Boquet, P., Popoff, M. R., Giry, M., Lemichez, E., & Bergez-Aullo, P. (1995). Inhibition of p21 Rho in intact cells by C3 diphtheria toxin chimera proteins. *Methods in Enzymology*, *256*(C), 297–306. https://doi.org/10.1016/0076-6879(95)56034-3

Bowman, B. J., & Bowman, E. J. (1986). H+-ATPases from mitochondria, plasma membranes, and vacuoles of fungal cells. *The Journal of Membrane Biology*, *94*(2), 83–97. https://doi.org/10.1007/BF01871190

Bradford, M. M. (1976). A rapid and sensitive method for the quantitation of microgram quantities of protein utilizing the principle of protein-dye binding. *Analytical Biochemistry*, *72*(1–2), 248–254. https://doi.org/10.1006/ABIO.1976.9999

Bradley, K. A., Mogridge, J., Mourez, M., Collier, R. J., & Young, J. A. T. (2001). Identification of the cellular receptor for anthrax toxin. *Nature*, *414*(6860), 225–229. https://doi.org/10.1038/N35101999

Bradley, Kenneth A., Mogridge, J., Jonah, G., Rainey, A., Batty, S., & Young, J. A. T. (2003). Binding of anthrax toxin to its receptor is similar to alpha integrin-ligand interactions. *The Journal of Biological Chemistry*, *278*(49), 49342–49347. https://doi.org/10.1074/JBC.M307900200

Brossier, F., Sirard, J. C., Guidi-Rontani, C., Duflot, E., & Mock, M. (1999). Functional analysis of the carboxy-terminal domain of Bacillus anthracis protective antigen. *Infection and Immunity*, *67*(2), 964–967. https://doi.org/10.1128/IAI.67.2.964-967.1999

Brown, M. J., Thoren, K. L., & Krantz, B. A. (2011). Charge requirements for proton gradient-driven translocation of anthrax toxin. *The Journal of Biological Chemistry*, *286*(26), 23189–23199. https://doi.org/10.1074/JBC.M111.231167

Bunch, T. J., Thalji, M. K., Pellikka, P. A., & Aksamit, T. R. (2002). Respiratory failure in tetanus: case report and review of a 25-year experience. *Chest*, *122*(4), 1488–1492. https://doi.org/10.1378/CHEST.122.4.1488

Buonocore, M., Demartini, L., Mandrini, S., Dall'Angelo, A., & Dalla Toffola, E. (2017). Effect of Botulinum Toxin on Disabling Neuropathic Pain: A Case Presentation Suggesting a New Therapeutic Strategy. *PM & R : The Journal of Injury, Function, and Rehabilitation*, *9*(2), 200–203. https://doi.org/10.1016/J.PMRJ.2016.10.014

Cao, S., Guo, A., Liu, Z., Tan, Y., Wu, G., Zhang, C., Zhao, Y., & Chen, H. (2009). Investigation of new dominant-negative inhibitors of anthrax protective antigen mutants for use in therapy and vaccination. *Infection and Immunity*, *77*(10),

4679–4687. https://doi.org/10.1128/IAI.00264-09

Carruthers, J. D. A., & Carruthers, A. (1992). Treatment of glabellar frown lines with C. botulinum-A exotoxin. *The Journal of Dermatologic Surgery and Oncology*, *18*(1), 17–21. https://doi.org/10.1111/J.1524-4725.1992.TB03295.X

Castro-Castro, A., Marchesin, V., Monteiro, P., Lodillinsky, C., Rossé, C., & Chavrier, P. (2016). Cellular and Molecular Mechanisms of MT1-MMP-Dependent Cancer Cell Invasion. *Http://Dx.Doi.Org/10.1146/Annurev-Cellbio-111315-125227*, *32*, 555–576. https://doi.org/10.1146/ANNUREV-CELLBIO-111315-125227

Chauhan, V., & Bhatnagar, R. (2002). Identification of amino acid residues of anthrax protective antigen involved in binding with lethal factor. *Infection and Immunity*, *70*(8), 4477–4484. https://doi.org/10.1128/IAI.70.8.4477-4484.2002

Collier, R. J. (1975). Diphtheria toxin: mode of action and structure. *Bacteriological Reviews*, *39*(1), 54–85. https://doi.org/10.1128/BR.39.1.54-85.1975

Collier, R. J., & Cole, H. A. (1969). Diphtheria toxin subunit active in vitro. *Science (New York, N.Y.)*, *164*(3884), 1179–1182. https://doi.org/10.1126/SCIENCE.164.3884.1179

Cunningham, K., Lacy, D. B., Mogridge, J., & Collier, R. J. (2002). Mapping the lethal factor and edema factor binding sites on oligomeric anthrax protective antigen. *Proceedings of the National Academy of Sciences of the United States of America*, *99*(10), 7049–7053. https://doi.org/10.1073/PNAS.062160399

Dal Molin, F., Tonello, F., Ladant, D., Zornetta, I., Zamparo, I., Di Benedetto, G., Zaccolo, M., & Montecucco, C. (2006). Cell entry and cAMP imaging of anthrax edema toxin. *The EMBO Journal*, *25*(22), 5405–5413. https://doi.org/10.1038/SJ.EMBOJ.7601408

De, S. N. (1959). Enterotoxicity of bacteria-free culture-filtrate of Vibrio cholerae. *Nature*, *183*(4674), 1533–1534. https://doi.org/10.1038/1831533A0

Desvignes, T., Pontarotti, P., Fauvel, C., & Bobe, J. (2009). Nme protein family evolutionary history, a vertebrate perspective. *BMC Evolutionary Biology*, *9*(1). https://doi.org/10.1186/1471-2148-9-256

Deuquet, J., Lausch, E., Superti-Furga, A., & Van Der Goot, F. G. (2012). The dark sides of capillary morphogenesis gene 2. *The EMBO Journal*, *31*(1), 3–13. https://doi.org/10.1038/EMBOJ.2011.442

Dmochewitz, L., Lillich, M., Kaiser, E., Jennings, L. D., Lang, A. E., Buchner, J., Fischer, G., Aktories, K., Collier, R. J., & Barth, H. (2011). Role of CypA and Hsp90 in membrane translocation mediated by anthrax protective antigen. *Cellular Microbiology*, *13*(3), 359–373. https://doi.org/10.1111/j.1462-5822.2010.01539.x

do Vale, A., Pereira, C., Osorio, C. R., & dos Santos, N. M. S. (2017). The Apoptogenic Toxin AIP56 Is Secreted by the Type II Secretion System of Photobacterium damselae subsp. piscicida. *Toxins*, *9*(11). https://doi.org/10.3390/TOXINS9110368

Dong, M., Masuyer, G., & Stenmark, P. (2019). Botulinum and Tetanus Neurotoxins. *Annual Review of Biochemistry*, *88*, 811. https://doi.org/10.1146/ANNUREV-BIOCHEM-013118-111654

Duesbery, N. S., Webb, C. P., Leppla, S. H., Gordon, V. M., Klimpel, K. R., Copeland, T. D., Ahn, N. G., Oskarsson, M. K., Fukasawa, K., Paull, K. D., & Vande Woude, G. F. (1998). Proteolytic inactivation of MAP-kinase-kinase by anthrax lethal factor. *Science (New York, N.Y.)*, *280*(5364), 734–737. http://www.ncbi.nlm.nih.gov/pubmed/9563949

Ernst, K., Langer, S., Kaiser, E., Osseforth, C., Michaelis, J., Popoff, M. R., Schwan, C., Aktories, K., Kahlert, V., Malesevic, M., Schiene-Fischer, C., & Barth, H. (2015). Cyclophilin-Facilitated Membrane Translocation as Pharmacological Target to Prevent Intoxication of Mammalian Cells by Binary Clostridial Actin ADP-Ribosylated Toxins. *Journal of Molecular Biology*, *427*(6), 1224–1238. https://doi.org/10.1016/j.jmb.2014.07.013

Ernst, K., Schnell, L., & Barth, H. (2016). Host Cell Chaperones Hsp70/Hsp90 and Peptidyl-Prolyl Cis/Trans Isomerases Are Required for the Membrane Translocation of Bacterial ADP-Ribosylating Toxins. In *Current topics in microbiology and immunology* (Vol. 406, pp. 163–198). https://doi.org/10.1007/82_2016_14

Ernst, K., Schnell, L., & Barth, H. (2017). Host Cell Chaperones Hsp70/Hsp90 and Peptidyl-Prolyl Cis/Trans Isomerases Are Required for the Membrane Translocation of Bacterial ADP-Ribosylating Toxins. *Current Topics in Microbiology and Immunology*, *406*, 163–198. https://doi.org/10.1007/82_2016_14

European Centre for Disease Prevention and Control (ECDC). (2019). *COMMUNICABLE DISEASE THREATS REPORT CDTR Week 18, 28 April-4 May 2019*. ecdc.europa.eu

Fahrer, J., Funk, J., Lillich, M., & Barth, H. (2011). Internalization of biotinylated compounds into cancer cells is promoted by a molecular Trojan horse based upon core streptavidin and clostridial C2 toxin. *Naunyn-Schmiedeberg's Archives of Pharmacology*, *383*(3), 263–273. https://doi.org/10.1007/S00210-010-0585-7

Fahrer, J., Rausch, J., & Barth, H. (2013). A Cell-Permeable Fusion Protein Based on Clostridium botulinum C2 Toxin for Delivery of p53 Tumorsuppressor into Cancer Cells. *PLoS ONE*, *8*(9), e72455. https://doi.org/10.1371/journal.pone.0072455

Fahrer, J., Rieger, J., van Zandbergen, G., & Barth, H. (2010). The C2-streptavidin delivery system promotes the uptake of biotinylated molecules in macrophages and T-leukemia cells. *Biological Chemistry*, *391*(11), 1315–1325. https://doi.org/10.1515/BC.2010.132

Falnes, P. O., Choe, S., Madshus, I. H., Wilson, B. A., & Olsnes, S. (1994). *Inhibition of membrane translocation of diphtheria toxin A-fragment by internal disulfide bridges - PubMed*. Inhibition of Membrane Translocation of Diphtheria Toxin A-Fragment by Internal Disulfide Bridges. https://pubmed.ncbi.nlm.nih.gov/8132565/

Falnes, P. O., & Olsnes, S. (1995). Cell-mediated reduction and incomplete membrane translocation of diphtheria toxin mutants with internal disulfides in the A fragment. *The Journal of Biological Chemistry*, *270*(35), 20787–20793. https://doi.org/10.1074/JBC.270.35.20787

FDA. (2008). *HIGHLIGHTS OF PRESCRIBING INFORMATION ONTAK® (denileukin diftitox) Solution for Intravenous use*.

FDA. (2016). *MEDICATION GUIDE BOTOX® BOTOX® Cosmetic (Boe-tox) (onabotulinumtoxinA) for Injection*.

Feld, G. K., Brown, M. J., & Krantz, B. A. (2012). Ratcheting up protein translocation with anthrax toxin. *Protein Science : A Publication of the Protein Society*, *21*(5), 606–624. https://doi.org/10.1002/PRO.2052

Felix, I., Lomada, S. K., Barth, H., & Wieland, T. (2020). *Bacillus anthracis ' PA 63 Delivers the Tumor Metastasis Suppressor Protein NDPK-A / NME1 into Breast Cancer Cells*. 1–20. https://doi.org/10.3390/ijms21093295

Foss, F. M. (2000). DAB(389)IL-2 (ONTAK): a novel fusion toxin therapy for lymphoma. *Clinical Lymphoma*, *1*(2), 110–116. https://doi.org/10.3816/CLM.2000.N.009

Friebe, S., van der Goot, F. G., & Bürgi, J. (2016). The ins and outs of anthrax toxin. In *Toxins* (Vol. 8, Issue 3). MDPI AG. https://doi.org/10.3390/toxins8030069

Fuhs, S. R., Meisenhelder, J., Aslanian, A., Ma, L., Zagorska, A., Stankova, M., Binnie, A., Al-Obeidi, F., Mauger, J., Lemke, G., Yates, J. R., & Hunter, T. (2015). Monoclonal 1- and 3-Phosphohistidine Antibodies: New Tools to Study Histidine Phosphorylation. *Cell*, *162*(1), 198–210. https://doi.org/10.1016/j.cell.2015.05.046

GALANOS, C., LÜDERITZ, O., RIETSCHEL, E. T., WESTPHAL, O., BRADE, H., BRADE, L., FREUDENBERG, M., SCHADE, U., IMOTO, M., YOSHIMURA, H., KUSUMOTO, S., & SHIBA, T. (1985). Synthetic and natural Escherichia coli free lipid A express identical endotoxic activities. *European Journal of Biochemistry*, *148*(1), 1–5. https://doi.org/10.1111/J.1432-1033.1985.TB08798.X

Gill, D. M. (1982). Bacterial toxins: a table of lethal amounts. *Microbiological Reviews*, *46*(1), 86. https://doi.org/10.1128/mmbr.46.1.86-94.1982

Goonetilleke, A., & Harris, J. B. (2004). Clostridial neurotoxins. *Journal of Neurology, Neurosurgery, and Psychiatry*, *75 Suppl 3*(Suppl 3). https://doi.org/10.1136/JNNP.2004.046102

Gravalos, C., & Jimeno, A. (2008). HER2 in gastric cancer: a new prognostic factor and a novel therapeutic target. *Annals of Oncology : Official Journal of the European Society for Medical Oncology*, *19*(9), 1523–1529. https://doi.org/10.1093/ANNONC/MDN169

Gülke, I., Pfeifer, G., Liese, J., Fritz, M., Hofmann, F., Aktories, K., & Barth, H. (2001). Characterization of the enzymatic component of the ADP-ribosyltransferase toxin CDTa from Clostridium difficile. *Infection and Immunity*, *69*(10), 6004–6011. https://doi.org/10.1128/IAI.69.10.6004-

6011.2001

Hatheway, C. L. (1990). Toxigenic clostridia. *Clinical Microbiology Reviews*, *3*(1), 66–98. https://doi.org/10.1128/CMR.3.1.66

Haug, G., Aktories, K., & Barth, H. (2004). The host cell chaperone Hsp90 is necessary for cytotoxic action of the binary iota-like toxins. *Infection and Immunity*, *72*(5), 3066–3068. https://doi.org/10.1128/iai.72.5.3066-3068.2004

Haug, G., Leemhuis, J., Tiemann, D., Meyer, D. K., Aktories, K., & Barth, H. (2003). The Host Cell Chaperone Hsp90 Is Essential for Translocation of the Binary Clostridium botulinum C2 Toxin into the Cytosol. *Journal of Biological Chemistry*, *278*(34), 32266–32274. https://doi.org/10.1074/jbc.M303980200

Haug, G., Wilde, C., Leemhuis, J., Meyer, D. K., Aktories, K., & Barth, H. (2003). Cellular Uptake of Clostridium botulinum C2 Toxin: Membrane Translocation of a Fusion Toxin Requires Unfolding of Its Dihydrofolate Reductase Domain †. *Biochemistry*, *42*(51), 15284–15291. https://doi.org/10.1021/bi0354278

Heimann, R., Ferguson, D. J., & Hellmann, S. (1998). The relationship between nm23, angiogenesis, and the metastatic proclivity of node-negative breast cancer - PubMed. *Cancer Res.*, *58*(13), 2766–2771. https://pubmed.ncbi.nlm.nih.gov/9661889/

Hirschenberger, M., Stadler, N., Fellermann, M., Sparrer, K. M. J., Kirchhoff, F., Barth, H., & Papatheodorou, P. (2021). CRISPA: A Non-viral, Transient Cas9 Delivery System Based on Reengineered Anthrax Toxin. *Frontiers in Pharmacology*, *12*. https://doi.org/10.3389/FPHAR.2021.770283

Holzer, C., & Maier, P. (1987). DNA and protein contents of hepatocytes in primary cultures monitored by flow cytometry: Effect of phenobarbital and dimethylsulphoxide. *Toxicology in Vitro : An International Journal Published in Association with BIBRA*, *1*(4), 203–213. https://doi.org/10.1016/0887-2333(87)90022-1

Horak, C. E., Lee, J. H., Elkahloun, A. G., Boissan, M., Dumont, S., Maga, T. K., Arnaud-Dabernat, S., Palmieri, D., Stetler-Stevenson, W. G., Lacombe, M.-L., Meltzer, P. S., & Steeg, P. S. (2007). Nm23-H1 Suppresses Tumor Cell Motility by Down-regulating the Lysophosphatidic Acid Receptor EDG2. *Cancer Research*, *67*(15), 7238–7246. https://doi.org/10.1158/0008-5472.CAN-07-0962

Hu, H., & Leppla, S. H. (2009). Anthrax toxin uptake by primary immune cells as determined with a lethal factor-beta-lactamase fusion protein. *PloS One*, *4*(11). https://doi.org/10.1371/JOURNAL.PONE.0007946

Ibidi. (2020, July 1). *Instructions Culture-Insert 2 Well*. https://ibidi.com/culture-inserts/24-culture-insert-2-well.html

Jack, S., Madhivanan, K., Ramadesikan, S., Subramanian, S., Edwards, D. F., Elzey, B. D., Dhawan, D., McCluskey, A., Kischuk, E. M., Loftis, A. R., Truex, N., Santos, M., Lu, M., Rabideau, A., Pentelute, B., Collier, J., Kaimakliotis, H., Koch, M., Ratliff, T. L., … Aguilar, R. C. (2020). A novel, safe, fast and efficient treatment for Her2-positive and negative bladder cancer utilizing an EGF-anthrax toxin chimera. *International Journal of Cancer*, *146*(2), 449–460. https://doi.org/10.1002/ijc.32719

Kaetzel, D. M., Zhang, Q., Yang, M., McCorkle, J. R., Ma, D., Craven, R. J., Kaetzel, D. M., Zhang, Q., Yang, M., McCorkle, J. R., Ma, D., & Craven, R. J. (2006). Potential roles of 3′-5′exonuclease activity of NM23-H1 in DNA repair and malignant progression. *Journal of Bioenergetics and Biomembranes 2006 38:3*, *38*(3), 163–167. https://doi.org/10.1007/S10863-006-9040-3

Kaiser, E., Böhm, N., Ernst, K., Langer, S., Schwan, C., Aktories, K., Popoff, M., Fischer, G., & Barth, H. (2012). FK506-binding protein 51 interacts with Clostridium botulinum C2 toxin and FK506 inhibits membrane translocation of the toxin in mammalian cells. *Cellular Microbiology*, *14*(8), 1193–1205. https://doi.org/10.1111/j.1462-5822.2012.01788.x

Kaiser, E., Pust, S., Kroll, C., & Barth, H. (2009). Cyclophilin A facilitates translocation of the *Clostridium botulinum* C2 toxin across membranes of acidified endosomes into the cytosol of mammalian cells. *Cellular Microbiology*, *11*(5), 780–795. https://doi.org/10.1111/j.1462-5822.2009.01291.x

Kantor, J. D., McCormick, B., Steeg, P. S., & Zetter, B. R. (1993). Inhibition of cell motility after nm23 transfection of human and murine tumor cells. *Cancer Research*, *53*(9), 1971–1973. http://www.ncbi.nlm.nih.gov/pubmed/8481897

Kaslow, H. R., & Burns, U. L. (1992). Pertussis toxin and target eukaryotic cells: binding, entry, and activation. *FASEB Journal : Official Publication of the Federation of American Societies for Experimental Biology*, *6*(9), 2684–2690. https://doi.org/10.1096/FASEBJ.6.9.1612292

Khan, I., Gril, B., & Steeg, P. S. (2019). Metastasis Suppressors NME1 and NME2 Promote Dynamin 2 Oligomerization and Regulate Tumor Cell Endocytosis, Motility, and Metastasis. *Cancer Research*, *79*(18), 4689–4702. https://doi.org/10.1158/0008-5472.CAN-19-0492

Kintzer, A. F., Thoren, K. L., Sterling, H. J., Dong, K. C., Feld, G. K., Tang, I. I., Zhang, T. T., Williams, E. R., Berger, J. M., & Krantz, B. A. (2009). The Protective Antigen Component of Anthrax Toxin Forms Functional Octameric Complexes. *Journal of Molecular Biology*, *392*(3), 614–629. https://doi.org/10.1016/J.JMB.2009.07.037

Kistner, A., & Habermann, E. (1992). Reductive cleavage of tetanus toxin and botulinum neurotoxin A by the thioredoxin system from brain. *Naunyn-Schmiedeberg's Archives of Pharmacology 1992 345:2*, *345*(2), 227–234. https://doi.org/10.1007/BF00165741

Klein, A. W. (1996). Cosmetic therapy with botulinum toxin, Anecdotal memoirs. *Dermatologic Surgery : Official Publication for American Society for Dermatologic Surgery [et Al.]*, *22*(9), 757–759. https://doi.org/10.1111/J.1524-4725.1996.TB00725.X

Klein, A. W., & Glogau, R. G. (2000). Botulinum toxin: beyond cosmesis. *Archives of Dermatology*, *136*(4), 539–541. https://doi.org/10.1001/ARCHDERM.136.4.539

Klimpel, K. R., Arora, N., & Leppla, S. H. (1994). Anthrax toxin lethal factor contains a zinc metalloprotease consensus sequence which is required for lethal toxin activity. *Molecular Microbiology*, *13*(6), 1093–1100.

https://doi.org/10.1111/J.1365-2958.1994.TB00500.X

Klimpel, K. R., Molloyt, S. S., Thomast, G., & Leppla, S. H. (1992). Anthrax toxin protective antigen is activated by a cell surface protease with the sequence specificity and catalytic properties of furin (Bacillus anthrwis/protein processing/paired basic rsdues/nutagenesis/consensus sequence). In *Biochemistry* (Vol. 89). https://www.pnas.org/content/pnas/89/21/10277.full.pdf

Krantz, B. A., Finkelstein, A., & Collier, R. J. (2006). Protein translocation through the anthrax toxin transmembrane pore is driven by a proton gradient. *Journal of Molecular Biology*, *355*(5), 968–979. https://doi.org/10.1016/J.JMB.2005.11.030

Krantz, B. A., Melnyk, R. A., Zhang, S., Juris, S. J., Lacy, D. B., Wu, Z., Finkelstein, A., & Collier, R. J. (2005). A phenylalanine clamp catalyzes protein translocation through the anthrax toxin pore. *Science (New York, N.Y.)*, *309*(5735), 777–781. https://doi.org/10.1126/science.1113380

Krüger, M., Kalbacher, H., Kastritis, P. L., Bischof, J., Barth, H., Henne-Bruns, D., Vorgias, C., Sarno, S., Pinna, L. A., & Knippschild, U. (2016). New potential peptide therapeutics perturbing CK1δ/α-tubulin interaction. *Cancer Letters*, *375*(2), 375–383. https://doi.org/10.1016/J.CANLET.2016.03.021

Lacombe, M. L., & Boissan, M. (2013). NME1 (NME/NM23 nucleoside diphosphate kinase 1). *Atlas of Genetics and Cytogenetics in Oncology and Haematology*. https://doi.org/DOI: 10.4267/2042/51139

Lacombe, M. L. L., Munier, A., Mehus, J. G., & Lambeth, D. O. (2000). The human Nm23/nucleoside diphosphate kinases. *Journal of Bioenergetics and Biomembranes*, *32*(3), 247–258. https://doi.org/10.1023/A:1005584929050

Lacy, D. B., Wigelsworth, D. J., Melnyk, R. A., Harrison, S. C., & Collier, R. J. (2004). Structure of heptameric protective antigen bound to an anthrax toxin receptor: A role for receptor in pH-dependent pore formation. *Proceedings of the National Academy of Sciences*, *101*(36), 13147–13151. https://doi.org/10.1073/pnas.0405405101

Laemmli, U. K. (1970). Cleavage of structural proteins during the assembly of the head of bacteriophage T4. *Nature*, *227*(5259), 680–685. https://doi.org/10.1038/227680A0

Lane, C. H., La Montagne, J., & Fauci, A. S. (2001). Bioterrorism: A clear and present danger. *Nature Medicine 2001 7:12*, *7*(12), 1271–1273. https://doi.org/10.1038/nm1201-1271

Lang, A. E., Ernst, K., Lee, H., Papatheodorou, P., Schwan, C., Barth, H., & Aktories, K. (2014). The chaperone Hsp90 and PPIases of the cyclophilin and FKBP families facilitate membrane translocation of Photorhabdus luminescensADP-ribosyltransferases. *Cellular Microbiology*, *16*(4), 490–503. https://doi.org/10.1111/cmi.12228

Lansigan, F., Stearns, D. M., & Foss, F. (2010). Role of denileukin diftitox in the treatment of persistent or recurrent cutaneous T-cell lymphoma. *Cancer Management and Research*, *2*, 53. https://doi.org/10.2147/CMAR.S5009

Lascu, I., & Gonin, P. (2000). The catalytic mechanism of nucleoside diphosphate kinases. *Journal of Bioenergetics and Biomembranes*, *32*(3), 237–246. https://doi.org/10.1023/A:1005532912212

Lemichez, E., Bomsel, M., Devilliers, G., VanderSpek, J., Murphy, J. R., Lukianov, E. V., Olsnes, S., & Boquet, P. (1997). Membrane translocation of diphtheria toxin fragment A exploits early to late endosome trafficking machinery. *Molecular Microbiology*, *23*(3), 445–457. https://doi.org/10.1111/J.1365-2958.1997.TB02669.X

Leppla, S. H. (1982). Anthrax toxin edema factor: a bacterial adenylate cyclase that increases cyclic AMP concentrations of eukaryotic cells. *Proceedings of the National Academy of Sciences of the United States of America*, *79*(10), 3162–3166. http://www.ncbi.nlm.nih.gov/pubmed/6285339

Leppla, S. H. (1984). Bacillus anthracis calmodulin-dependent adenylate cyclase: chemical and enzymatic properties and interactions with eucaryotic cells. *Advances in Cyclic Nucleotide and Protein Phosphorylation Research*, *17*, 189–198. http://www.ncbi.nlm.nih.gov/pubmed/6328915

Leppla, S. H., Arora, N., & Varughese, M. (1999). Anthrax toxin fusion proteins for intracellular delivery of macromolecules. *Journal of Applied Microbiology*, *87*(2), 284. https://doi.org/10.1046/j.1365-2672.1999.00890.x

Liao, X., Rabideau, A. E., & Pentelute, B. L. (2014). Delivery of antibody mimics into mammalian cells via anthrax toxin protective antigen. *Chembiochem : A European Journal of Chemical Biology*, *15*(16), 2458–2466. https://doi.org/10.1002/CBIC.201402290

Lillich, M., Chen, X., Weil, T., Barth, H., & Fahrer, J. (2012). Streptavidin-conjugated C3 protein mediates the delivery of mono-biotinylated RNAse A into macrophages. *Bioconjugate Chemistry*, *23*(7), 1426–1436. https://doi.org/10.1021/bc300041z

Lingwood, C. (2021). Therapeutic Uses of Bacterial Subunit Toxins. *Toxins*, *13*(6). https://doi.org/10.3390/TOXINS13060378

Liu, S., Netzel-Arnett, S., Birkedal-Hansen, H., & Leppla, S. H. (2000). Tumor cell-selective cytotoxicity of matrix metalloproteinase-activated anthrax toxin - PubMed. *Cancer Res.*, *60*, 6061–6067. https://pubmed.ncbi.nlm.nih.gov/11085528/

Liu, Shihui, & Leppla, S. H. (2003). Cell surface tumor endothelium marker 8 cytoplasmic tail-independent anthrax toxin binding, proteolytic processing, oligomer formation, and internalization. *The Journal of Biological Chemistry*, *278*(7), 5227–5234. https://doi.org/10.1074/JBC.M210321200

Liu, Shihui, Leung, H. J., & Leppla, S. H. (2007). Characterization of the interaction between anthrax toxin and its cellular receptors. *Cellular Microbiology*, *9*(4), 977–987. https://doi.org/10.1111/J.1462-5822.2006.00845.X

Liu, W., & Nestorovich, E. M. (2021). Anthrax toxin channel: What we know based on over 30 years of research. *Biochimica et Biophysica Acta. Biomembranes*, *1863*(11). https://doi.org/10.1016/J.BBAMEM.2021.183715

Locht, C., Coutte, L., & Mielcarek, N. (2011). The ins and outs of pertussis toxin.

FEBS Journal, *278*(23), 4668–4682. https://doi.org/10.1111/j.1742-4658.2011.08237.x

Lodillinsky, C., Fuhrmann, L., Irondelle, M., Pylypenko, O., Li, X. Y., Bonsang-Kitzis, H., Reyal, F., Vacher, S., Calmel, C., De Wever, O., Bièche, I., Lacombe, M. L., Eiján, A. M., Houdusse, A., Vincent-Salomon, A., Weiss, S. J., Chavrier, P., & Boissan, M. (2021). Metastasis-suppressor NME1 controls the invasive switch of breast cancer by regulating MT1-MMP surface clearance. *Oncogene 2021 40:23*, *40*(23), 4019–4032. https://doi.org/10.1038/s41388-021-01826-1

Lubran, M. M. (1988). Bacterial toxins. *Annals of Clinical and Laboratory Science*, *18*(1), 58–71.

Makurumidze, R., Gombe, N. T., Magure, T., & Tshimanga, M. (2021). Investigation of an anthrax outbreak in Makoni District, Zimbabwe. *BMC Public Health*, *21*(1), 1–10. https://doi.org/10.1186/S12889-021-10275-0/TABLES/2

Marino, N., Marshall, J. C., Collins, J. W., Zhou, M., Qian, Y., Veenstra, T., & Steeg, P. S. (2013). Nm23-H1 binds to Gelsolin and inactivates its actin-severing capacity to promote tumor cell motility and metastasis. *Cancer Research*, *73*(19), 5949–5962. https://doi.org/10.1158/0008-5472.CAN-13-0368

Marino, N., Marshall, J. C., & Steeg, P. S. (2011). Protein-protein interactions: A mechanism regulating the anti-metastatic properties of Nm23-H1. *Naunyn-Schmiedeberg's Archives of Pharmacology*, *384*(4–5), 351–362. https://doi.org/10.1007/s00210-011-0646-6

Marino, N., Nakayama, J., Collins, J. W., & Steeg, P. S. (2012). Insights into the biology and prevention of tumor metastasis provided by the Nm23 metastasis suppressor gene. *Cancer Metastasis Reviews*, *31*(3–4), 593–603. https://doi.org/10.1007/s10555-012-9374-8

McCluskey, A. J., & Collier, R. J. (2013). Receptor-directed chimeric toxins created by sortase-mediated protein fusion. *Molecular Cancer Therapeutics*, *12*(10), 2273–2281. https://doi.org/10.1158/1535-7163.MCT-13-0358

McCluskey, A. J., Olive, A. J., Starnbach, M. N., & Collier, R. J. (2013). Targeting HER2-positive cancer cells with receptor-redirected anthrax protective antigen. *Molecular Oncology*, *7*(3), 440–451. https://doi.org/10.1016/J.MOLONC.2012.12.003

Mechaly, A., McCluskey, A. J., & John Collier, R. (2012). Changing the receptor specificity of anthrax toxin. *MBio*, *3*(3), 1–6. https://doi.org/10.1128/mBio.00088-12

Miller, C. J., Elliott, J. L., & Collier, R. J. (1999). Anthrax protective antigen: prepore-to-pore conversion. *Biochemistry*, *38*(32), 10432–10441. https://doi.org/10.1021/BI990792D

Milne, J. C., Furlong, D., Hanna, P. C. ., Wall, J. S., & Collier, R. J. (1994). Anthrax protective antigen forms oligomers during intoxication of mammalian cells - PubMed. *J Biol Chem.* , *269*(32), 20607–20612. https://pubmed.ncbi.nlm.nih.gov/8051159/

Milne, J C, Blanke, S. R., Hanna, P. C., & Collier, R. J. (1995). Protective antigen-binding domain of anthrax lethal factor mediates translocation of a heterologous protein fused to its amino- or carboxy-terminus. *Molecular Microbiology*, *15*(4), 661–666. http://www.ncbi.nlm.nih.gov/pubmed/7783638

Milne, Jill C., & Collier, R. J. (1993). pH-dependent permeabilization of the plasma membrane of mammalian cells by anthrax protective antigen. *Molecular Microbiology*, *10*(3), 647–653. https://doi.org/10.1111/J.1365-2958.1993.TB00936.X

Moayeri, M., Leppla, S. H., Vrentas, C., Pomerantsev, A. P., & Liu, S. (2015). Anthrax Pathogenesis. *Annual Review of Microbiology*, *69*(1), 185–208. https://doi.org/10.1146/annurev-micro-091014-104523

Mogridge, J., Mourez, M., & Collier, R. J. (2001). Involvement of domain 3 in oligomerization by the protective antigen moiety of anthrax toxin. *Journal of Bacteriology*, *183*(6), 2111–2116. https://doi.org/10.1128/JB.183.6.2111-2116.2001

Mourez, M., Yan, M., Lacy, D. B., Dillon, L., Bentsen, L., Marpoe, A., Maurin, C., Hotze, E., Wigelsworth, D., Pimental, R. A., Ballard, J. D., Collier, R. J., & Tweten, R. K. (2003). Mapping dominant-negative mutations of anthrax protective antigen by scanning mutagenesis. *Proceedings of the National Academy of Sciences of the United States of America*, *100*(24), 13803–13808. https://doi.org/10.1073/PNAS.2436299100

Murphy, J. R., Bishai, W., Borowski, M., Miyanohara, A., Boyd, J., & Nagle, S. (1986). Genetic construction, expression, and melanoma-selective cytotoxicity of a diphtheria toxin-related alpha-melanocyte-stimulating hormone fusion protein. *Proceedings of the National Academy of Sciences of the United States of America*, *83*(21), 8258–8262. https://doi.org/10.1073/PNAS.83.21.8258

Nanda, A., Carson-Walter, E. B., Seaman, S., Barber, T. D., Stampfl, J., Singh, S., Vogelstein, B., Kinzler, K. W., & St Croix, B. (2004). TEM8 interacts with the cleaved C5 domain of collagen alpha 3(VI). *Cancer Research*, *64*(3), 817–820. http://www.ncbi.nlm.nih.gov/pubmed/14871805

Nassi, S., Collier, R. J., & Finkelstein, A. (2002). PA63 channel of anthrax toxin: an extended beta-barrel. *Biochemistry*, *41*(5), 1445–1450. https://doi.org/10.1021/BI0119518

Neumeyer, T., Tonello, F., Dal Molin, F., Schiffler, B., & Benz, R. (2006). Anthrax edema factor, voltage-dependent binding to the protective antigen ion channel and comparison to LF binding. *The Journal of Biological Chemistry*, *281*(43), 32335–32343. https://doi.org/10.1074/JBC.M606552200

Ost, G. S., Ng'ang'a, P. N., Lang, A. E., & Aktories, K. (2019). Photorhabdus luminescens Tc toxin is inhibited by the protease inhibitor MG132 and activated by protease cleavage resulting in increased binding to target cells. *Cellular Microbiology*, *21*(3), e12978. https://doi.org/10.1111/cmi.12978

Papini, E., Cabrini, G., & Montecucco, C. (1993). The sensitivity of cystic fibrosis cells to diphtheria toxin. *Toxicon : Official Journal of the International Society on Toxinology*, *31*(3), 359–362. https://doi.org/10.1016/0041-0101(93)90154-

B

Papini, E., Rappuoli, R., Murgia, M., & Montecucco, C. (1993). Cell penetration of diphtheria toxin. Reduction of the interchain disulfide bridge is the rate-limiting step of translocation in the cytosol. *Journal of Biological Chemistry*, *268*(3), 1567–1574. https://doi.org/10.1016/S0021-9258(18)53890-4

Pappenheimer, A. M. (1937). Diphtheria Toxin. I. Isolation and Characterization of a Toxic Protein from Corynebacterium diphtheriae Filtrates. *Journal of Biological Chemistry* , *120*, 543–553.

Petosa, C., Collier, R. J., Klimpel, K. R., Leppla, S. H., & Liddington, R. C. (1997). Crystal structure of the anthrax toxin protective antigen. *Nature*, *385*(6619), 833–838. https://doi.org/10.1038/385833A0

Pirazzini, M., Tehran, D. A., Zanetti, G., Megighian, A., Scorzeto, M., Fillo, S., Shone, C. C., Binz, T., Rossetto, O., Lista, F., & Montecucco, C. (2014). Thioredoxin and Its Reductase Are Present on Synaptic Vesicles, and Their Inhibition Prevents the Paralysis Induced by Botulinum Neurotoxins. *Cell Reports*, *8*(6), 1870–1878. https://doi.org/10.1016/J.CELREP.2014.08.017

Plaut, R. D., & Carbonetti, N. H. (2008). Retrograde transport of pertussis toxin in the mammalian cell. *Cellular Microbiology*, *10*(5), 1130–1139. https://doi.org/10.1111/J.1462-5822.2007.01115.X

Pruitt, R. N., & Lacy, D. B. (2012). Toward a structural understanding of Clostridium difficile toxins A and B. *Frontiers in Cellular and Infection Microbiology*, *2*, 28. https://doi.org/10.3389/FCIMB.2012.00028/BIBTEX

Rabideau, A. E., Liao, X., Akçay, G., & Pentelute, B. L. (2015). Translocation of Non-Canonical Polypeptides into Cells Using Protective Antigen. *Scientific Reports*, *5*(1), 11944. https://doi.org/10.1038/srep11944

Rabideau, A. E., & Pentelute, B. L. (2016). Delivery of Non-Native Cargo into Mammalian Cells Using Anthrax Lethal Toxin. *ACS Chemical Biology*, *11*(6), 1490–1501. https://doi.org/10.1021/acschembio.6b00169

Rainey, G. J. A., Wigelsworth, D. J., Ryan, P. L., Scobie, H. M., Collier, R. J., & Young, J. A. T. (2005). Receptor-specific requirements for anthrax toxin delivery into cells. *Proceedings of the National Academy of Sciences of the United States of America*, *102*(37), 13278–13283. https://doi.org/10.1073/PNAS.0505865102

Reeves, C. V., Dufraine, J., Young, J. A. T., & Kitajewski, J. (2010). Anthrax toxin receptor 2 is expressed in murine and tumor vasculature and functions in endothelial proliferation and morphogenesis. *Oncogene*, *29*(6), 789–801. https://doi.org/10.1038/ONC.2009.383

Rosovitz, M. J., Schuck, P., Varughese, M., Chopra, A. P., Mehra, V., Singh, Y., McGinnis, L. M., & Leppla, S. H. (2003). Alanine-scanning mutations in domain 4 of anthrax toxin protective antigen reveal residues important for binding to the cellular receptor and to a neutralizing monoclonal antibody. *The Journal of Biological Chemistry*, *278*(33), 30936–30944. https://doi.org/10.1074/JBC.M301154200

Rummel, A. (2016). *Two Feet on the Membrane: Uptake of Clostridial Neurotoxins*

(pp. 1–37). https://doi.org/10.1007/82_2016_48

Sakurai, J., Nagahama, M., Hisatsune, J., Katunuma, N., & Tsuge, H. (2003). Clostridium perfringens iota-toxin, ADP-ribosyltransferase: structure and mechanism of action. *Advances in Enzyme Regulation*, *43*, 361–377.

Salerno, M., Ouatas, T., Palmieri, D., & Steeg, P. S. (2003). Inhibition of signal transduction by the nm23 metastasis suppressor: possible mechanisms. *Clinical & Experimental Metastasis*, *20*(1), 3–10. https://doi.org/10.1023/A:1022578000022

Sánchez, J., & Holmgren, J. (2008). Cholera toxin structure, gene regulation and pathophysiological and immunological aspects. *Cellular and Molecular Life Sciences : CMLS*, *65*(9), 1347–1360. https://doi.org/10.1007/S00018-008-7496-5

Sandvig, K., & Olsnes, S. (1980). Diphtheria toxin entry into cells is facilitated by low pH. *The Journal of Cell Biology*, *87*(3 Pt 1), 828–832. https://doi.org/10.1083/JCB.87.3.828

Sandvig, K., Spilsberg, B., Lauvrak, S. U., Torgersen, M. L., Iversen, T. G., & Van Deurs, B. (2004). Pathways followed by protein toxins into cells. *International Journal of Medical Microbiology : IJMM*, *293*(7–8), 483–490. https://doi.org/10.1078/1438-4221-00294

Santelli, E., Bankston, L. A., Leppla, S. H., & Llddington, R. C. (2004). Crystal structure of a complex between anthrax toxin and its host cell receptor. *Nature*, *430*(7002), 905–908. https://doi.org/10.1038/NATURE02763

Schantz, E. J., & Johnson, E. A. (1997). Botulinum toxin: the story of its development for the treatment of human disease. *Perspectives in Biology and Medicine*, *40*(3), 317–327. https://doi.org/10.1353/PBM.1997.0032

Schleberger, C., Hochmann, H., Barth, H., Aktories, K., & Schulz, G. E. (2006). Structure and Action of the Binary C2 Toxin from Clostridium botulinum. *Journal of Molecular Biology*, *364*(4), 705–715. https://doi.org/10.1016/j.jmb.2006.09.002

Schnell, L., Dmochewitz-Kück, L., Feigl, P., Montecucco, C., & Barth, H. (2016). Thioredoxin reductase inhibitor auranofin prevents membrane transport of diphtheria toxin into the cytosol and protects human cells from intoxication. *Toxicon*. https://doi.org/10.1016/j.toxicon.2015.04.012

Schuster, M., Schnell, L., Feigl, P., Birkhofer, C., Mohr, K., Roeder, M., Carle, S., Langer, S., Tippel, F., Buchner, J., Fischer, G., Hausch, F., Frick, M., Schwan, C., Aktories, K., Schiene-Fischer, C., & Barth, H. (2017). The Hsp90 machinery facilitates the transport of diphtheria toxin into human cells. *Scientific Reports*, *7*(1). https://doi.org/10.1038/s41598-017-00780-x

Scobie, H. M., Rainey, G. J. A., Bradley, K. A., & Young, J. A. T. (2003). Human capillary morphogenesis protein 2 functions as an anthrax toxin receptor. *Proceedings of the National Academy of Sciences of the United States of America*, *100*(9), 5170–5174. https://doi.org/10.1073/PNAS.0431098100

Scott, A. B., & Rosenbaum, A. (1973). Pharmacologic weakening of extraocular muscles. *Invest Ophthalmol.* https://pubmed.ncbi.nlm.nih.gov/4203467/

Sellman, B. R., Nassi, S., & Collier, R. J. (2001). Point Mutations in Anthrax Protective Antigen That Block Translocation. *Journal of Biological Chemistry*, *276*(11), 8371–8376. https://doi.org/10.1074/jbc.M008309200

Shapiro, R. L., Hatheway, C., & Swerdlow, D. L. (1998). Botulism in the United States: a clinical and epidemiologic review. *Annals of Internal Medicine*, *129*(3), 221–228. https://doi.org/10.7326/0003-4819-129-3-199808010-00011

Sharma, O., & Collier, R. J. (2014). Polylysine-mediated translocation of the diphtheria toxin catalytic domain through the anthrax protective antigen pore. *Biochemistry*, *53*(44), 6934–6940. https://doi.org/10.1021/bi500985v

Singh, Y., Chaudhary, V. K. ., & Leppla, S. H. (1989). A deleted variant of Bacillus anthracis protective antigen is non-toxic and blocks anthrax toxin action in vivo - PubMed. *J Biol Chem.*, *265*(32), 19103–19107. https://pubmed.ncbi.nlm.nih.gov/2509473/

Singh, Y., Khanna, H., Chopra, A. P., & Mehra, V. (2001). A dominant negative mutant of Bacillus anthracis protective antigen inhibits anthrax toxin action in vivo. *The Journal of Biological Chemistry*, *276*(25), 22090–22094. https://doi.org/10.1074/JBC.M010222200

Singh, Y., Klimpel, K. R., Quinn, C. P., CHaudhary V. K., & Leppla, S. H. (1991). The carboxyl-terminal end of protective antigen is required for receptor binding and anthrax toxin activity - PubMed. *J Biol Chem.*, *226*(23). https://pubmed.ncbi.nlm.nih.gov/1651334/

Slamon, D. J., Godolphin, W., Jones, L. A., Holt, J. A., Wong, S. G., Keith, D. E., Levin, W. J., Stuart, S. G., Udove, J., Ullrich, A., & Press, M. F. (1989). Studies of the HER-2/neu proto-oncogene in human breast and ovarian cancer. *Science (New York, N.Y.)*, *244*(4905), 707–712. https://doi.org/10.1126/SCIENCE.2470152

Stanley, J. L., & Smith, H. (1961). Purification of factor I and recognition of a third factor of the anthrax toxin. *Journal of General Microbiology*, *26*, 49–63. https://doi.org/10.1099/00221287-26-1-49

Steeg, P. S., Bevilacqua, G., Kopper, L., Thorgeirsson, U. P., Talmadge, J. E., Liotta, L. A., & Sobel, M. E. (1988). Evidence for a novel gene associated with low tumor metastatic potential. *Journal of the National Cancer Institute*, *80*(3), 200–204. https://doi.org/10.1093/JNCI/80.3.200

Stiles, B. G., Wigelsworth, D. J., Popoff, M. R., & Barth, H. (2011). Clostridial binary toxins: iota and C2 family portraits. *Frontiers in Cellular and Infection Microbiology*, *1*, 11. https://doi.org/10.3389/fcimb.2011.00011

Tamaoki, T., Nomoto, H., Takahashi, I., Kato, Y., Morimoto, M., & Tomita, F. (1986). Staurosporine, a potent inhibitor of phospholipid/Ca++dependent protein kinase. *Biochemical and Biophysical Research Communications*, *135*(2), 397–402. https://doi.org/10.1016/0006-291X(86)90008-2

Texas Animal Health Commssion. (2021). *2021 Texas Anthrax Situational Update*.

Ting, P. T., & Freiman, A. (2004). The story of Clostridium botulinum: from food poisoning to Botox. *Clinical Medicine (London, England)*, *4*(3), 258–261. https://doi.org/10.7861/CLINMEDICINE.4-3-258

Tsuge, H., Nagahama, M., Nishimura, H., Hisatsune, J., Sakaguchi, Y., Itogawa, Y., Katunuma, N., & Sakurai, J. (2003). Crystal structure and site-directed mutagenesis of enzymatic components from Clostridium perfringens iota-toxin. *Journal of Molecular Biology*, *325*(3), 471–483. http://www.ncbi.nlm.nih.gov/pubmed/12498797

van der Goot, G., & Young, J. A. T. (2009). Receptors of anthrax toxin and cell entry. *Molecular Aspects of Medicine*, *30*(6), 406–412. https://doi.org/10.1016/J.MAM.2009.08.007

Varughese, M., Teixeira, A. V., Liu, S., & Leppla, S. H. (1999). Identification of a receptor-binding region within domain 4 of the protective antigen component of anthrax toxin. *Infection and Immunity*, *67*(4), 1860–1865. https://doi.org/10.1128/IAI.67.4.1860-1865.1999

Verheyden, J., Blitzer, A., & Brin, M. F. (2001). Other noncosmetic uses of BOTOX. *Seminars in Cutaneous Medicine and Surgery*, *20*(2), 121–126. https://doi.org/10.1053/SDER.2001.25136

Vitale, G., Bernardi, L., Napolitani, G., Mock, M., & Montecucco, C. (2000). Susceptibility of mitogen-activated protein kinase kinase family members to proteolysis by anthrax lethal factor - PubMed. *Biochem J.*, *352*(3), 739–745. https://pubmed.ncbi.nlm.nih.gov/11104681/

Vitale, G., Pellizzari, R., Recchi, C., Napolitani, G., Mock, M., & Montecucco, C. (1998). Anthrax Lethal Factor Cleaves the N-Terminus of MAPKKs and Induces Tyrosine/Threonine Phosphorylation of MAPKs in Cultured Macrophages. *Biochemical and Biophysical Research Communications*, *248*(3), 706–711. https://doi.org/10.1006/bbrc.1998.9040

Werner, G., Hagenmeier, H., Drautz, H., Baumgartner, A., & Zähner, H. (1984). Metabolic products of microorganisms. 224. Bafilomycins, a new group of macrolide antibiotics. Production, isolation, chemical structure and biological activity. *The Journal of Antibiotics*, *37*(2), 110–117. https://doi.org/10.7164/antibiotics.37.110

Wesche, J., Elliott, J. L., Falnes, P., Olsnes, S., & Collier, R. J. (1998). Characterization of membrane translocation by anthrax protective antigen. *Biochemistry*, *37*(45), 15737–15746. https://doi.org/10.1021/BI981436I

Westphal, O., & Lüderitz, O. (1954). Chemische Erforschung von Lipopolysacchariden gramnegativer Bakterien. *Angewandte Chemie*, *66*(13–14), 407–417. https://doi.org/10.1002/ANGE.19540661312

Williams, D. P., Parker, K., Bacha, P., Bishai, W., Borowski, M., Genbauffe, F., Strom, T. B., Murphy, J. R., & Charles, ’. (1987). Diphtheria toxin receptor binding domain substitution with interleukin-2: genetic construction and properties of a diphtheria toxin-related interleukin-2 fusion protein. *Protein Engineering*, *1*(6), 493–498. http://peds.oxfordjournals.org/

Wu, G., Feng, C., Cao, S., Guo, A., & Liu, Z. (2012). Identification of new dominant-negative mutants of anthrax protective antigen using directed evolution. *Applied Biochemistry and Biotechnology*, *168*(5), 1302–1310. https://doi.org/10.1007/S12010-012-9858-6

Yamaizumi, M., Mekada, E., Uchida, T., & Okada, Y. (1978). One molecule of

diphtheria toxin fragment A introduced into a cell can kill the cell. *Cell*, *15*(1), 245–250. https://doi.org/10.1016/0092-8674(78)90099-5

Young, J. A. T., & Collier, R. J. (2007). Anthrax Toxin: Receptor Binding, Internalization, Pore Formation, and Translocation. *Annual Review of Biochemistry*, *76*(1), 243–265. https://doi.org/10.1146/annurev.biochem.75.103004.142728

Zanetti, G., Azarnia Tehran, D., Pirazzini, M., Binz, T., Shone, C. C., Fillo, S., Lista, F., Rossetto, O., & Montecucco, C. (2015). Inhibition of botulinum neurotoxins interchain disulfide bond reduction prevents the peripheral neuroparalysis of botulism. *Biochemical Pharmacology*, *98*(3), 522–530. https://doi.org/10.1016/J.BCP.2015.09.023

Zanetti, G., Mattarei, A., Lista, F., Rossetto, O., Montecucco, C., & Pirazzini, M. (2021). Novel Small Molecule Inhibitors That Prevent the Neuroparalysis of Tetanus Neurotoxin. *Pharmaceuticals 2021, Vol. 14, Page 1134*, *14*(11), 1134. https://doi.org/10.3390/PH14111134

Zhang, S., Finkelstein, A., & Collier, R. J. (2004). Evidence that translocation of anthrax toxin's lethal factor is initiated by entry of its N terminus into the protective antigen channel. *Proceedings of the National Academy of Sciences of the United States of America*, *101*(48), 16756–16761. https://doi.org/10.1073/PNAS.0405754101

6. List of Publications

Felix I, Lomada SK, Barth H[#], Wieland T[#]. Bacillus anthracis' PA63 Delivers the Tumor Metastasis Suppressor Protein NDPK-A/NME1 into Breast Cancer Cells. Int J Mol Sci. 2020 May 6;21(9):3295. doi: 10.3390/ijms21093295

Schnell L, **Felix I**, Müller B, Sadi M, von Bank F, Papatheodorou P, Popoff MR, Aktories K, Waltenberger E, Benz R, Weichbrodt C, Fauler M, Frick M, Barth H[#]. Revisiting an old antibiotic: bacitracin neutralizes binary bacterial toxins and protects cells from intoxication. FASEB J. 2019 Apr;33(4):5755-5771. doi: 10.1096/fj.201802453R

Martin T*, Möglich A*, **Felix I**, Förtsch C, Rittlinger A, Palmer A, Denk S, Schneider J, Notbohm L, Vogel M, Geiger H, Paschke S[#], Huber-Lang M[#], Barth H[#]. Rho-inhibiting C2IN-C3 fusion toxin inhibits chemotactic recruitment of human monocytes ex vivo and in mice in vivo. Arch Toxicol. 2018 Jan;92(1):323-336. doi: 10.1007/s00204-017-2058-y

*authors contributed equally to this work

[#]corresponding authors

7. Curriculum Vitae

Personal Information

Name:	Ina Felix
Year of Birth:	1991
Place of Birth:	Überlingen, Germany

Education

2017 - 2022	**PhD**, International Graduate School in Molecular Medicine Ulm University, Germany
2015 - 2017	**M.Sc.**, Biology, Ulm University, Germany
2011 - 2015	**B.Sc.**, Biology, Ulm University, Germany
2007 - 2010	**A-Levels** Justus von Liebig Schule, Ueberlingen, Germany
2001 - 2007	**General Certificate of Secondary Education** (GCSE) (2.0) Bildungszentrum Salem, Germany

8. Acknowledgements

First and foremost, I would like to thank Prof. Dr. Holger Barth for giving me the opportunity to work in his group. He was always open for ideas and discussions, had solutions at an instant and was never far from a word of wisdom.

Furthermore, I would like to thank my thesis advisory committee Prof. Dr. Manfred Frick and Prof. Dr. Thomas Wieland for their support.

I would especially like to thank my amazing former colleagues, who created a warm, free-spirited and hilarious atmosphere during my time in the institute. Special thanks goes to Stefan Carle, Tobias Martin, Katharina Sessler, Anna Anastasia, Maximilian Fellermann, Stephan Fischer, Leonie Schnell und Katharina Ernst. Without you my time would have been much less fun.

Of course, I would also like to thank Carolin Weiß who made a lot of not so sound ideas possible and never grew tired of my questions.

In the end I would like to thank the International Graduate School in Molecular Medicine Ulm for funding and all the staff for their support and organization.

Finally, I would like to express my deepest gratitude to my family and friends for their continuous support and understanding, especially during the stressful times.

9. Statutory Declaration

I hereby declare that I wrote the present dissertation with the topic:

"Bacillus anthracis´ protective antigen as molecular transporter for the pharmacologically relevant biomolecule His-NDPK-A"

independently and used no other aids that those cited. In each individual case, I have clearly identified the source of the passages that are taken word for word or paraphrased from other works.

I also hereby declare that I have carried out my scientific work according to the principles of good scientific practice in accordance with the current „Satzung der Universität Ulm zur Sicherung guter wissenschaftlicher Praxis" [Rules of the University of Ulm for Assuring Good Scientific Practice].

Ulm,

_____

(Ina Felix)